

1,3,5-Triazine-Functionalized Thermally Activated Delayed Fluorescence Emitters for Organic Light-Emitting Diodes

Dianming Sun, Changfeng Si, Tao Wang, and Eli Zysman-Colman*

The 1,3,5-triazine electron acceptor has become one of the most popular building blocks for the design of thermally activated delayed fluorescence (TADF) materials. Many TADF design strategies are first applied in compounds that contain triazines, and there are numerous examples of organic light-emitting diodes (OLEDs) with triazine-containing emitters that show high efficiencies and long operating lifetimes. A comprehensive review of triazine-containing TADF emitters is provided. This review is organized according to the triazine-derived structural motifs, such as number and position of electron-donor groups in donor–acceptor-type emitters, the π -bridging linkers employed, orientation control of the transition dipole moment, and the design of chiral and through-space charge-transfer emitters. The structure of the compounds with their optoelectronic properties and the corresponding performance of the OLED devices is correlated.

1. Introduction


Since 1987, when the first viable electroluminescent device was reported by Tang and Van Slyke,^[1] significant progress has been made in terms of materials development such that organic light-emitting diodes (OLEDs) have now been commercialized in both the solid-state lighting and display markets. The current mature OLED products heavily rely on the phosphorescent emitters that contain noble metals such as iridium because these materials permit 100% utilization of the electrogenerated singlet and triplet excitons to produce light. The breakthrough of TADF materials in 2012 by Adachi and co-workers^[2] provides an alternative route to reach equally efficient OLEDs and without the use of these scarce metals. To date, thousands of TADF materials have been reported, and their use in red, green, and blue OLEDs has been demonstrated. Importantly, there are now many examples of devices that show high external quantum efficiency (EQE),

device stability, and color purity, these reports demonstrate that TADF OLEDs are attractive alternatives to phosphorescent devices. Indeed, the first commercialized TADF OLED devices are now on the market.^[3] For instance, one of the best red TADF OLED, which uses TPA-PZCN as the emitter, has realized a record high maximum EQE (EQE_{max}) of 28.1% with an electroluminescence maximum, λ_{EL} , of 648 nm.^[4] For green OLEDs, the use of CzDBA as the emitter resulted in a device with an EQE_{max} of 37.8% with the λ_{EL} at 528 nm.^[5] Blue OLED employing TDBA-DI as the emitter showed a comparable high EQE_{max} of 38.2% with CIE coordinates of (0.15, 0.28)^[6] and an OLED using a multiple resonance TADF (MR-TADF) emitter, ν -DABNA, achieved an EQE_{max}

of 34.4% with a λ_{EL} at 469 nm and a full-width at half-maximum (FWHM) of only 18 nm.^[7]

All these achievements in terms of device performance are inextricably linked to the development of high-performance highly twisted donor–acceptor emitter architectures. The vast majority of electron-donor groups used within TADF emitters are hole-transporting *N*-heterocycles and are typically chosen from carbazole and its derivatives (e.g., bicarbazole, benzofurocarbazole, thienocarbazole, and indolocarbazole), arylamine, acridan, phenoxazine, phenothiazine, and phenazine, and their derivatives. There is more structural diversity in the electron-acceptor moiety, with popular motifs containing borane, sulfone, ketone, pyrimidine, benzonitrile, phthalonitrile, triazole, oxadiazole, thiadiazole, benzothiazole, benzooxazole, quinoxaline, anthraquinone, heptazine, and, of course, triazine. In particular, 1,3,5-triazine has been one of the most popular electron-deficient heteroaromatic acceptors used in green and blue TADF emitters and is also a popular component used in host materials design due to its moderate electron affinity with the LUMO values in the range of -2.7 to 3.1 eV.^[8] Most commonly, the 1,3,5-triazine is decorated by three phenyl groups attached to the 2,4,6-position of triazine in a triphenyltriazine structure (TRZ). There are also examples of triazine-containing materials where the electron donor is directly attached to the triazine. However, in many of these materials, as there are negligible steric interactions between the triazine and the donor, thus leading to a predominantly coplanar conformation, there is significant overlap between the highest occupied molecular orbital (HOMO) and lowest unoccupied molecular orbital (LUMO), thereby resulting in a correspondingly large singlet and triplet energy splitting (ΔE_{ST}) and no TADF. For example, DPPhCzT,^[9] a compound

D. Sun, C. Si, T. Wang, E. Zysman-Colman
Organic Semiconductor Centre
EaStCHEM School of Chemistry
University of St Andrews
St Andrews KY16 9ST, UK
E-mail: eli.zysman-colman@st-andrews.ac.uk

 The ORCID identification number(s) for the author(s) of this article can be found under <https://doi.org/10.1002/adpr.202200203>.

© 2022 The Authors. Advanced Photonics Research published by Wiley-VCH GmbH. This is an open access article under the terms of the Creative Commons Attribution License, which permits use, distribution and reproduction in any medium, provided the original work is properly cited.

DOI: 10.1002/adpr.202200203

containing a carbazole directly coupled to a diphenyltriazine, was reported as a host material, but did not show any TADF properties due to its large ΔE_{ST} of 0.3 eV (Figure 1).

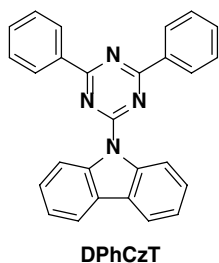


Figure 1. Chemical structure of DPhCzT.

The genesis of organic TADF materials as emitters for OLEDs was in 2011 and relied on a triazine-based compound (Figure 2). A sufficient separation between HOMO and LUMO was induced by strengthening the electron donor by extending the conjugation length as was done in PIC-TRZ ($\Delta E_{ST} = 0.11$ eV), the first example of a purely organic TADF emitter. The design of PIC-TRZ also paved the way for the adoption of one of the most successful design strategies for TADF emitters, which is based on a strongly twisted donor- π -acceptor motif. Exciplex systems are another route to small ΔE_{ST} as the weak intermolecular interactions between electron-donor and electron-acceptor compounds ensure suitable physical separation of the HOMO and LUMO. Triazine-containing electron acceptors appear prominently in exciplex systems due to their largely planar conformation since the first exciplex system was reported in 2012.^[10] PO-T2T, for instance, has

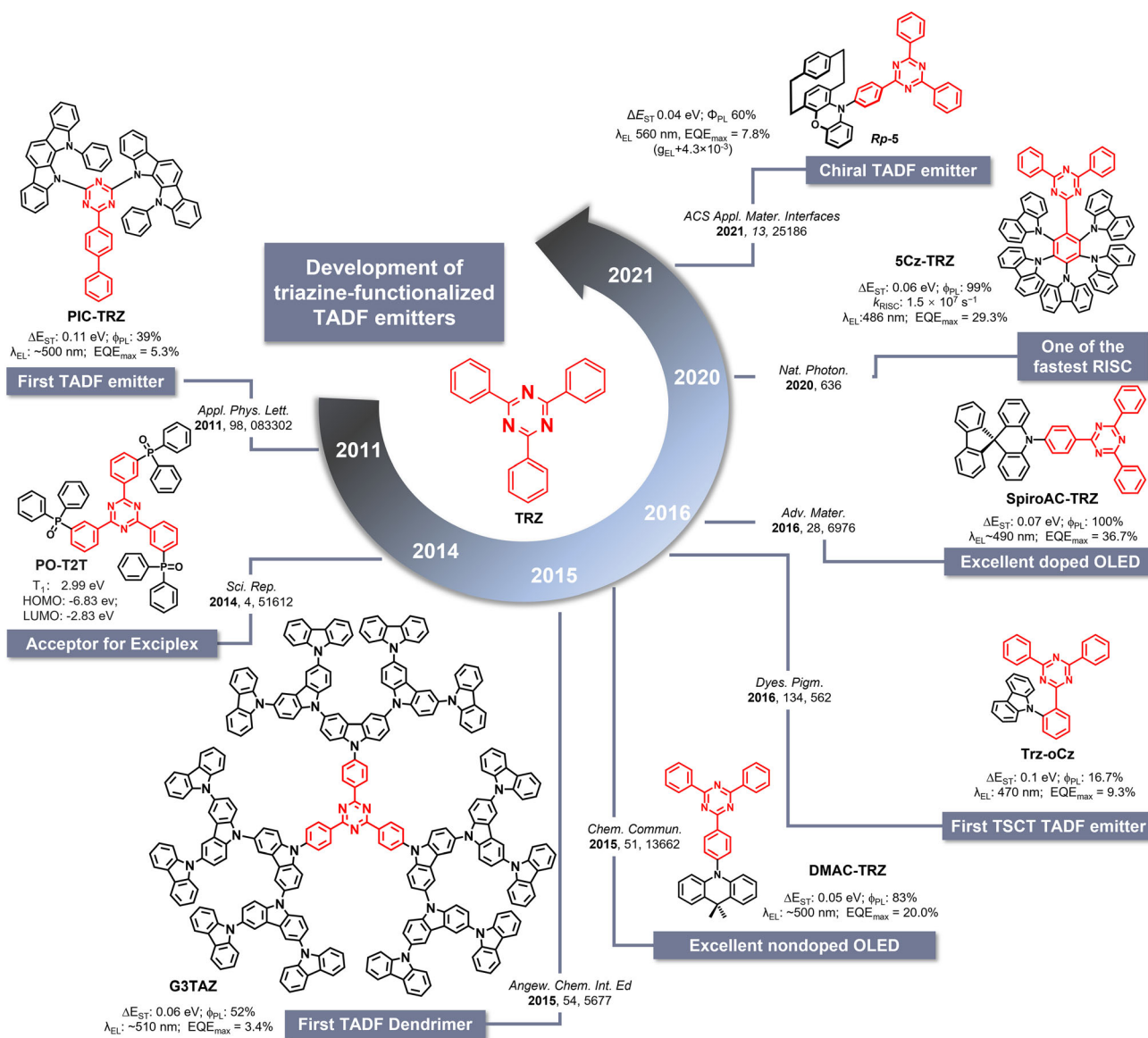


Figure 2. Timeline of the development of 1,3,5-triazine-based TADF materials for OLEDs.

been widely used as the acceptor for exciplex since it was first reported in 2014.^[11] Triazine electron acceptors were incorporated into some of the first TADF dendrimer emitters in 2015, such as **G3TAZ**, this due in part to the D_3 -symmetric structure of the TRZ and the ease with which chemical modification of this core can occur. High-efficiency nondoped OLEDs ($\text{EQE}_{\text{max}} = 20\%$) using the small molecule emitter **DMAC-TRZ** showed comparable performance to the doped device, indicating that it is possible to design a compound that shows significantly suppressed concentration quenching in neat films. **DMAC-TRZ** is still one of the most widely studied donor-acceptor-type TADF emitters. Disposing the electron-donor adjacent to the TRZ results in improved performance in the OLED, as exemplified by **TRZ-oCz** ($\text{EQE}_{\text{max}} = 9.3\%$). This is partially due to the more strongly twisted conformation that must be adopted for this compound and the additional through space charge transfer (TSCT) state that is induced. Since the first example in 2017, TRZ-containing TSCT TADF emitters have developed rapidly. Presently, the highest performing TRZ-based TADF emitter is **SpiroAC-TRZ**. Compared to the OLED with **DMAC-TRZ**, the EQE_{max} of the OLED with **SpiroAC-TRZ** is improved to 36.7%. Here, by employing a related electron donor in 10 H-spiro [acridine-9,9'-fluorene] (**SpiroAC**), a highly horizontally orientated transition dipole moment (TDM) was achieved, leading to enhanced light outcoupling.^[12] Recently, a triazine-containing TADF emitter **5Cz-TRZ** with five carbazoles closely packed onto a central phenylene bridge afforded a material with one of the fastest reverse intersystem crossing (RISC) rate constants of $k_{\text{RISC}} = 1.5 \times 10^7 \text{ s}^{-1}$.

There are several advantages for the use of triazine within TADF materials. These include (1) triazine and its derivatives are easy to synthesize from inexpensive starting materials; (2) triazine is easily functionalized at the 2,4,6 positions and can be done both symmetrically or asymmetrically, thereby increasing structural diversity; (3) the linkage between the electron donor and the triazine core can be rationally adjusted; and (4) triazine is a stable aromatic structure that contributes to improved operational lifetimes of the devices. Documenting the popularity of this moiety, in this review, we summarize the recent progress of triazine-containing TADF materials. First, the TADF emitters based on carbazole-triazine structures are introduced and classified according to 1) the number and substitution position of the carbazole; 2) the influence of the bridge between the donor and the triazine acceptor; 3) the influence of the structure on the orientation of the emitter within the emitter layer, which will affect the orientation of the TDM and hence the light outcoupling efficiency in the device; 4) trisubstitution about the triazine core; 5) dimerization strategies where there are at least two triazines within the material; 6) examples where the linker group goes beyond a phenylene; 7) adjustment of the triazine electron-withdrawing strength through peripheral decoration; and 8) examples where there is TSCT in addition to through-bond charge transfer (TBCT). Finally, moving beyond carbazole-based electron donors, examples of emitters using other donors will be summarized (Figure 3).

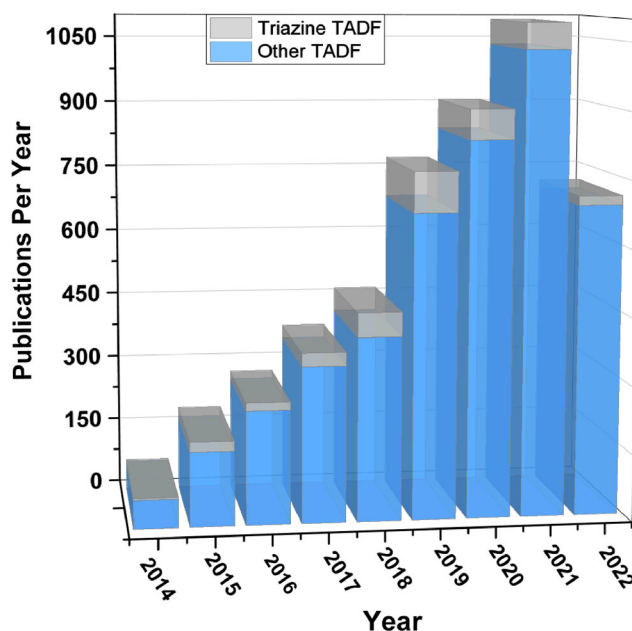


Figure 3. Number of publications for TADF materials and the proportion that contain triazine. Keyword: “triazine” or “TADF”. Scifinder search conducted: 30/06/2022.

2. Influence of Carbazole (Number and Position) on the Properties of TRZ-Based TADF Emitters

Carbazole (Cz) has been widely used as an electron-donating group in optoelectronic materials because of its moderate donor strength and the ease with which chemical derivatization can occur.^[13] Carbazole is also a fully aromatic structure, with no bonds to a sp^3 -centre as exists in acridine, phenoxazine, and phenothiazine, bonds that are prone to scission and routes to degradation in the device.

First, we compare the optoelectronic properties of Cz-TRZ derivatives where the Cz is either *ortho*, *meta* or *para* disposed with respect to the diphenyltriazine, as shown in Figure 4. The *para*-analog **CzTRZ** (here, it is renamed as **p-CzTRZ**), first reported by Lee et al.,^[14] is not a TADF emitter due to its too strong conjugation between Cz and TRZ, leading to a large ΔE_{ST} of 0.36 eV; the compound is a blue emitter with a λ_{PL} of 449 nm and a photoluminescence quantum yield, Φ_{PL} , of 71% (10 wt% DPEPO). A blue OLED with CIE coordinates of (0.17, 0.11) showed only an EQE_{max} of 4.2%. A slightly improved OLED efficiency (EQE_{max} of 5.8%) was later reported by our group,^[15] which provided further confirmation that in the device **p-CzTRZ** acts as a fluorescent emitter. Liao et al.^[16] designed two analogs, **SFCCN** and **SFCCNO** (Figure 5), based on the strategy of introducing a secondary donor group onto the carbazole moiety of **p-CzTRZ**. The solution-state properties remained unchanged because the spiro-carbon linkage between the secondary donor with carbazole is not conjugated. However, in the neat films, the aggregation of these molecules triggered the TADF as a result of the intermolecular TSCT. The planar molecular conformation is believed to facilitate face-to-face

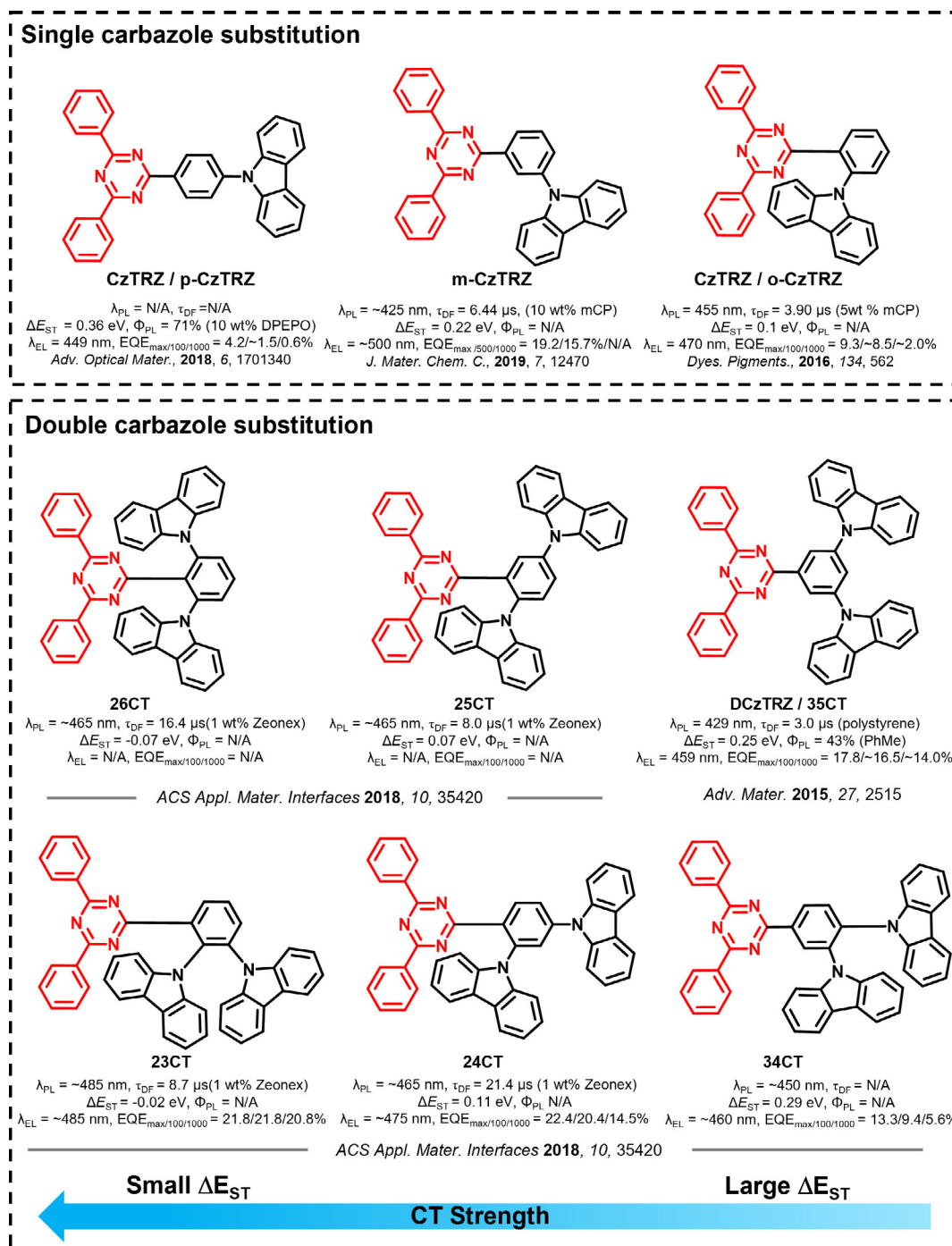


Figure 4. Molecular structures and properties of TADF emitters containing carbazole-triazine motifs.

intermolecular interactions required for the TSCT to occur. The nondoped device based on **SFCCNO** exhibited an EQE of 12.9% at 100 cd m^{-2} , which is much improved compared to the device based on the non-TADF emitter **p-CzTRZ** (1.5% at 100 cd m^{-2}).

The *meta*- and *ortho*- analogs, by contrast, are efficient TADF emitters. **CzTRZ** (renamed as **o-CzTRZ**; $\lambda_{PL} = 455 \text{ nm}$, $\tau_d = 3.90 \mu\text{s}$ in 5 wt% mCP film) possesses a much smaller overlap between the HOMO and LUMO as a result of the more

strongly twisted conformation (87.3° for the dihedral angle between carbazole and phenylene bridge determined from the crystal structure^[17]), which translates into a compound with a ΔE_{ST} of 0.1 eV in 5 wt% mCP film. By doping 5 wt% **o-CzTRZ** in mCP host as the emitting layer, the OLED exhibited a blue emission with a λ_{EL} at 470 nm and an EQE_{max} of 9.3% despite the Φ_{PL} of **o-CzTRZ** being only 16.7% (5 wt% mCP), which likely implies that the Φ_{PL} has been underestimated, considering the

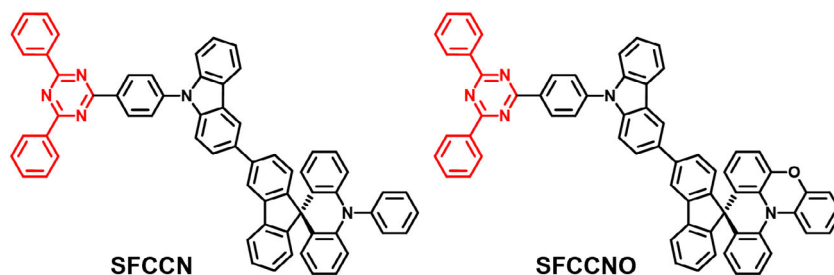


Figure 5. Molecular structures of SFCCN and SFCCNO.

device performance. Interestingly, the full-width at half-maximum (FWHM) of the blue TADF device is only 66 nm, which we attribute to a much reduced geometric reorganization in the excited state to the small degree of conformational freedom present in the *ortho*-linked system. Indeed, many other compounds containing *ortho*-linked donors and acceptors also show narrow emission spectra (in section 9 related to TSCT). Normally, *meta*-disposed electron donors^[18] and electron acceptors in D–A-type emitters show the weakest conjugation compared to their *ortho*- and *para*- analogs, which should lead to a correspondingly smaller ΔE_{ST} . However, it was observed by Wu et al.^[19] that the ΔE_{ST} of *m*-CzTRZ (0.22 eV in 10 wt% in mCP film) is indeed larger than 0.03 eV for *o*-CzTRZ (determined again by Wu et al.^[19] although these values are extracted from the energy difference between the PL at room temperature and the phosphorescence spectra at 77 K in 2-MeTHF and so differ from those of Gong et al.^[17]). The authors contended that the smaller observed ΔE_{ST} for *o*-CzTRZ resulted from the near orthogonal conformation of the donor, leading to near complete suppression of the conjugation between Cz and TRZ. The DFT calculations (Figure 6) from their work suggest that the ³LE state of *m*-CzTRZ is much more stabilized than the ³CT state, while the ³LE state of *o*-CzTRZ is much closer in energy to its ³CT state. The stabilized ³LE state explains the greater ΔE_{ST} of *m*-CzTRZ

than that of *o*-CzTRZ due to their similar energy in ¹CT state, resulting in calculated ΔE_{ST} of 0.06 eV and 0.23 eV for *o*-CzTRZ and *m*-CzTRZ, respectively, which are consistent with the experimental values. The OLEDs exhibited high EQE_{max} of 17.5% and 19.2% for the devices with *o*-CzTRZ and *m*-CzTRZ, respectively (10 wt% doped in mCP host). Further, the EQE_{max} of the corresponding nondoped OLEDs remains nearly as high at 17.6% and 16.7% for the devices with *o*-CzTRZ and *m*-CzTRZ, respectively.

In comparison to the three aforementioned triazine-based TADF emitters, each possessing only one carbazole donor, emitters with more than one carbazole have also been investigated. Lee et al.^[20] reported a stable deep blue emitter DCzTRZ (λ_{PL} : 459 nm; Φ_{PL} : 43% in toluene) in which the two carbazole donor groups are disposed mutually *meta* to each other and to the triazine acceptor. The ΔE_{ST} of DCzTRZ is 0.25 eV, which is similar to that of *m*-CzTRZ (0.22 eV in 10 wt% mCP). The blue OLED has an EQE_{max} of 17.8% at CIE coordinates of (0.15, 0.15), which is slight less efficient than that of *m*-CzTRZ (19.2%). It is surprising to observe a much bluer emission spectrum in comparison with the device based on *m*-CzTRZ, although the solution PL spectrum in toluene is exactly the same. The blue-shift of the EL may be caused by the different device configurations, choice of host, and doping concentration between the two devices.

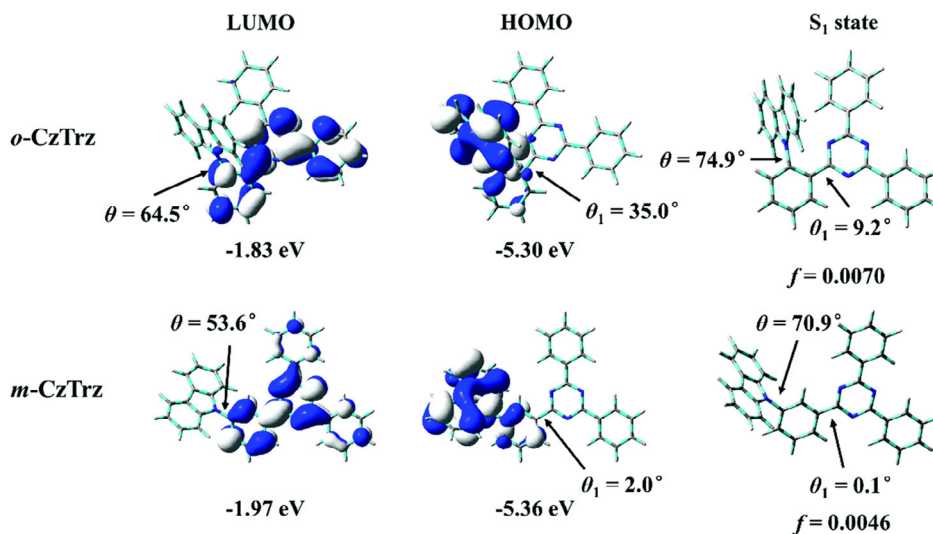


Figure 6. HOMO and LUMO distribution and their energy levels, optimized S_1 geometry with oscillator strengths (f) for *o*-CzTRZ and *m*-CzTRZ. Reproduced with permission.^[19] Copyright 2019, Royal Society of Chemistry.

A number of other analogs containing two carbazole donors were also prepared by Lee et al.^[21] The different substitution patterns of the two carbazoles for six emitters **23CT**, **24CT**, **25CT**, **26CT**, **34CT**, and **35CT** (here **DCzTRZ** was renamed as **35CT**) are correlated with their photophysical properties. *Ortho*-substitution to the triazine acceptor induces a large dihedral angle between the carbazole and triazine moieties, thus leading to a stronger charge transfer state and smaller ΔE_{ST} , which is evident by comparing **23CT** (ΔE_{ST} : -0.02 eV, 1 wt% in Zeonex), **24CT** (ΔE_{ST} : 0.11 eV, 1 wt% in Zeonex), **25CT** (ΔE_{ST} : 0.07, 1 wt% in Zeonex), and **26CT** (ΔE_{ST} : -0.07 eV, 1 wt% in Zeonex) with **34CT** (ΔE_{ST} : 0.29 eV, 1 wt% in Zeonex) and **35CT** (ΔE_{ST} : 0.24 eV, 1 wt% in Zeonex). The difference of ΔE_{ST} may result from different conformers, showing the various CT strength. The emitters with no *ortho*-substituted carbazole have larger ΔE_{ST} and long-to-negligible delayed fluorescence. The EQE_{max} of the OLEDs with **23CT**, **24CT**, and **34CT** as emitters are 21.8%, 22.4%, and 13.3%, respectively, which align with both the smaller ΔE_{ST} and faster RISC rates of the former two emitters.

There are also a number of analog emitters possessing three carbazole donors. Compared with **35CT** (ΔE_{ST} : 0.23 eV; Φ_{PL} : 43% in toluene), **TCzTRZ**^[22] (ΔE_{ST} : 0.16 eV; Φ_{PL} : 100% in toluene), as shown in **Figure 7**, possesses a smaller ΔE_{ST} coupled with a significantly improved Φ_{PL} . The structural difference between these two compounds is the addition of a third carbazole *para* to the triazine, which results in a HOMO that is distributed

over the three donor carbazoles. The even distribution of the electron density of the HOMO across multiple donors also is in operation in **TmCzTRZ** (ΔE_{ST} : 0.07 eV; Φ_{PL} : 99% in toluene), which also possesses a smaller ΔE_{ST} and a higher Φ_{PL} than **DCzmCzTRZ** (ΔE_{ST} : 0.20 eV; Φ_{PL} : 84% in toluene), which has two different carbazole-based donors. OLEDs with these three emitters achieved comparably high efficiencies, with EQE_{max} of 25% and CIE coordinates of (0.18, 0.33) for the device with **TCzTRZ** and an EQE_{max} of 25.5% and CIE coordinates of (0.25, 0.50) for the device with **TmCzTRZ**; the red-shift in the EL of the latter is due to the use of a stronger dimethylcarbazole donor. The EQE_{max} decreased to 21.3%, with CIE coordinates of (0.23, 0.46) for the device with **DCzmCzTRZ**, reflecting to the lower Φ_{PL} for the emitter.

Lee et al.^[23] later probed the effect of the regiochemistry of the three carbazole donors on the photophysical properties of the emitters. A cross-comparison of the photophysical properties of compounds **234CzTRZ** (ΔE_{ST} : 0.07 eV; Φ_{PL} : 90% in DPEPO; τ_d : 4.1 μ s), **235CzTRZ** (ΔE_{ST} : 0.14 eV; Φ_{PL} : 100% in DPEPO; τ_d : 8.4 μ s), and **245CzTRZ** (ΔE_{ST} : 0.17 eV; Φ_{PL} : 98.4% in DPEPO; τ_d : 9.7 μ s) revealed that the substitution pattern of the three carbazole donors affects both ΔE_{ST} and τ_d ; all three compounds possess a shorter delayed fluorescence lifetime than that of **TCzTRZ** (τ_d : 13.5 μ s). As shown in **Figure 8**, the *ortho*-substituted carbazoles to the diphenyltriazine acceptor adopt a large dihedral angle, which leads to a shortened delayed fluorescence lifetime, compound **234CzTRZ**, with three

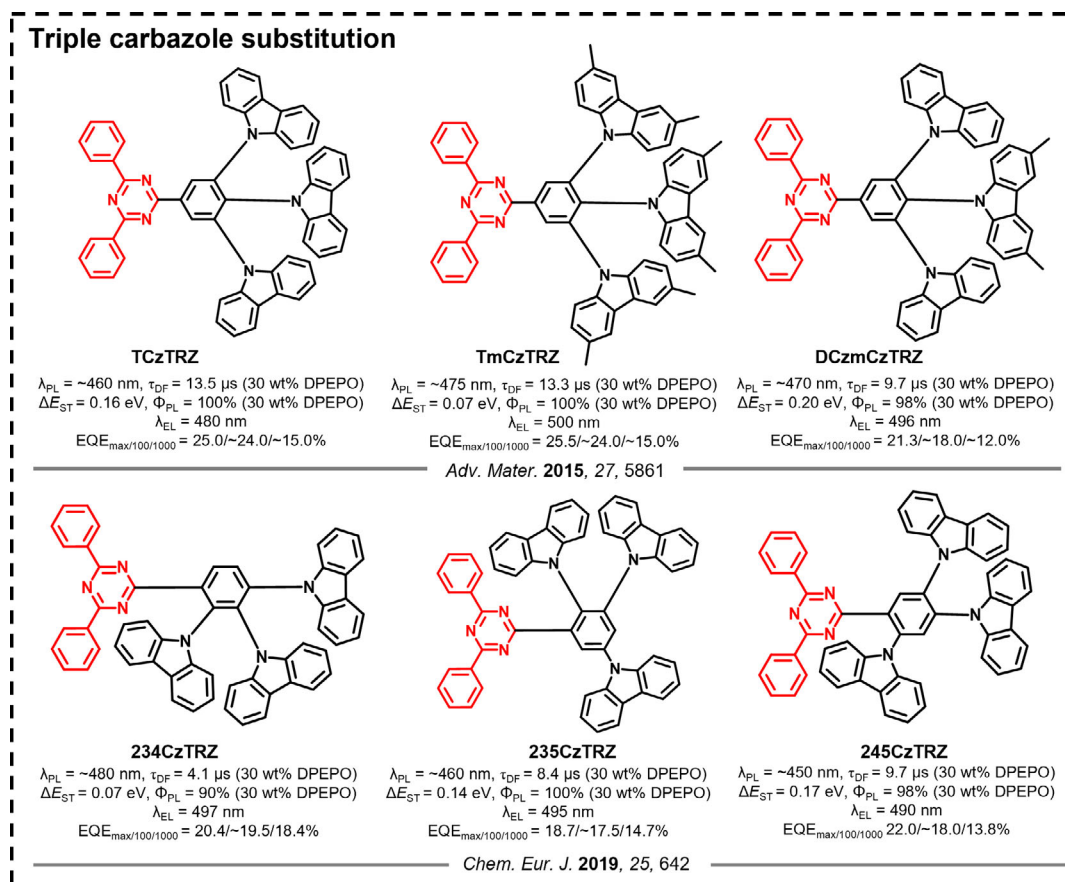


Figure 7. Molecular structures and properties of TADF emitters containing three carbazole donors and a triazine acceptor.

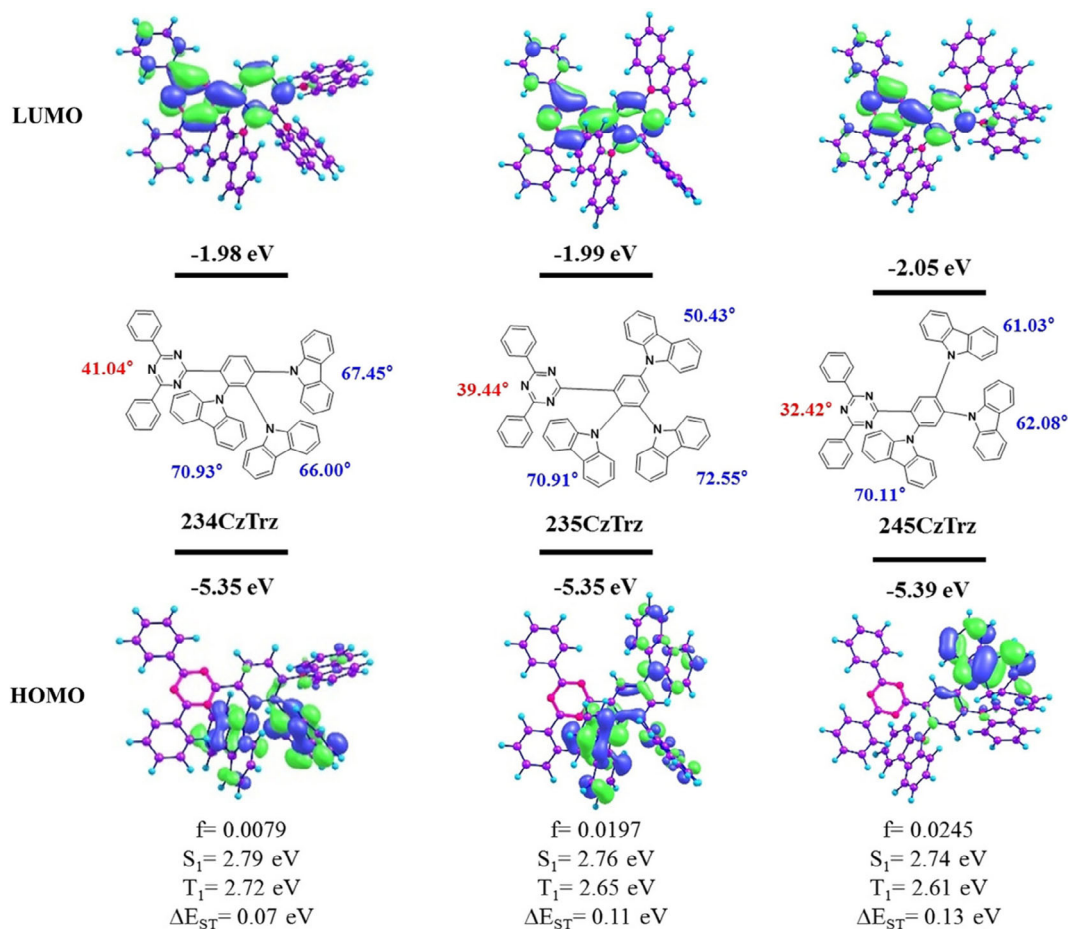


Figure 8. Results of molecular orbital calculations showing frontier molecular orbitals distribution and geometry of **234CzTRZ**, **235CzTRZ**, and **245CzTRZ**. Reproduced with permission.^[23] Copyright 2019, Wiley-VCH.

carbazoles packed closely to each other, showed the shortest delayed lifetime of 4.1 μs . The EQE_{max} of the OLEDs using **234CzTRZ** (λ_{EL} : 497 nm; CIE = (0.20, 0.44)), **235CzTRZ** (λ_{EL} : 495 nm; CIE = (0.20, 0.45)), and **245CzTRZ** (λ_{EL} : 490 nm; CIE = (0.17, 0.39)) are all quite similar at 20.4%, 18.7%, and 22.0%, respectively. At a luminance of 1000 cd m^{-2} , the device with **234CzTRZ** can still maintain 18.4%, while the EQE_{1000} of the OLEDs with **235CzTRZ** and **245CzTRZ** drops to 14.7% and 13.8%, respectively. However, even though these emitters exhibited shorter τ_{DF} and smaller ΔE_{ST} than those of **TCzTRZ**, their devices performance is inferior to the OLED based on **TCzTRZ**.

Recently, a TADF emitter **5Cz-TRZ** (ΔE_{ST} : 0.06; Φ_{PL} : 99% (15 wt% mCPB); τ_{d} : 0.8 μs in DMF) was reported (Figure 9c) that contains five carbazole donors.^[24] Compound **5Cz-TRZ** possesses a very high k_{RISC} of $1.5 \times 10^7 \text{ s}^{-1}$, which is in part due to the large density of excited states and the small ΔE_{ST} . The authors contended that the fast RISC in **5Cz-TRZ** would contribute to a smaller efficiency roll-off in the device as efficiency roll-off is typically caused by the accumulation of long-lived triplet excitons. The resulting device showed an outstanding performance with an EQE_{max} of 29.3%, which decreased a mere 2.3% at 1000 cd m^{-2} and a device lifetime, T_{90} , of ≈ 600 h from an initial brightness of 1,000 cd m^{-2} . All the photophysics and

electrochemical characteristics of the aforementioned materials are summarized in Table 1. Representative device performance is summarized in Table 2.

3. Importance of Conjugated Bridge between TRZ and Carbazole/Carbazole Derivatives

PIC-TRZ^[25] (λ_{PL} : 466 nm; τ_{d} : 120 μs ; ΔE_{ST} : 0.11 eV; Φ_{PL} : 39%; 6 wt% in mCP) was the first reported purely organic TADF emitter for use in OLEDs (Figure 2). Unlike the most commonly used design strategy for TADF emitters, which is to separate electron-donor and electron-acceptor groups by a conjugated phenylene bridge, **PIC-TRZ** contains two carbazole derivatives that are directly connected to a triazine core. A relatively small ΔE_{ST} (0.11 eV) was obtained due to the large twist angle between the carbazole-based donors and the triazine acceptor. Even though the reported EQE_{max} could only reach 5.3% for the sky-blue OLED, this nevertheless indicated that upconversion of triplet excitons to singlet excitons was occurring as the theoretical EQE_{max} of the device was limited to 2% based on its relatively low Φ_{PL} of 39% and assuming no triplet exciton harvesting (Figure 10).

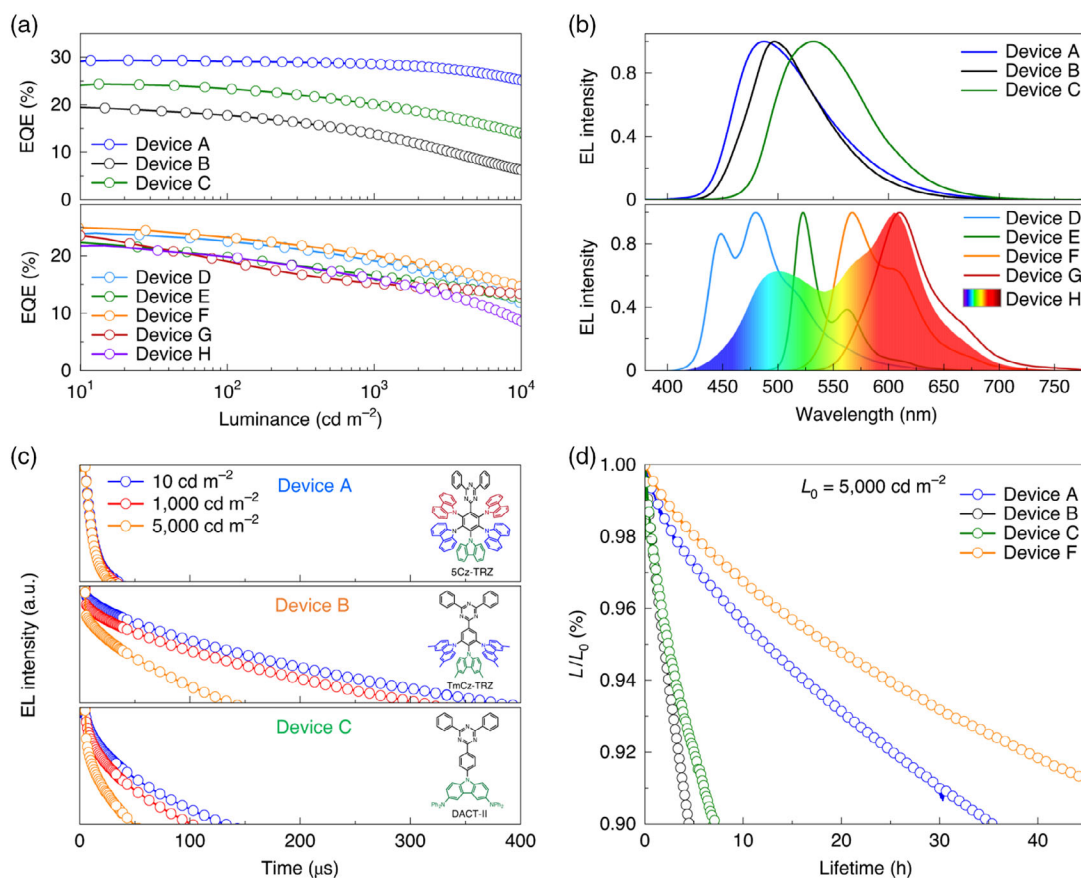


Figure 9. a) EQE versus luminance characteristics. b) Normalized EL spectra. c) Transient EL decay characteristics of devices A, B, and C at 10, 1000, and 5000 cd m⁻². a.u., arbitrary units. d) Operational lifetimes of the TADF and hyperfluorescent OLEDs. Reproduced with permission.^[24] Copyright 2020, Nature Portfolio.

Table 1. Summary of photophysical and electrochemical properties.

Emitter	Solution $\lambda_{PL}/\Phi_{PL}/\tau_d$ (medium) [nm/%/μs]	Solid State $\lambda_{PL}/\Phi_{PL}/\tau_d$ (medium) [nm/%/μs]	ΔE_{ST} [eV]	HOMO [eV]	LUMO [eV]	Ref.
CzTrz	/-/	-/71/- (10 wt% in DPEPO)	0.36	-6.04	-3.39	[14]
<i>m</i> -CzTrz	431/-/(PhMe)	≈425/-/6.44(10 wt% in mCP)	0.22	-5.62	-2.77	[19]
<i>o</i> -CzTRZ	-/-	455/-/3.9(5 wt% in mCP)	0.10	-6.12	-3.26	[17]
26CT	≈465/-/(PhMe)	-/-/16.4 ± 0.9(1% wt in ZEONEX)	-0.07	-	-	[21]
25CT	≈465/-/(PhMe)	-/-/8.0 ± 1.2(1% wt in ZEONEX)	0.07	-	-	[20]
DCzTrz	≈440/0.43/(PhMe)	429/-/3.1(polystyrene)	0.25	-5.88	-2.86	[21]
23CT	≈485/-/(PhMe)	-/-/8.7 ± 0.3(1% wt in ZEONEX)	-0.02	-6.12	-3.52	[21]
24CT	≈465/-/(PhMe)	-/-/21.4 ± 1.9(1% wt in ZEONEX)	0.11	-6.14	-3.55	[21]
34CT	≈450/-/(PhMe)	-/-/(1% wt in ZEONEX)	0.29	-6.16	-3.50	[21]
TCzTrz	-/100/(PhMe)	≈460/100/13.5(30 wt% in DPEPO)	0.16	-	-	[22]
TmCzTrz	-/99/(PhMe)	≈475/100/13.3(30 wt% in DPEPO)	0.07	-	-	[22]
DCzmCzTrz	-/89/(PhMe)	≈470/98/9.7(30 wt% in DPEPO)	0.20	-	-	[22]
235CzTrz	≈480/-/(PhMe)	≈460/100/8.4	0.14	-	-	[23]
245CzTrz	≈500/-/(PhMe)	≈450/98.4/9.7	0.17	-	-	[23]
5Cz-TRZ	486/92/(PhMe)	486/99/2.1(15 wt% in mCBP)	0.03	-5.92	-	[24]

Table 2. Summary of device structures and performance.

Emitter	Device Structure	λ_{EL} [nm]	CIE	V_{on} [V]	EQE/PE/CE ^(a) [%/lm W ⁻¹ /cd A ⁻¹]	EQE _{100/1000} [[cd] [m ⁻²]	Ref.
CzTRZ	ITO/PEDOT:PSS/TAPC/mCP/ CzTrz /TSPO1/TBPI/LiF/Al	449	(0.17, 0.11)	–	4.2/2.7/3.8	≈1.5/0.6	[14]
m-CzTRZ	ITO/PEDOT:PSS/TAPC/10 wt% m-CzTrz:mCP/TmPyPB/LiF/Al	≈500	(0.25, 0.44)	3.3	19.2/40.3/51.3	15.7/N/A	[19]
o-CzTRZ	ITO/PEDOT:PSS/TAPC/mCP/mCP:5%CzTrz/TSPO1//LiF/Al	470	(0.15, 0.22)	–	9.3/–/14.59	–/–	[17]
DCzTRZ	ITO/PEDOT:PSS/TAPC/mCP/25 wt% DCzTrz:DPEPO/TSPO1/TPBi/LiF/Al	459	(0.15, 0.15)	5.9	17.8/22.4/26.8	≈8.5/≈2.0	[20]
23CT	ITO/PEDOT:PSS/TAPC/mCP/DPEPO:30 wt% 23CT /TSPO1/TPBi/LiF/Al	–	(0.17, 0.33)	≈3.8	21.8/30.9/45.9	21.8/20.8	[21]
24CT	ITO/PEDOT:PSS/TAPC/mCP/DPEPO:30 wt% 24CT /TSPO1/TPBi/LiF/Al	–	(0.15, 0.26)	≈3.8	22.4/–/40	20.4/14.5	[21]
34CT	ITO (120 nm)/PEDOT:PSS/TAPC/mCP/DPEPO:30 wt% 34CT/TSPO1/TPBi/LiF/Al	–	(0.15, 0.17)	≈3.8	13.3/–/21.5	9.4/5.6	[21]
TCzTRZ	ITO/PEDOT:PSS/TAPC/mCP/40 wt% TCzTrz:DPEPO/TSPO1/TPBi/LiF/Al	480	(0.18, 0.33)	–	25/42.7/–	≈24.0/≈15.0	[22]
234CzTRZ	ITO/PEDOT:PSS/TAPC/mCP/DPEPO:30% 234CzTrz/TSPO1/TPBi/LiF/Al	497	(0.20, 0.44)	≈3.6	20.4/–/–	≈19.5/18.4	[23]
235CzTRZ	ITO/PEDOT:PSS/TAPC/mCP/DPEPO:30% 235CzTrzor/TSPO1/TPBi/LiF/Al	495	(0.20, 0.45)	≈3.6	18.7/–/–	≈17.5/14.7	[23]
245CzTRZ	ITO/PEDOT:PSS/TAPC/mCP/DPEPO:30% 235CzTrzor/TSPO1/TPBi/LiF/Al	490	(0.17, 0.39)	≈3.6	22/–/–	≈18.0/13.8	[23]
5Cz–TRZ	ITO/HAT–CN/α–NPD/Tris–PCz/mCBP / 15 wt% 5Cz–TRZ: mCBP/CF3–TRZ/30 wt% Liq:BPPB/Liq/Al	486	–	–	29.3/–/–	≈29.0/28.6	[24]

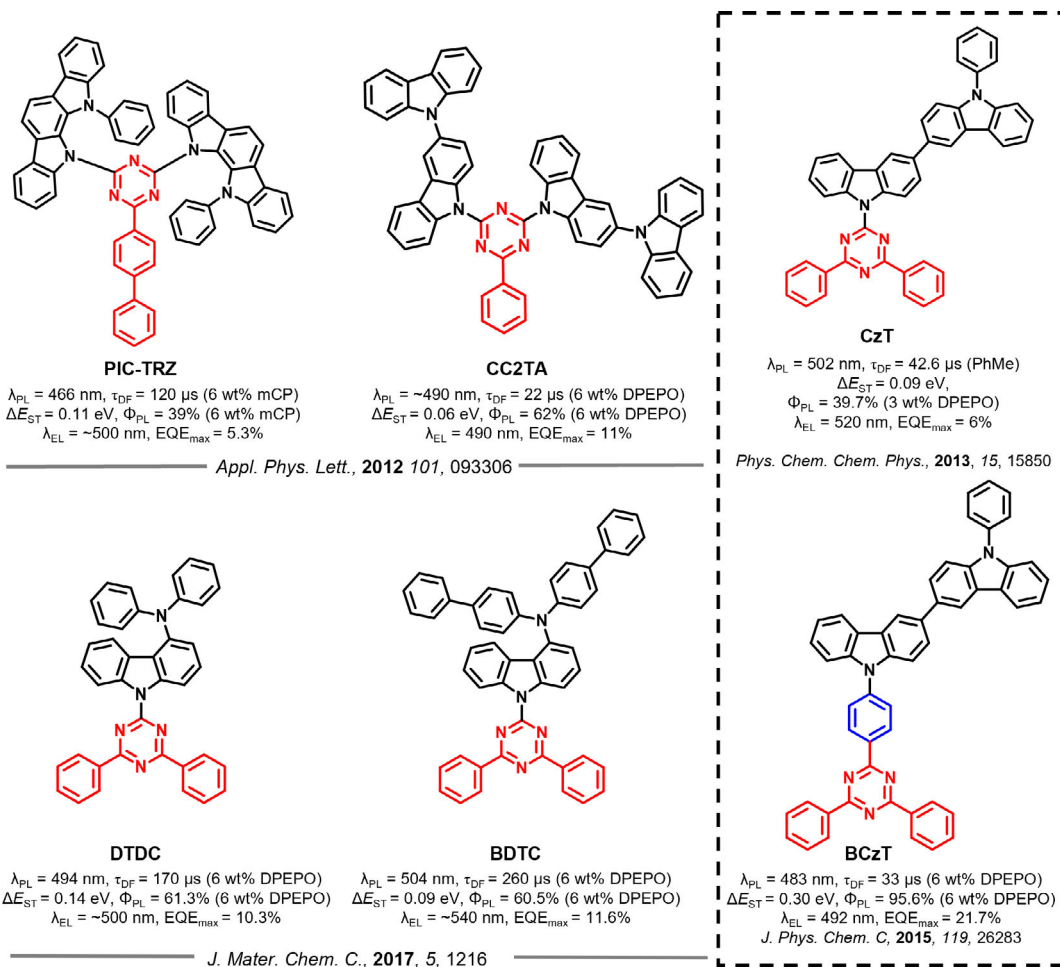


Figure 10. Comparison of TADF emitters with and without a phenylene bridge between triazine and carbazole derivatives.

In lieu of an indolocarbazole donor, compound **CC2TA**^[26] (λ_{PL} : 490 nm; τ_{d} : 22 μs ; ΔE_{ST} : 0.06 eV; Φ_{PL} : 62%; 6 wt% in DPEPO) contains a carbazole dendron-type donor structure. **CC2TA** exhibited a much improved Φ_{PL} of 62% (6 wt% in DPEPO) as well as a reduced ΔE_{ST} (0.06 eV) compared to **PIC-TRZ**, and the corresponding device showed an EQE_{max} of 11%. **DTDC** (ΔE_{ST} : 0.14; τ_{d} : 170 μs ; Φ_{PL} : 61.3%; 6 wt% in DPEPO) and **BDTC** (ΔE_{ST} : 0.09; τ_{d} : 260 μs ; Φ_{PL} : 60.5%; 6 wt% in DPEPO), each containing only one functionalized carbazole donor, were also prepared by Adachi and co-workers.^[27] These two compounds are randomly oriented in the neat films; however, the orientation of the TDMs (orientation order parameter θ : -0.18 for DTDC; -0.12 for BDTC) of these two TADF emitters is significantly more horizontally aligned when they are dispersed in the DPEPO matrix. The best OLEDs showed comparable efficiencies to that of the **CC2TA** device with EQE_{max} values of 10.3% and 11.6% for the **DTDC** and **BDTC** devices, respectively.

Adachi et al.^[28] also performed a study to elucidate the importance of the bridging phenylene by comparing **CzT** (λ_{PL} : 502 nm; ΔE_{ST} : 0.09 eV; τ_{d} : 43 μs ; Φ_{PL} : 40%; 3 wt% in DPEPO) with **BCzT** (λ_{PL} : 483 nm; ΔE_{ST} : 0.3 eV; τ_{d} : 33 μs ; Φ_{PL} : 96%; 6 wt% in DPEPO) and demonstrated that the bridging phenylene contributes to increasing the overlap density between the electronic wave functions of the ground state and the lowest excited singlet

state, leading to both a larger ΔE_{ST} and higher Φ_{PL} , yet surprisingly a blue-shifted λ_{PL} . **CzT**, first reported in 2013 by Adachi et al.,^[29] shows a small ΔE_{ST} of 0.09 eV. The reported OLED shows an EQE_{max} of only 6% due to the relatively low Φ_{PL} of 40%. The $S_1 \rightarrow S_0$ radiative decay of **BCzT** is significantly enhanced, leading to a much higher Φ_{PL} of 96% (6 wt% in DPEPO), while the emission blue-shifted by 19 nm with a higher doping concentration in DPEPO matrix. Despite **BCzT** obtaining a near unity Φ_{PL} , the observed ΔE_{ST} was dramatically raised to 0.3 eV. Despite the larger ΔE_{ST} , the delayed fluorescence lifetimes are of a similar magnitude, which can only be explained by the implication of intermediate triplet states in the RISC process of **BCzT**. The **BCzT**-based sky-blue OLED exhibits an EQE_{max} of 21.7% with λ_{EL} at 492 nm, which is significantly improved compared to the 6% EQE_{max} of the **CzT**-based OLED. The photophysical and electrochemical data of the aforementioned materials are summarized in Table 3. Representative device performance is summarized in Table 4.

4. Orientation of TADF Materials Containing TRZ and Carbazole/Carbazole Derivatives as Donors

The EQE of the OLEDs also depend on the orientation of the TDM of the emitters, which affects the light out-coupling

Table 3. Summary of photophysical and electrochemical properties.

Emitter	Solution $\lambda_{\text{PL}}/\Phi_{\text{PL}}/\tau_{\text{d}}$ (medium) [nm/%/ μs]	Solid State $\lambda_{\text{PL}}/\Phi_{\text{PL}}/\tau_{\text{d}}$ (medium) [nm/%/ μs]	ΔE_{ST} [eV]	HOMO [eV]	LUMO [eV]	Ref.
PIC-TRZ	-/35/120(PhMe)	/39/120(6 wt% in mCP)	0.11	-	-	[25]
CC2TA	435/-/(cyclohexane)	\approx 490/62/22(6 wt% in DPEPO)	0.06	-	-	[26]
CzT	512/45.6/42.6(PhMe)	502/39.7/- (3 wt% in DPEPO)	0.09	-	-	[28]
DTDC	-/-/-	494/61.3/0.17 ms(6 wt% in DPEPO)	0.14	5.80	2.60	[27]
BDTC	-/-/-	504/60.5/0.26 ms(6 wt% in DPEPO)	0.09	5.70	2.70	[27]
BCzT	460/-/(PhMe)	483/95.6/33(6 wt% in DPEPO)	\approx 0.30	-	-	[28]

Table 4. Summary of device structures and performances.

Emitter	Device Structure	$E_{\text{L,max}}$ [nm]	CIE	V_{on} [V]	$\text{EQE}/\text{PE}/\text{CE}^{\text{a}}$ [%/lm W^{-1} /cd A^{-1}]	$\text{EQE}_{100/1000}$ [cd] [m^{-2}]	Ref.
PIC-TRZ	ITO/ α -NPD/ m -CP/6 wt% PIC-TRZ: m -CP/BP4mPy/LiF/Al	\approx 500	-	-	0.053/-/-	NA	[25]
CC2TA	ITO/ α -NPD/ 6 wt% CC2TA:mCP/ 6 wt% CC2TA:DPEPO/ DPEPO/TPBi /LiF/Al	490	-	-	0.11/-/-	NA	[26]
CzT	ITO/ α -NPD/TCTA/CzSi/3 wt% CzT:DPEPO/DPEPO/TPBi/LiF/Al	520	(0.23, 0.40)	-	0.06/9.7-	NA	[28]
DTDC	glass/ITO/ a -NPD/TCTA/ m CP /6 wt% DTDC:DPEPO/DPEPO/TPBi/LiF/Al	\approx 500	-	3.8	10.3/-/-	NA	[27]
BDTC	glass/ITO/ a -NPD/TCTA/ m CP/6 wt% BDTC:DPEPO /DPEPO/TPBi/LiF/Al	\approx 540	-	4.7	11.6/-/-	NA	[27]
BCzT	ITO/ α -NPD/ m -CBP/6 wt% BCzT:DPEPO/TPBi/LiF/Al	492	-	-	21.7/-/-	NA	[28]

efficiency of the device.^[30] Wang et al.^[31] prepared two TADF emitters **IndCzpTr-1** (Φ_{PL} : 75.2%, 10 wt% in mCBP) and **IndCzpTr-2** (Φ_{PL} : 71.9%, 20 wt% in mCBP) containing an indolocarbazole-based donor (**Figure 11**). **IndCzpTr-2** possesses a slightly smaller ΔE_{ST} of 0.11 eV than the 0.13 eV for **IndCzpTr-1**. The more extended structure of **IndCzpTr-2** leads to a preferential horizontal orientation of the TDM in the neat film with an orientation order parameter, S , of -0.264 (estimated by VASE). The S value of **IndCzpTr-1** in the neat film is only -0.1 , which is far away from the theoretical value of $S = -0.5$ for a perfectly horizontal orientation of the TDM. From these measurements in neat films, the orientation factor θ was calculated as 0.70 for **IndCzpTr-1** and 0.77 for **IndCzpTr-2**, where a value of 1

indicates a perfectly horizontally aligned TDM and a value of 0.66 indicates an isotropic orientation. As a result of greater horizontal orientation of the TDM of **IndCzpTr-2**, there is a strong divergence in the efficiencies of the OLEDs. The optimized OLEDs within this study realized EQE_{max} values of 14.5% and 30.0% for **IndCzpTr-1** (λ_{EL} : 472 nm; CIE = (0.17, 0.27)) and **IndCzpTr-2** (λ_{EL} : 496 nm; CIE = (0.23, 0.50)), respectively. Even though the EQE_{max} of the device with **IndCzpTr-1** only reached 14.5%, it is still much improved compared with **PIC-TRZ**, demonstrating the link between improved performance and the presence of the phenylene bridge, as both compounds contain the same donor and diphenyltriazine acceptor.

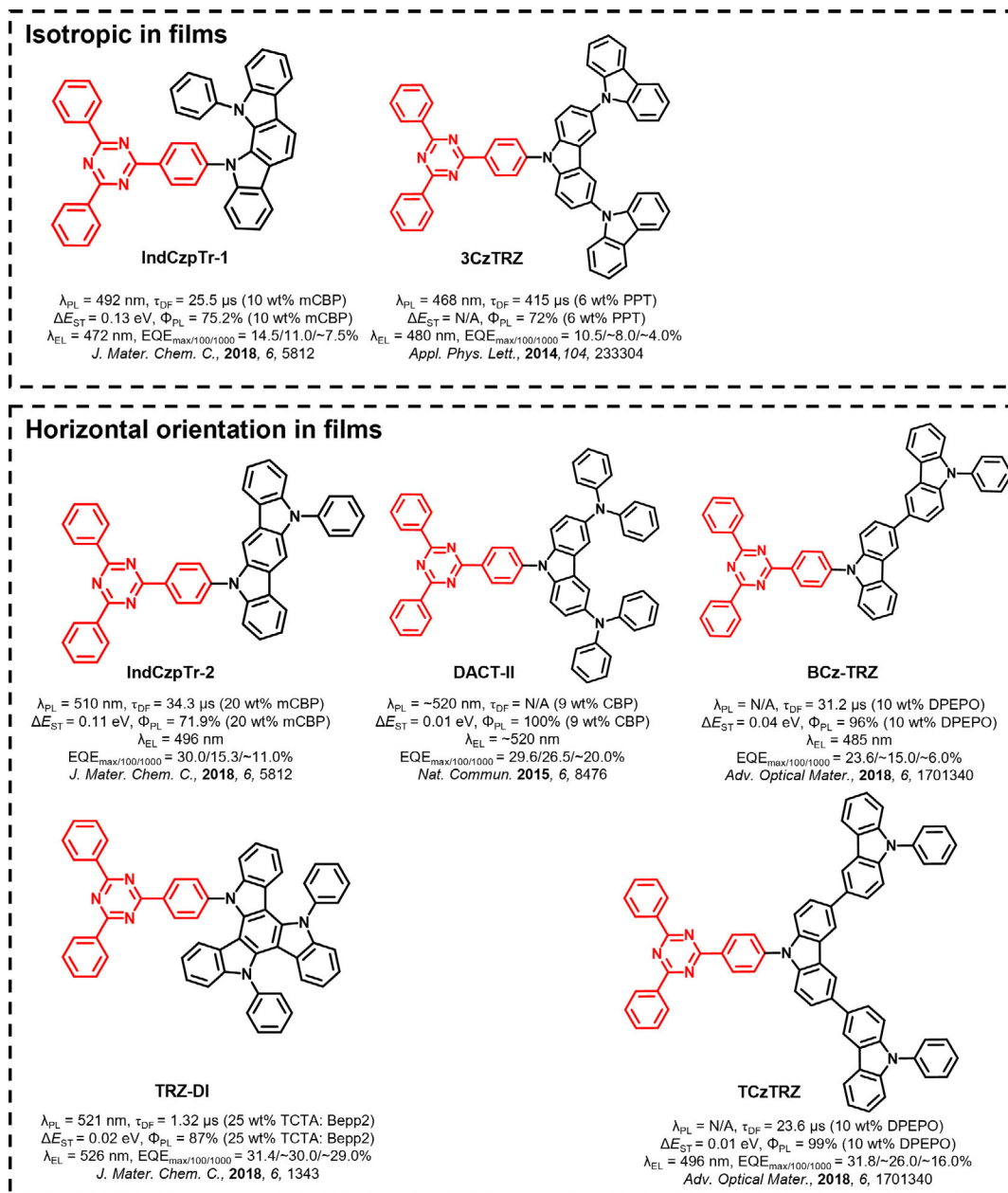


Figure 11. Molecular structures of triazine-based TADF emitters with/without preference of horizontal orientation in films.

The emitter **DACT-II** (ΔE_{ST} : 0.009 eV; Φ_{PL} : 100% as 9 wt% doped film in CBP)^[32] is a derivative of **Cz-TRZ** but contains peripheral diphenylamino groups decorating the Cz donor. Their addition significantly strengthens the donor and turns on TADF compared to **Cz-TRZ**. **DACT-II** exhibits a near zero ΔE_{ST} of 0.009 eV yet a large oscillator strength, f , reflected in the unity Φ_{PL} (9 wt% in CBP film). These desirable traits translate into a green OLED that shows an impressive EQE_{max} of 29.6% with λ_{EL} at ≈ 520 nm. The high efficiency of the device is also due to the preferential horizontal orientation of the TDM of **DACT-II** as determined by VASE measurements ($S = -0.32$) in **Figure 12a** and angular-dependent PL measurements ($S = -0.29$) in **Figure 12b**. Kim et al.^[33] later showed that efficiency roll-off can be suppressed in the OLED if the CBP host is replaced by a TCTA:B3YPMPM exciplex-forming host, as the authors found a 1.5-fold increased RISC rate in this system (k_{risc} : CBP $1.37 \times 10^5 s^{-1}$; TCTA:B3PYMPM $2.06 \times 10^5 s^{-1}$). As a result, the device gives a higher efficiency with an EQE_{max} of 34.2%, which only slightly decreased to 31% at a luminescence of $1000 cd m^{-2}$.

However, the close structural analog, **3CzTRZ**^[34] (λ_{PL} : 468 nm; τ_d : 415 μs ; ΔE_{ST} : not reported; Φ_{PL} 72%; 6 wt% in

PPT), seems to be oriented randomly in the solid state. **3CzTRZ** presents a blue-shifted emission at 468 nm and a lower Φ_{PL} of 72% as a 6 wt% doped PPT film compared with **DACT-II** (9 wt% in CBP). The OLED with **3CzTRZ** thus shows much poorer performance with an EQE_{max} of 10.5% [λ_{EL} : 480 nm; CIE = (0.17, 0.26)], which implies that there is not even a 100% IQE, assuming an outcoupling efficiency of 0.2–0.25 based on an isotropic orientation of the TDM. However, a structural analog of **3CzTRZ**, **TCzTRZ** (ΔE_{ST} : 0.01 eV; Φ_{PL} : 99%; 10 wt% in DPEPO), developed by Lee et al.,^[14] who replaced the C–N bonded tercarbazole dendron of **3CzTRZ** with a C–C bonded tercarbazole dendron, does show 95% horizontal orientation of the TDM; a similar analog, **BCzTRZ**, also shows a horizontal dipole orientation of its TDM as high as 89%, indicating the preferential in-plane alignment is formed both in tercarbazole and bicarbazole-containing compounds. Thus, subtle changes in molecular design can have profound effects on both the propensity for horizontal orientation of the TDM and the efficiency of the device. The Φ_{PL} values of the 10 wt% doped DPEPO film are 99% and 96% for **TCzTRZ** and **BCzTRZ**, respectively, both of which are significantly higher than that of **3CzTRZ** (72% in DPEPO matrix). Thanks to the near unity Φ_{PL} and near perfect horizontal

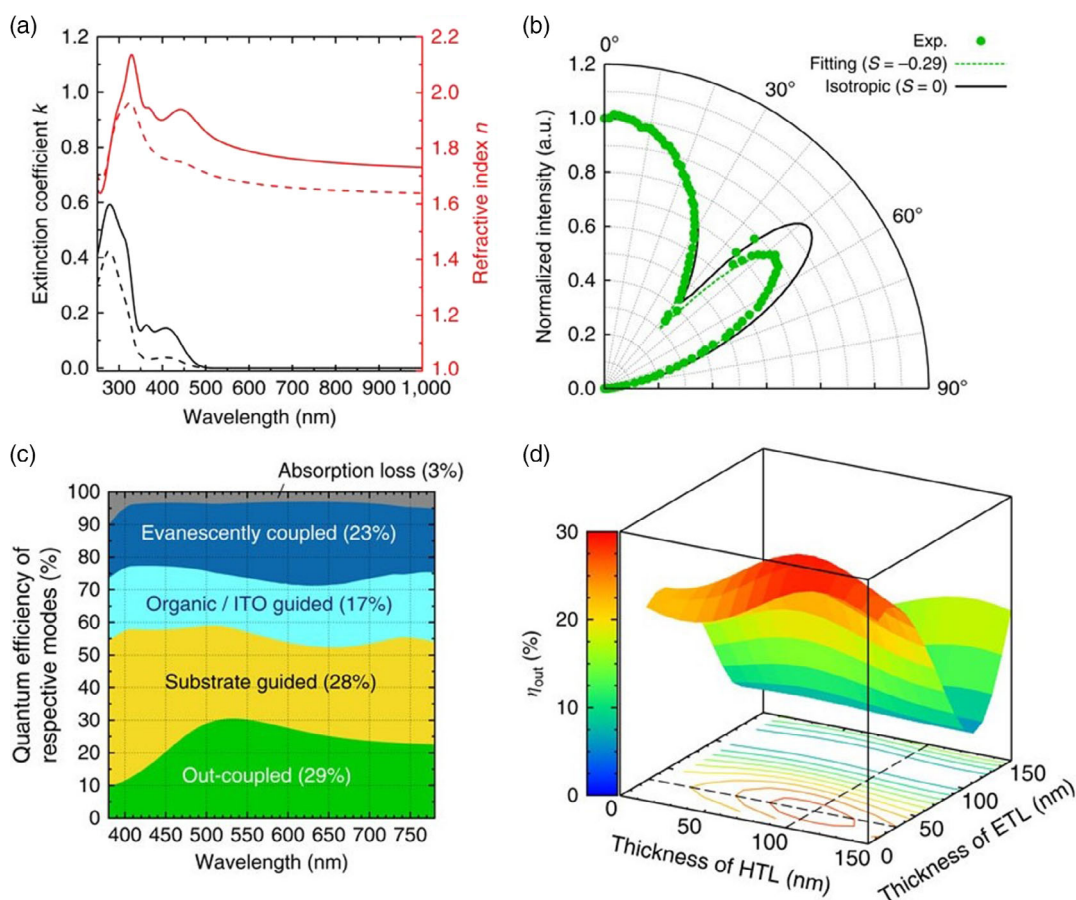


Figure 12. a) Results of VASE measurements; extinction coefficient k (black) and refractive index n (red). The solid and dashed lines represent spectra for the ordinary and extraordinary optical constants, respectively. b) Results of angular-dependent PL experiments. c) Optical simulations for the **DACT-II-9** device. The numbers in parentheses for respective modes are obtained by the integration with respect to emission wavelengths with weighting of the PL intensity. d) Dependence of the out-coupling mode on the thicknesses of hole and electron-transport layers.^[32]

orientation, the blue OLED shows an outstanding EQE_{max} of 31.8% at a λ_{EL} of 496 nm and CIE coordinates of (0.20, 0.44).

TRZ-DI (ΔE_{ST} : 0.023 eV), designed by Kwon et al.,^[35] incorporates a D_3 -symmetric triazatruxene donor. Compared with Cz in Cz-TRZ, the extended conjugation within triazatruxene effectively localizes the HOMO only on the donor group, leading to a very small ΔE_{ST} of 0.02 eV. A small dihedral angle (24.5°) between the plane of triazatruxene and the TRZ acceptor, along with the rigid molecular structure, contributes to a Φ_{PL} of 87% (25 wt% in TCTA: Bepp2 exciplex host). A green OLED using **TRZ-DI** [λ_{EL} : 526 nm; CIE = (0.31, 0.57)] as the emitter exhibits an outstanding EQE_{max} of 31.4%. The orientation of the TDM of **TRZ-DI** was not investigated, but it is not unreasonable to hypothesize that **TRZ-DI** possesses a highly horizontally oriented TDM based on the analysis of the Φ_{PL} and the EQE_{max} .

TRZ-SBA-NAI (ΔE_{ST} : 0.16 eV; Φ_{PL} : 87%; 3 wt% in mCPCN), designed by Yang et al.,^[36] contains an A-D-A' motif, where a spirobiacridine (SBA) donor is used to link the acceptors NAI and TRZ, as shown in **Figure 13**. Because of the weak electronic communication through the central sp^3 carbon on the SBA donor, two distinct CT emission bands at λ_{PL} of around 474 and 586 nm were observed in toluene, with the former assigned to **TRZ-SBA** and the later to **SBA-NAI**. By contrast, the solid-state emission 3.0 wt% doped in mCPCN matrix only showed a band at λ_{PL} of 577 nm from the **SBA-NAI** moiety, suggesting efficient energy conversion from the high-lying excited states of **TRZ-SBA** to **SBA-NAI**. The different PL character in toluene and film was ascribed to the higher intramolecular charge transfer rate via FRET to the radiative decay rate of the **TRZ-SBA** counterpart.

The TDM vector aligns with the molecular long axis, which contributes to the high horizontal dipole ratios (Θ_{\parallel}) of 88% in the mCPCN host matrix (**Figure 14**). Finally, the orange-red OLED based on **TRZ-SBA-NAI** showed an EQE_{max} of 31.7% at λ_{EL} of 593 nm and CIE coordinates of (0.55, 0.45).

A similar design using SBA as the donor and triazine as the acceptor has also been explored by Kido et al.^[37] to enable the horizontal orientation of the TDM of emitters in OLEDs. Three molecules, **tBuTZ-SBA-Ph**, **TZ-SBA-Ph**, and **tBuPhTZ-SBA-Ph**, were prepared with the difference in structure associated with the choice of distal groups on the triazine acceptor unit. The Φ_{PL} values of **tBuTZ-SBA-Ph**, **TZ-SBA-Ph**, and **tBuPhTZ-SBA-Ph** in toluene are modest at 34%, 55%, and 43%, respectively. However, the Φ_{PL} values in neat films increased to 41% for **tBuTZ-SBA-Ph**, 90% for **TZ-SBA-Ph**, and 65% for **tBuPhTZ-SBA-Ph**. By comparing with the Φ_{PL} values of the 10 wt% doped films in DPEPO matrix (87% for **tBuTZ-SBA-Ph**, 100% for **TZ-SBA-Ph**, and 97% for **tBuPhTZ-SBA-Ph**), the similarly high Φ_{PL} values for **TZ-SBA-Ph** in both neat and doped films indicate a strong suppression of intermolecular concentration quenching. The orientation ratio (Θ) in evaporated doped films was quantified to be 56%, 82%, and 82% for **tBuTZ-SBA-Ph**, **TZ-SBA-Ph**, and **tBuPhTZ-SBA-Ph**, respectively, as shown in **Figure 15**. The larger π -plane in **TZ-SBA-Ph** and **tBuPhTZ-SBA-Ph**, as asserted by the authors, would be more likely to interact with the deposition surface, thus enhancing the horizontal orientation. The OLEDs achieved EQE_{max} of 24.1%, 31.2%, and 28.3% for the devices with **tBuTZ-SBA-Ph**, **TZ-SBA-Ph**, and **tBuPhTZ-SBA-Ph**, respectively. The

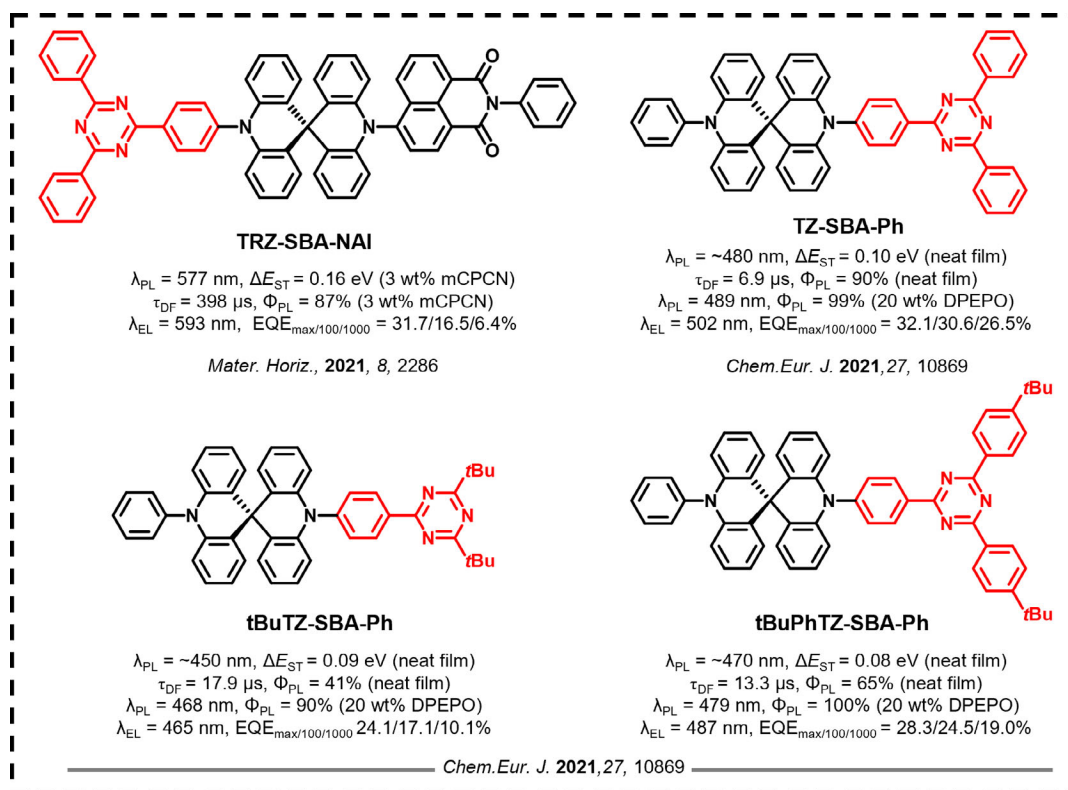


Figure 13. Molecular structures and properties of TADF emitters with preference of horizontal orientation in films.

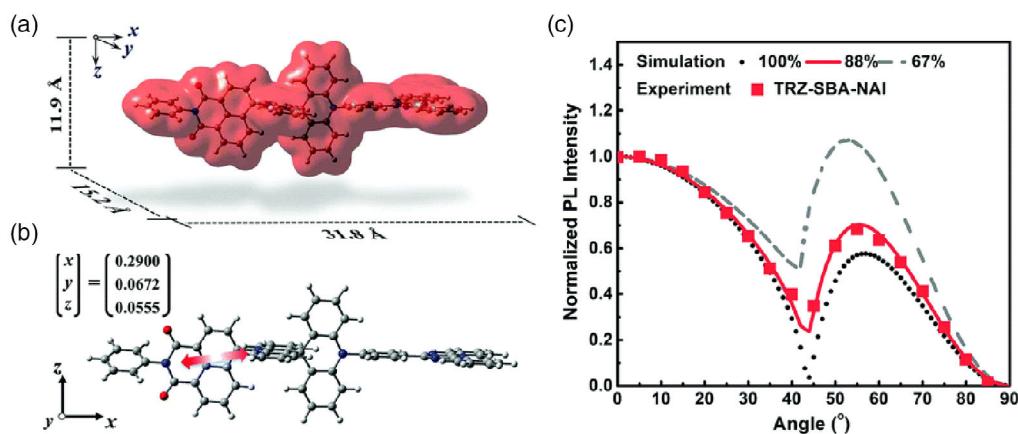


Figure 14. a) Isodensity surface of TRZ-SBA-NAI with $\rho = 0.001 \text{ e bohr}^{-3}$ and their spatial range in the Cartesian axes based on optimized S_0 structure. b) The direction of the calculated S_0-S_1 transition dipole moment (as indicated by the arrow) of TRZ-SBA-NAI based on the optimized S_1 structure. c) Measured p -polarized PL intensity (at PL peak wavelength) versus emission angle curve of 3.0 wt% TRZ-SBA-NAI doped into mPCPN host. Reproduced with permission.^[36] Copyright 2021, Royal Society of Chemistry.

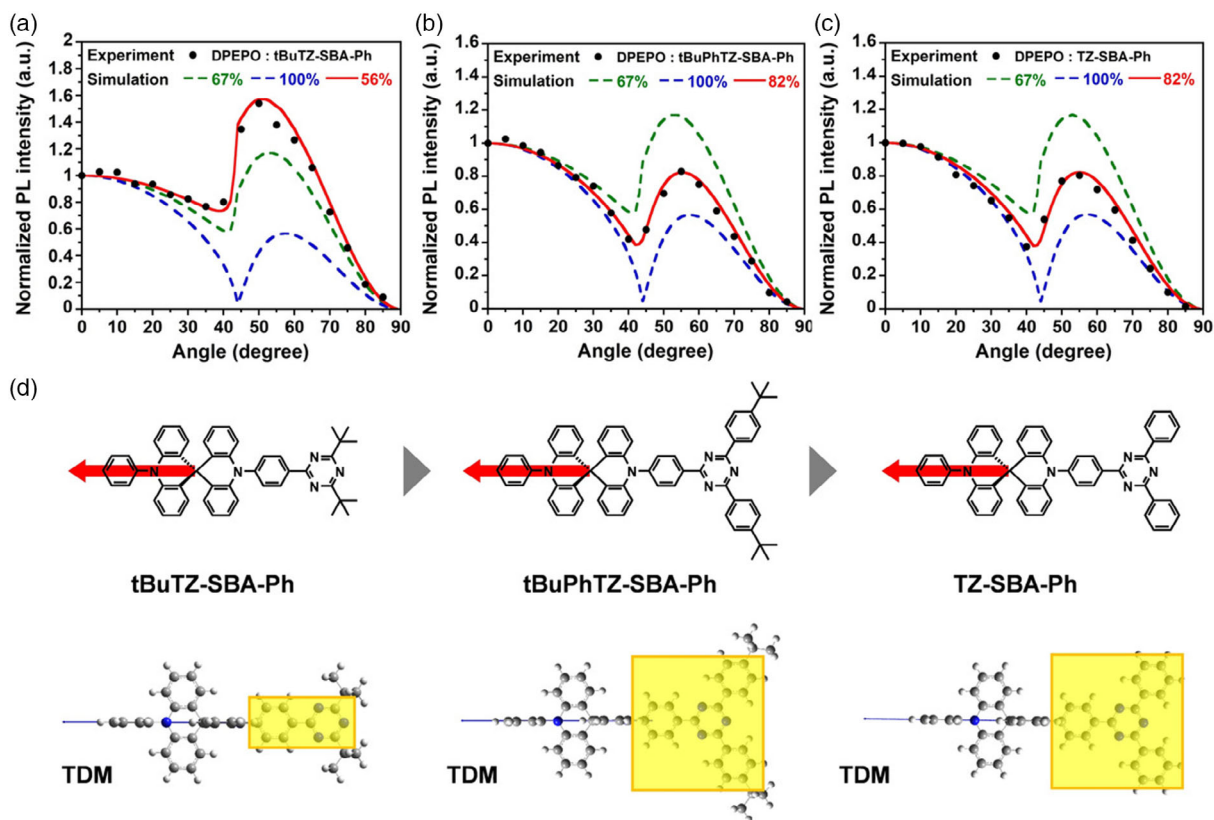


Figure 15. PL intensity of 10 wt% a) tBuTZ-SBA-Ph, b) tBuPhTZ-SBA-Ph, and c) TZ-SBA-Ph-doped host films at different angles. The experimental data are compared with the fitting curve for different horizontal dipole ratios (Θ) for X-SBA-Ph derivatives doped in a host film of DPEPO. d) The direction of the calculated S_0-S_1 transition dipole moment. Reproduced with permission.^[37] Copyright 2021, Wiley-VCH.

performance is in line with the properties in doped films in terms of Φ_{PL} and Θ values. The photophysics and electrochemical characteristics of the aforementioned materials are summarized in Table 5, and representative device performance metrics are summarized in Table 6.

5. Symmetric Substitution of Carbazole/Carbazole Dendrons on Triphenyltriazine Core

In this section, we focus on trisubstituted triazine-based dendrimer emitters. The very first TADF dendrimers, G_nTAZ

Table 5. Summary of photophysical and electrochemical properties.

Emitter	Solution $\lambda_{PL}/\Phi_{PL}/\tau_d$ (medium) [nm/%/ μ s]	Solid State $\lambda_{PL}/\Phi_{PL}/\tau_d$ (medium) [nm/%/ μ s]	ΔE_{ST} [eV]	HOMO [eV]	LUMO [eV]	Ref.
IndCzpTr-1	480//25.48(2Me-THF)	492/75.2/-(mCBP)	0.13	-5.47	-2.91	[31]
IndCzpTr-2	490//34.31(2Me-THF)	510/71.9/-(mCBP)	0.11	-5.29	-2.95	[31]
3CzTRZ	-/-/-	468/72/415(6 wt% in PPT)	-	-	-	[34]
DACT-II	-/-/-	-/96/-(TCTA:B3YPMPM (1:1):DACT-II (7 wt%))	-	-	-	[32]
DACT-II	-/63.7/-(PhMe)	\approx 520/100/-(9 wt% in CBP)	0.009	5.5	3.2	[32]
BCzTrz	-/-/-	-/96/31.2(10 wt% in DPEPO)	0.04	-5.8	-3.24	[14]
TCzTrz	-/-/-	-/99 /23.6(10 wt% in DPEPO)	0.01	-5.75	-3.41	[14]
TRZ-DI	506/-/1.61(PhMe)	521/87/1.32(25 wt% TCTA:Bepp2)	0.023	5.7	3	[35]

Table 6. Summary of device structures and performance.

Emitter	Device Structure	EL_{max} [nm]	CIE	V_{on} [V]	$EQE/PE/CE^a)$ [%/lm W ⁻¹ /cd A ⁻¹]	$EQE_{100/1000}$ [cd] [m] ⁻²	Ref.
IndCzpTr-1	ITO/MoO3/TAPC/mCP/EML/DPEPO/TmPyPB/LiF/Al	472	0.17, 0.27	3.8	14.5/23.2/28.1	11.0/ \approx 7.5	[31]
IndCzpTr-2	ITO/MoO3/TAPC/mCP/EML/DPEPO/TmPyPB/LiF/Al	496	0.23, 0.50	4	30/61.8/82.6	15.3/ \approx 11	[31]
3CzTRZ	ITO/HAT-CN/Tris-PCz /10 wt% 3CzTRZ:PPT/PPT/LiF/Al	480	(0.17, 0.26)	-	10.5/-/-	\approx 8./ \approx 4	[34]
DACT-II	ITO/TAPC/TCTA/TCTA:B3YPMPM:7 wt% DACT-II/B3YPMPM/LiF/Al	-	-	-	34.2/121.3/114	26.5/ \approx 20	[32]
DACT-II	ITO/TAPC/9 wt% DACT-II:CBP/BAlq/Liq/Al	\approx 520	-	-	29.6/-/-	NA	[32]
BCzTrz	ITO/PEDOT:PSS/TAPC/mCP/ 10 wt% BCzTrz in DPEPO/TSPO1/TBPI/LiF/Al	485	(0.23, 0.42)	-	23.6/46.6/53.3	\approx 15/ \approx 6	[14]
TCzTrz	ITO/PEDOT:PSS/TAPC/mCP/ 10 wt% TCzTrz in DPEPO/TSPO1/TBPI/LiF/Al	496	(0.20, 0.44)	-	31.8/61.5/86.4	\approx 26/ \approx 16	[14]
TRZ-DI	ITO/HATCN/NPB/TAPC/TCTA:Bepp2:25% TRZ-DI/TmPyPB/LiF/A	526	0.31, 0.57	2.6	31.4/91.6/87.5	\approx 30/29	[35]

(n refers to the generation of the dendrons) (**Figure 16**), were developed by Yamamoto et al.^[38] These compounds contain three symmetrical carbazole donor dendrons (from second generation to fourth generation; 1st generation with only Cz as the donor was not studied due to the insolubility of this compound) attached to a central TRZ acceptor. All three dendrimers showed near unity Φ_{PL} and very small ΔE_{ST} in toluene solution: **G2TAZ** (ΔE_{ST} : 0.03 eV; Φ_{PL} : 94% in toluene), **G3TAZ** (ΔE_{ST} : 0.06 eV; Φ_{PL} : 100% in toluene), and **G4TAZ** (ΔE_{ST} : 0.06 eV; Φ_{PL} : 94% in toluene). However, the Φ_{PL} decreased significantly for the neat films to 52%, 31%, and 8.5%, respectively, which was rationalized in terms of increasing concentration quenching in the neat films along the series. OLEDs with neat films of **GnTAZ** dendrimers as the emitting layer performed poorly, with the highest EQE_{max} of 3.4% at CIE coordinates of (0.27, 0.49) for the device with **G3TAZ**.

Yamamoto et al.^[39] showed how substitution about the periphery of the donor dendron in **G2TAZ** analogs can affect the Φ_{PL} . Compared to **G2TAZ**, methyl (**MeG2TAZ**) (Φ_{PL} : 40%; τ_d : 3.3 μ s; ΔE_{ST} : 0.07 eV; in neat film), *tert*-butyl (**tBuG2TAZ**) (Φ_{PL} : 45%; τ_d : 5.3 μ s; ΔE_{ST} : 0.07 eV; in neat film), phenyl (**PhG2TAZ**) (Φ_{PL} : 49%; τ_d : 1.9 μ s; ΔE_{ST} : 0.08 eV; in neat film), and 7H-dibenzo[c,g]carbazole (**dbG2TAZ**) (Φ_{PL} : 9.1%; ΔE_{ST} : 0.53 eV; in neat film) analogs all showed similar PL spectra and comparably high Φ_{PL} in toluene, with **tBuG2TAZ** showing the highest Φ_{PL} of 96%. These dendrimers suffered a similarly lower Φ_{PL} as neat films compared to toluene solutions. Apart from **dbG2TAZ**, which has the lowest Φ_{PL} in the neat film, all of the other dendrimers

have only modestly lower Φ_{PL} than **G2TAZ** (52%). However, the EQE_{max} based on the solution-processed OLEDs improved from 6.0% (**G2TAZ**) to 9.4% (**MeG2TAZ**), 9.5% (**tBuG2TAZ**), and 8.2% (**PhG2TAZ**), respectively.

Although the EQE_{max} of the OLED based on **tBuG2TAZ** improved to 9.5%, this performance is still not comparable to the efficiencies reported for nondoped vacuum-deposited devices based on small-molecule TADF emitters. This is due to the low Φ_{PL} (<50%) in the neat film that results from concentration quenching. To solve the problem and further improve the device performance, Yamamoto et al.^[40] developed two carbazole-based dendrimers (**G3Ph** and **G4Ph** as shown in **Figure 17**) as host materials to suppress the observed concentration quenching of **tBuG2TAZ** (λ_{PL} : 500 nm; Φ_{PL} : 76%; ΔE_{ST} : 0.07 eV; 15 wt% in **G3Ph**). The doping concentration of 15% was chosen to optimize the Φ_{PL} in the blended film. The emission spectra remain unchanged at 500 nm between the neat film and the films doped in **G3Ph** and **G4Ph**. However, the Φ_{PL} increased from 44% in neat film to 76% and 70% in **G3Ph** and **G4Ph** (15 wt%), respectively. The EQE_{max} of the green-emitting OLED was significantly improved to 16.1% at CIE coordinates of (0.28, 0.49).

Recently, our group^[41] has developed a series of green TADF dendrimers that contain carbazole dendron donors surrounding a TRZ core acceptor unit, linked via either a *para*/*meta*-phenylene (**tBuCz2pTRZ**/ **tBuCz2mTRZ**) or combination of both connections (**tBuCz2m2pTRZ**), as shown in **Figure 18**. The design strategy of **tBuCz2m2pTRZ** (λ_{PL} : 520 nm; Φ_{PL} : 86%; ΔE_{ST} : 0.04 eV; neat film) demonstrates that **tBuCz2m2pTRZ**

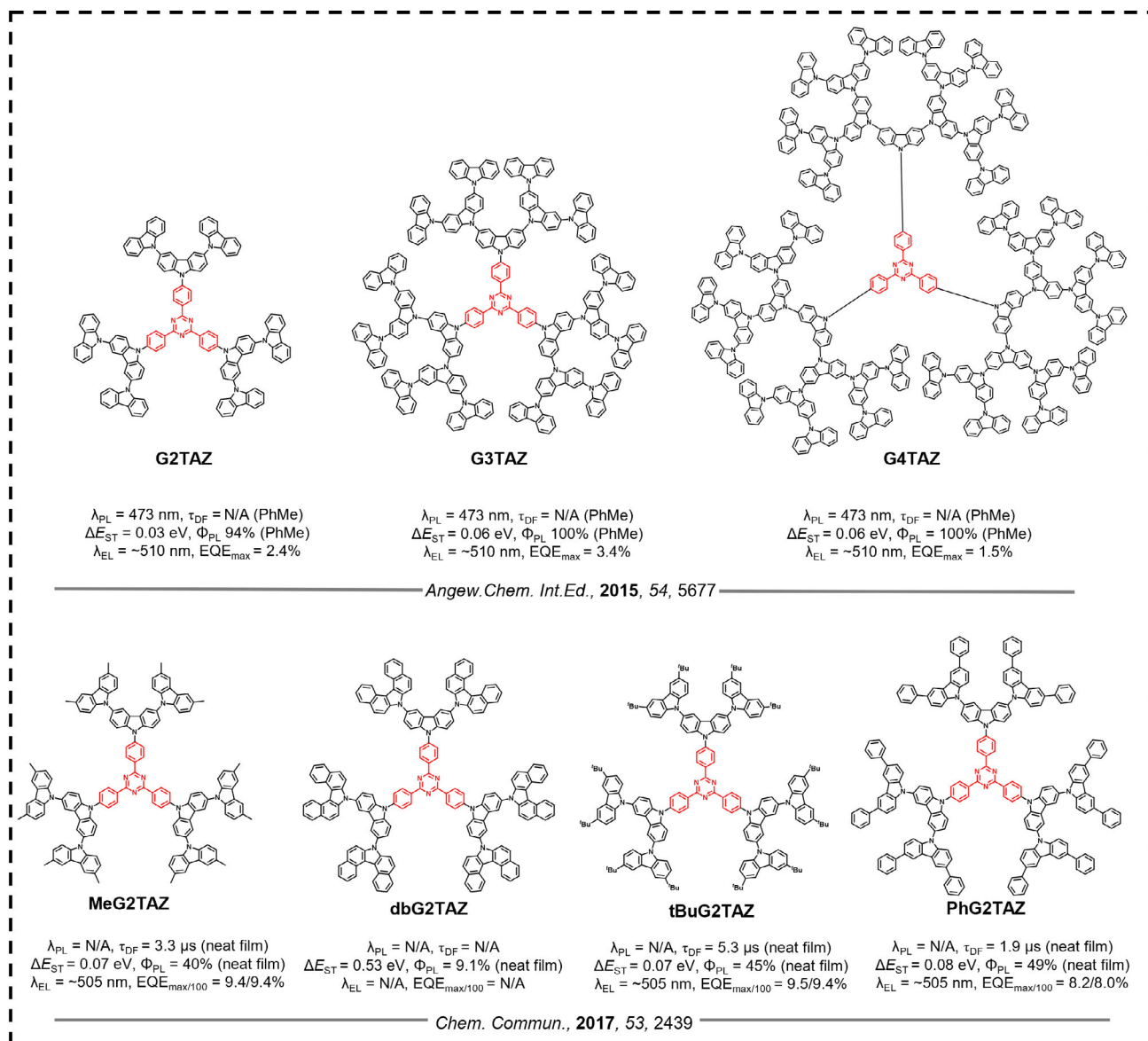


Figure 16. Molecular structures and properties of TADF dendrimer emitters with symmetric trisubstitution of carbazole dendrons.

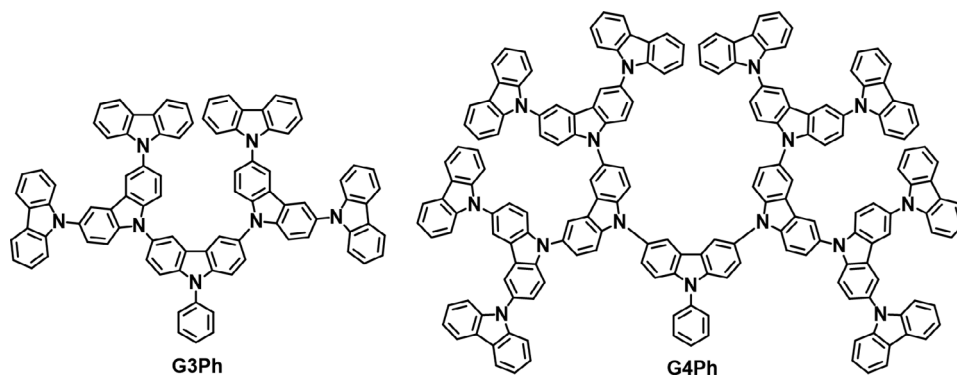


Figure 17. Molecular structures of dendrimer host materials G3Ph and G4Ph.

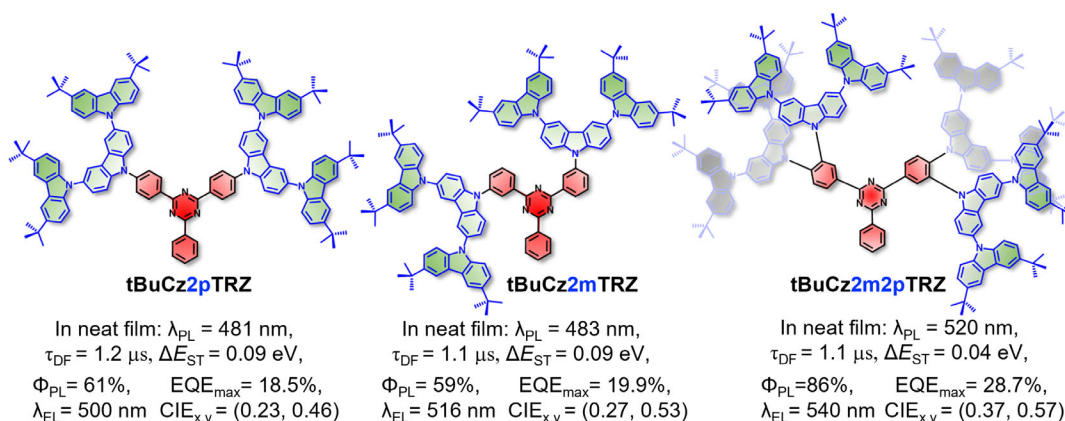


Figure 18. Molecular structures and properties of TADF dendrimer emitters with symmetric disubstitution of carbazole dendrons. Reproduced with permission.^[41] Copyright 2022, Wiley-VCH.

is capable of inheriting key properties from both **tBuCz2pTRZ** (λ_{PL} : 481 nm; Φ_{PL} : 61%; ΔE_{ST} : 0.09 eV; neat film) and **tBuCz2mTRZ** (λ_{PL} : 483 nm; Φ_{PL} : 59%; ΔE_{ST} : 0.09 eV; neat film), with the excited-state behavior being modulated as a result of the interactions between the two adjacent donor dendrons. The *para*-connection of the donor dendrons in **tBuCz2m2pTRZ** leads to strong electronic coupling between donor and acceptor, as evidenced by the strong molar absorption for the ICT transition, while the additional *meta*-connection in **tBuCz2m2pTRZ** results in a small ΔE_{ST} as the *meta*-disposed donor and acceptor groups

are electronically decoupled. The λ_{PL} of **tBuCz2pTRZ** is similar to that of **tBuCz2mTRZ**, indicating similar energies of their 1CT states regardless of the electronic coupling between donor and acceptor. The spectral red-shift of **tBuCz2m2pTRZ** indicates the stabilized 1CT states with more dendritic moieties than **tBuCz2pTRZ** and **tBuCz2mTRZ**. Nondoped solution-processed OLEDs using a simple device configuration (Figure 19) without exciton barrier layers and containing only the dendrimers in the emissive layer exhibited the EQE_{max} of 18.5%, 19.9%, and 28.7% for **tBuCz2pTRZ**, **tBuCz2mTRZ**, and **tBuCz2m2pTRZ**,

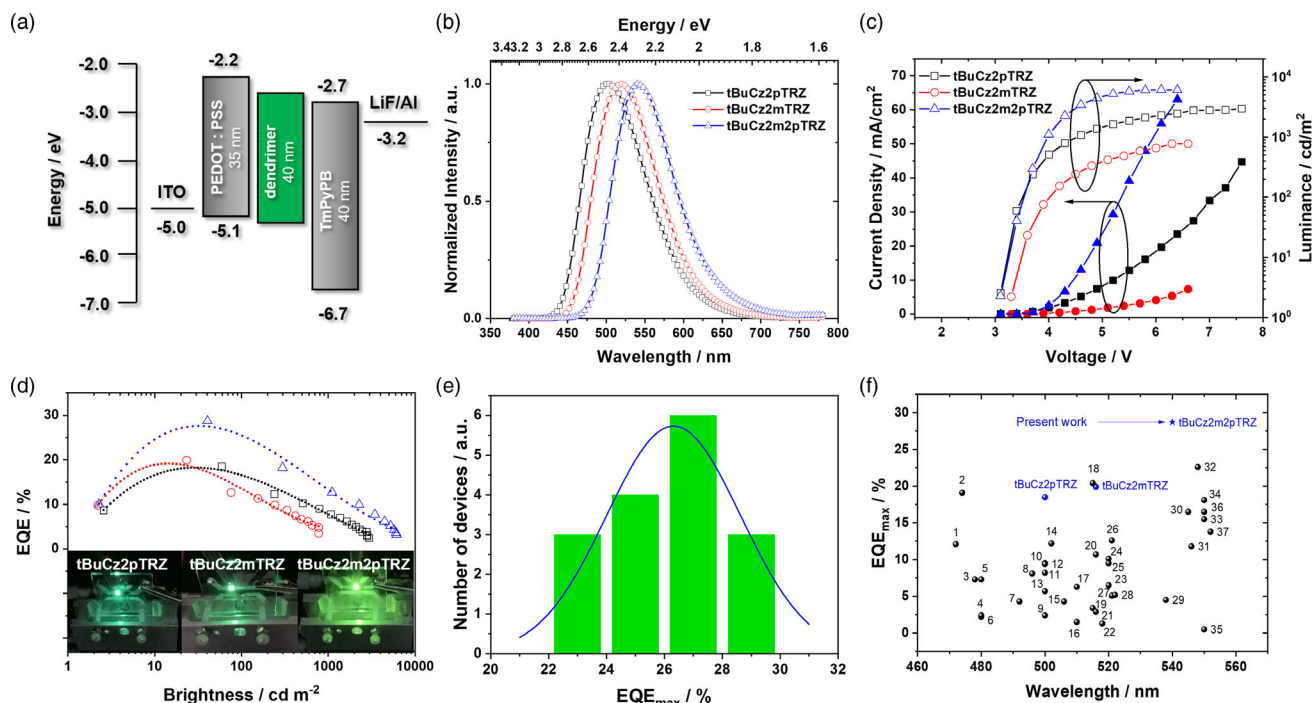


Figure 19. Electroluminescence characteristics of host-free OLEDs using **tBuCz2pTRZ**, **tBuCz2mTRZ**, and **tBuCz2m2pTRZ** as emitters. a) Device configuration. b) Normalized electroluminescence spectra. c) Current density and luminance versus driving voltage characteristics. d) EQE versus brightness for **tBuCz2pTRZ** (black), **tBuCz2mTRZ** (red), and **tBuCz2m2pTRZ** (blue) based devices. (The photos shown from bottom left to right for **tBuCz2pTRZ**, **tBuCz2mTRZ**, and **tBuCz2m2pTRZ**-based devices, respectively). e) Statistical histogram of EQE_{max} for **tBuCz2m2pTRZ**-based OLEDs. f) The EQE_{max} of all reported solution-processed host-free TADF OLEDs as a function of wavelength.

respectively. The performance of the device with **tBuCz2m2pTRZ** represents a step change in the efficiency of the nondoped solution-processed OLEDs. Importantly, the efficiency roll-off of the OLED based on **tBuCz2m2pTRZ** is significantly improved by doping 30 wt% OXD-7, an electron-transporting material, into the emissive layer. As a result of the improved charge balance, the EQE of the optimized device not only reached a similar EQE_{max} of 28.4% but also maintained its efficiency of 22.7% at a luminance of 500 cd m⁻².

A related work^[42] documents a detailed photophysical investigation to rationalize the structure–property relationship of the TADF dendrimers **tBuCz3pTRZ** and **tBuCz3mTRZ** (the DFT optimized structures without peripheral tertbutyl groups are shown in **Figure 19**). Both dendrimers exhibit high Φ_{PL} values (89% for **tBuCz3pTRZ** and 81% for **tBuCz3mTRZ**, 10 wt% doped in mCP). While **tBuCz3mTRZ** (2.92 eV) possesses a slightly higher S₁ state than that of **tBuCz3pTRZ** (2.84 eV) due to the weak electron coupling of *meta*-connection, both have a similarly small ΔE_{ST} (0.1 eV for **tBuCz3pTRZ** and 0.08 eV for **tBuCz3mTRZ**). The activation energy barriers (E_{act}) for RISC are approximately half those of the corresponding ΔE_{ST} values. However, the contribution of the delayed emission to the total emission (19% for **tBuCz3pTRZ** and 63% for **tBuCz3mTRZ**) and the k_{RISC} (0.5 × 10⁵ s⁻¹ for **tBuCz3pTRZ** and 3.7 × 10⁵ s⁻¹ for **tBuCz3mTRZ**), both reflecting the efficiency of the RISC process, are much greater/faster in the case of the *meta*-connected dendrimer **tBuCz3mTRZ**.

The comparison of the DFT calculation for the model dendrimers without *tert*-butyl groups is shown in **Figure 20**. Unlike **Cz3pTRZ**, **Cz3mTRZ** has negligible overlap between the hole and electron NTO distribution in the T₁ states. This leads to a greater CT character in the T₁ state of **Cz3mTRZ** (ω_{CT} = 0.54) as compared to **Cz3pTRZ** (ω_{CT} = 0.38). The calculated spin–orbital coupling (SOC) matrix element was found to be higher for **Cz3mTRZ** (0.53 cm⁻¹) as compared to **Cz3pTRZ** (0.31 cm⁻¹). The intramolecular (λ_{intra}) reorganization energy for **Cz3pTRZ** (275 meV) was also calculated to be higher than that of

Cz3mTRZ (155 meV). Most TADF molecule design strategies focus on the minimization the ΔE_{ST}; however, it is observed that the enhancement of the SOC for the T₁ → S₁ transition and the reduced reorganization energy also significantly contribute to the faster k_{RISC} in **tBuCz3mTRZ** compared to **tBuCz3pTRZ**, despite their similar ΔE_{ST} values. This work demonstrates the importance of the regiochemistry of the donor dendrons on the control of the SOC and reorganization energies, which is a heretofore unexploited strategy that is distinct from the involvement of intermediate triplet states through a nonadiabatic (vibronic) coupling with the lowest singlet charge transfer state.

The introduction of *tert*-butyl groups to carbazole donor dendrons in **G1TAZ** was reported by Ulanski et al.^[43] Dendrimers **TR1** and **TR2** (**Figure 21**) contain one and two *tert*-butyl groups on each carbazole unit, respectively, their inclusion was designed to improve the solubility of the dendrimers. Similar to **Cz-TRZ**, both **TR1** (λ_{PL}: 398 nm; Φ_{PL}: 83% in hexane) and **TR2** (λ_{PL}: 407 nm; Φ_{PL}: 74% in hexane) are deep blue emitters, with only very short lifetimes of a few nanoseconds, suggesting that these dendrimers do not show TADF. A subsequent study^[44] compared the *para*-substituted compound **TR2** (renamed as **TpCz**) with a newly designed *meta*-linked donor dendron dendrimer **TmCz**. The photophysical properties of **TmCz** (λ_{PL}: ≈450 nm; Φ_{PL}: 25%; τ_d: 80 μs (1 wt% in PMMA); ΔE_{ST}: 0.125 eV) and **TpCz** (λ_{PL}: ≈440 nm; Φ_{PL}: 35%; τ_d: 500 μs (1 wt% in PMMA); ΔE_{ST}: 0.249 eV) revealed that **TpCz** possesses a larger oscillator strength leading to a higher Φ_{PL}, but at the expense of a lower triplet energy, stronger charge transfer character, and larger ΔE_{ST}. A blue vacuum-deposited OLED using **TmCz** as the emitter showed an EQE_{max} of 9.5% at CIE coordinates of (0.16, 0.23) and λ_{EL} at 475 nm, demonstrating that **TmCz** emits via TADF in the device.

Another design strategy, developed by Sun et al.,^[45] for TADF dendrimers incorporates nonconjugated aliphatic chains linked to distal carbazole moieties that act as host units. Compounds **TZ-Cz** and **TZ-3Cz** (**Figure 21**) are based on a *para*-connected

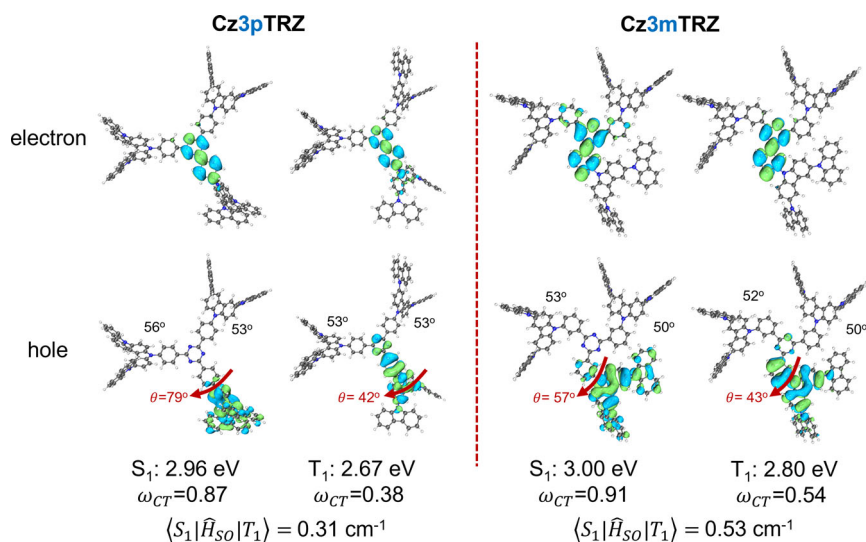


Figure 20. Natural transition orbital (NTO) pairs for the S₁ and T₁ states of **Cz3pTRZ** and **Cz3mTRZ**. The spin–orbital coupling (SOC) matrix elements are also provided.

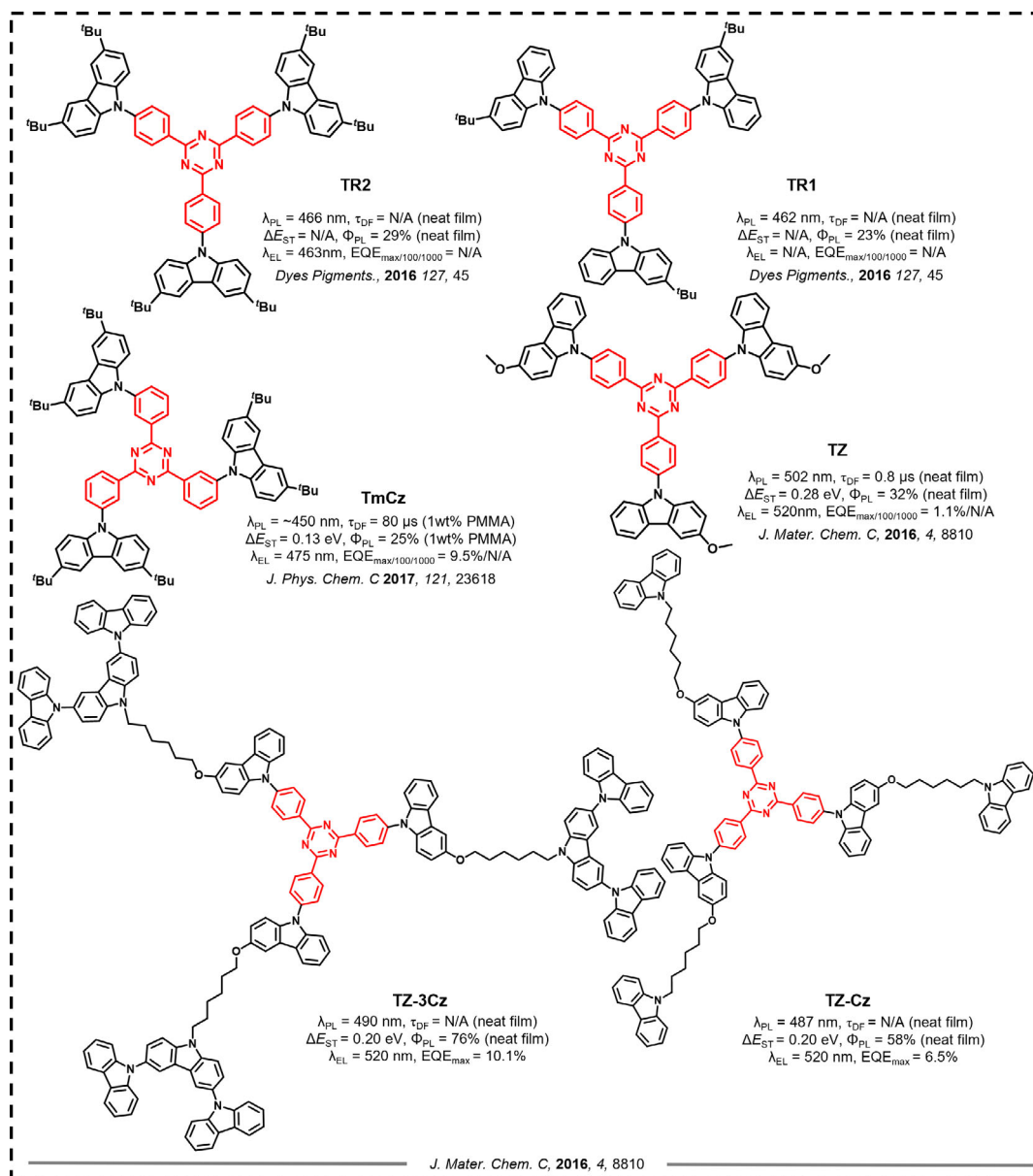


Figure 21. Molecular structures and properties of TADF emitters with trisubstitution of carbazole/carbazole derivatives.

C₃ symmetric carbazole-triazine reference compound, **Tz**. The authors contend that the emissive core is encapsulated by the nonconjugated dendrons, thus suppressing concentration quenching. Similar to **TR1** and **TR2**, **Tz** (λ_{PL} : 502 nm; Φ_{PL} : 25%; ΔE_{ST} : 0.28 eV; in neat film) is only a fluorescent emitter and does not show TADF. However, TADF turns on in **TZ-Cz** (λ_{PL} : 490 nm; Φ_{PL} : 58% in neat film; ΔE_{ST} : 0.20 eV) and **TZ-3Cz** (λ_{PL} : 487 nm; Φ_{PL} : 76% in neat film; ΔE_{ST} : 0.20 eV), which the authors assert is due to the change in local environment that results from the encapsulation. The best solution-processed OLED was achieved using **TZ-3Cz** (λ_{EL} : 520 nm; CIE = (0.24, 0.51)) in a host-free configuration and showed a much-improved EQE_{max} of 10.1% compared to the OLED based on **TZ** (1.09%). The photophysics and electrochemical characteristics of the aforementioned

materials are summarized in **Table 7**, and representative device performance metrics are summarized in **Table 8**.

6. TADF Emitters Containing Two TRZ and Carbazole/Carbazole Derivative Donors

There are a small number of examples of emitters containing two triazine acceptors. Many of these examples are based on a dimerization strategy. As shown in **Figure 22**, Lee et al.^[46] reported two related green TADF emitters **mCBPTRZ-1** (λ_{PL} : 472 nm; Φ_{PL} : 95%; τ_d : 5.65 μs ; ΔE_{ST} : 0.20 eV; 10 wt% in DPEPO) and **mCBPTRZ-2** (λ_{PL} : 482 nm; Φ_{PL} : 74%; τ_d : 3.21 μs ; ΔE_{ST} : 0.19 eV; 10 wt% in DPEPO), which are dimers of the TADF

Table 7. Summary of photophysical and electrochemical properties.

Emitter	Solution $\lambda_{PL}/\Phi_{PL}/\tau_d$ (medium) [nm/%/ μ s]	Solid State $\lambda_{PL}/\Phi_{PL}/\tau_d$ (medium) [nm/%/ μ s]	ΔE_{ST} [eV]	HOMO [eV]	LUMO [eV]	Ref.
G2TAZ	473/94/(PhMe)	–/52/(in neat film)	0.03	–5.76	–3.01	[38]
G3TAZ	473/100/(PhMe)	–/31/(in neat film)	0.06	–5.72	–2.97	[38]
G4TAZ	473/94/(PhMe)	–/8.5/(in neat film)	0.06	–5.68	–2.80	[38]
MeG2TAZ	–/92/(PhMe)	–/40/3.3 (in neat film)	0.07	–5.73	–2.85	[39]
tBuG2TAZ	–/96/(PhMe)	–/45/5.3 (in neat film)	0.07	–5.79	–2.88	[39]
PhG2TAZ	–/95/(PhMe)	–/49/1.9 (in neat film)	0.08	–5.79	–2.90	[39]
dbG2TAZ	–/86/(PhMe)	–/9.1/(in neat film)	0.53	–5.76	–2.99	[39]
TR1	398/83/(hexane)	462/23/(neat film)	–	5.49	2.86	[43]
TR2	407/74/(hexane)	466/29/(neat film)	–	5.70	2.83	[43]
TmCZ	≈475/–/(PhMe)	≈450/25/80 (in PMMA)	0.13	–5.65	–2.78	[44]
Tz	535/–/(DCM)	502/32/(neat)	0.28	–5.11	–2.22	[45]
TZ–Cz	535/–/(DCM)	490/58/(neat film)	0.20	–5.20	–2.31	[45]
TZ–3Cz	535/–/(DCM)	487/76/(neat film)	0.20	–5.00	2.11	[45]

Table 8. Summary of device structures and performance.

Emitter	Device Structure	$E_{L,max}$ [nm]	CIE	V_{on} [V]	$EQE/PE/CE^a$ [%/lm $W^{-1}/cd A^{-1}$]	$EQE_{100/1000}$ [cd] $[m]^{-2}$	Ref.
G2TAZ	ITO/PEDOT:PSS/G2TAZ/TPBI/Ca/Al	–	(0.252, 0.493)	3.3	2.4/–/–	N/A	[38]
G3TAZ	ITO/PEDOT:PSS/G3TAZ/TPBI/Ca/Al	–	(0.266, 0.485)	3.5	3.4/–/–	N/A	[38]
G4TAZ	ITO/PEDOT:PSS/G4TAZ/TPBI/Ca/Al	–	(0.232, 0.368)	3.5	1.5/–/–	N/A	[38]
G2TAZ	ITO/PEDOT–PSS/PVK/G2TAZ/TPBi/Ca/Al	–	–	3.7	6.2/–/–	N/A	[39]
MeG2TAZ	ITO/PEDOT–PSS/PVK/MeG2TAZ/TPBi/Ca/Al	–	–	3.0	9.4/–/–	9.4/NA	[39]
tBuG2TAZ	ITO/PEDOT–PSS/PVK/tBuG2TAZ/TPBi/Ca/Al	–	–	3.5	9.5/–/–	9.4/N/A	[39]
PhG2TAZ	ITO/PEDOT–PSS/PVK/PhG2TAZ/TPBi/Ca/Al	–	–	3.2	8.2/–/–	8.0/N/A	[39]
tBuG2TAZ	A:ITO/PEDOTPSS/15 wt% tBuG2TAZ in Gn3Ph/SPPO13/LiF/Al;	503	(0.28, 0.48)	2.9	16.1/19.3/22.7		[40]
tBuG2TAZ	A:ITO/PEDOTPSS/15 wt% tBuG2TAZ in Gn4Ph/SPPO13/LiF/Al	508	(0.29, 0.51)	2.9	10.5/27.3/28.6		[40]
TR1	ITO/PEDOT:PSS/PVK:PBD (40 wt%):TR2 (3 wt%)/LiF/A	463	(0.15, 0.13)	8	–/–/0.51	N/A	[43]
TR2	ITO/PEDOT:PSS/PVK:PBD (40 wt%):TR3 (3 wt%)/LiF/A	515	(0.21, 0.33)	9.5	–/–/0.46	N/A	[43]
TmCZ	ITO/ <i>m</i> –MTDATA/NPB/mCP/5 wt%– TmCZ:DPEPO/TPBi/LiF/Al	475	(0.16, 0.23)	5.0≈6.0	9.5/–/–	N/A	[44]
TZ	ITO/PEDOT:PSS/TZ–Cz/TPBI/Cs ₂ CO ₃ /Al	520	(0.32, 0.51)	4.7	1.09/–/3.4	N/A	[45]
TZ–Cz	ITO/PEDOT:PSS/TZ–Cz/TPBI/Cs ₂ CO ₃ /Al	520	(0.24, 0.51)	4	6.5/–/20	N/A	[45]
TZ–3Cz	ITO/PEDOT:PSS/TZ–3Cz/TPBI/Cs ₂ CO ₃ /Al	520	(0.24, 0.51)	3.6	10.1/–/30.5	N/A	[45]

emitter ***o*-CzTRZ** (λ_{PL} 455 nm; Φ_{PL} : 16.7%; τ_d : 3.90 μ s; ΔE_{ST} : 0.10 eV; 5 wt% in mCP). The Φ_{PL} of these two compounds are significantly enhanced compared to that of the parent emitter ***o*-CzTRZ** (16.7%). Dimerization is expected to enhance the overlap between frontier molecular orbitals (FMOs), which leads to an increase of the oscillator strength, thus resulting in higher Φ_{PL} , but at the expense of a red-shifted emission along with a larger ΔE_{ST} . The OLED using **mCBPTRZ-1** (λ_{EL} : 503 nm; CIE = (0.23, 0.52) emits in the green with an EQE_{max} of 20.8%, while the device using **mCBPTRZ-2** (λ_{EL} : 521 nm; CIE = (0.31, 0.59)) that contains the more electron-rich 3,6-di-*tert*-butylcarbazole shows a red-shifted emission and a

significantly lower EQE_{max} of 9.3% despite of the high Φ_{PL} of the emitter. The low device efficiency was rationalized by the authors as due to the weak exciton conversion efficiency of 41% in the **mCBPTRZ-2**-based device compared to 90% in the **mCBPTRZ-1**-based device. However, this explanation does not seem plausible given their similar molecular structures and photophysics.

Lee et al.^[47] also reported two triazine analog emitters to **2CzTPN** and **2CzIPN**, **p2Cz2TRZ** and **m2Cz2TRZ** (Figure 22), which contain *ortho*-disposed carbazole units to the bis(diphenyl-triazine) moiety. According to the computed FMOs in Figure 23, the HOMOs of **p2Cz2TRZ** and **m2Cz2TRZ** are evenly distributed over two carbazole donors whereas the LUMOs are evenly

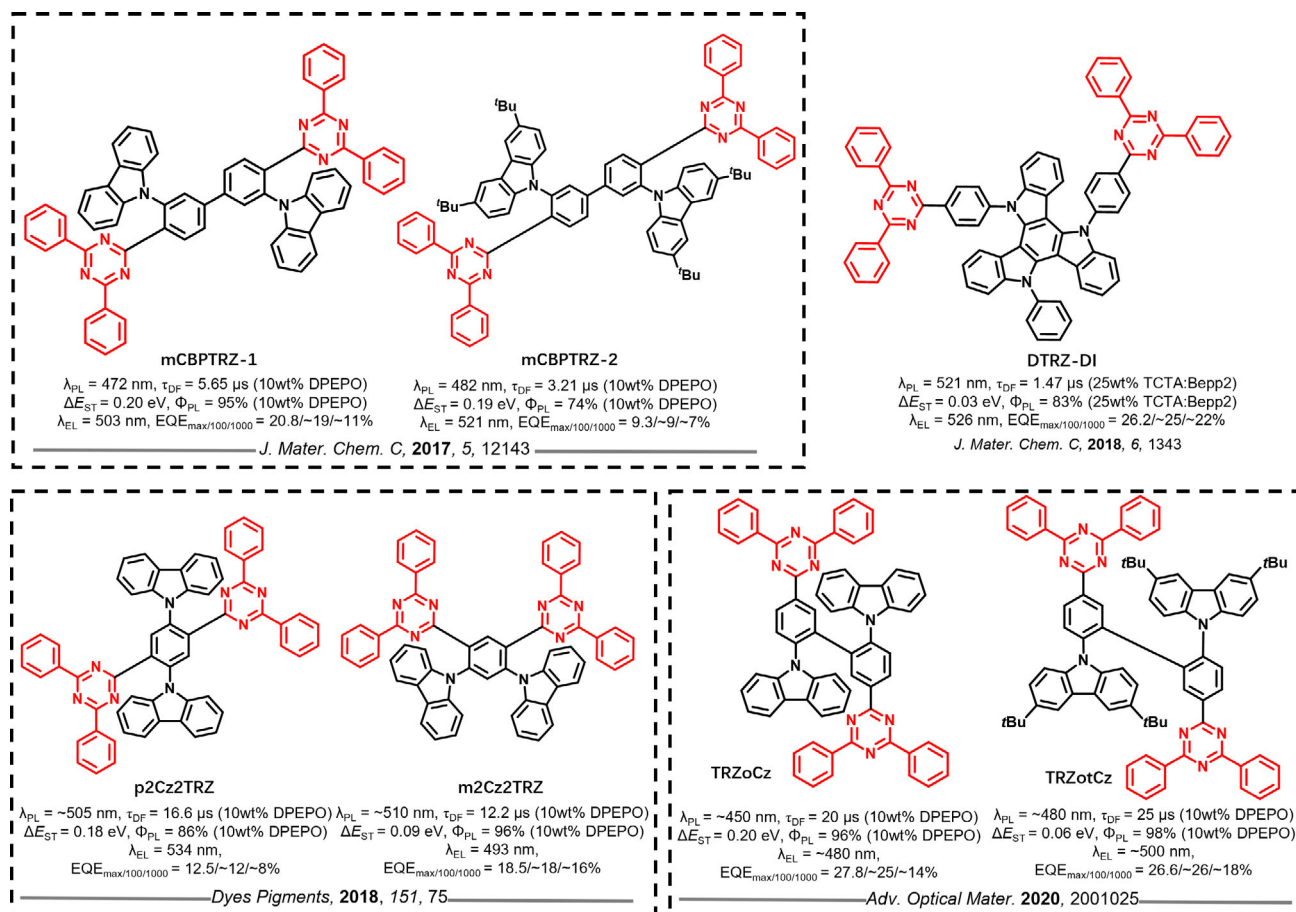


Figure 22. Molecular structures and properties of TADF emitters based on two diphenyltriazine TRZ and carbazole/carbazole derivative donors.

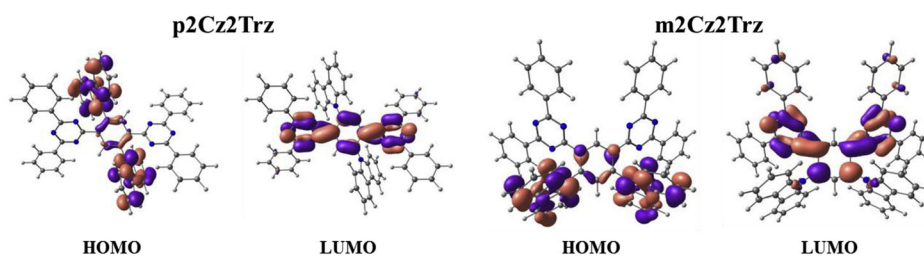


Figure 23. Calculated HOMO and LUMO distributions of the p2Cz2TRZ and m2Cz2TRZ. Reproduced with permission.^[47] Copyright 2017, Elsevier.

distributed over the two TRZ acceptors. A strong overlap between the HOMO and LUMO at the central phenyl moiety contributes to the high Φ_{PL} . Compounds **p2Cz2TRZ** ($\lambda_{PL} \approx 505 \text{ nm}$; Φ_{PL} : 86%; τ_d : 16.6 μs ; ΔE_{ST} : 0.18 eV; 10 wt% in DPEPO) and **m2Cz2TRZ** ($\lambda_{PL} \approx 510 \text{ nm}$; Φ_{PL} : 96%; τ_d : 12.2 μs ; ΔE_{ST} : 0.09 eV; 10 wt% in DPEPO) each showed green delayed fluorescence, with **m2Cz2TRZ** having a higher Φ_{PL} and a smaller ΔE_{ST} than **p2Cz2TRZ**. The OLED with **m2Cz2TRZ** showed a correspondingly higher EQE_{max} of 18.5% coupled with a bluer emission [λ_{EL} : 493 nm; CIE = (0.20, 0.47)] compared with the device using **p2Cz2TRZ**, which showed an EQE_{max} of 12.5% [λ_{EL} : 534 nm; CIE = (0.39, 0.58)].

Kwon et al.^[35] used a diindolocarbazole as a central donor core to connect two diphenyltriazine moieties (Figure 22). Like the diindolocarbazole analog **TRZ-DI** (λ_{PL} : 521 nm; Φ_{PL} : 87%; τ_d : 1.32 μs ; ΔE_{ST} : 0.02 eV; 25 wt% in TCTA:Bepp2) shown in Figure 9, **DTRZ-DI** (λ_{PL} : 521 nm; Φ_{PL} : 83%; τ_d : 1.47 μs ; ΔE_{ST} : 0.03 eV; 25 wt% in TCTA:Bepp2) showed the same green emission and similar photophysical properties. The introduction of a second TRZ acceptor did not improve the Φ_{PL} as other studies^[46,48] had documented. The performance of the OLED based on **DTRZ-DI** is poorer with an EQE_{max} of 26.2% [λ_{EL} : 526 nm; CIE = (0.32, 0.58)] in contrast to that for the **TRZ-DI** device where the EQE_{max} is 31.4%.

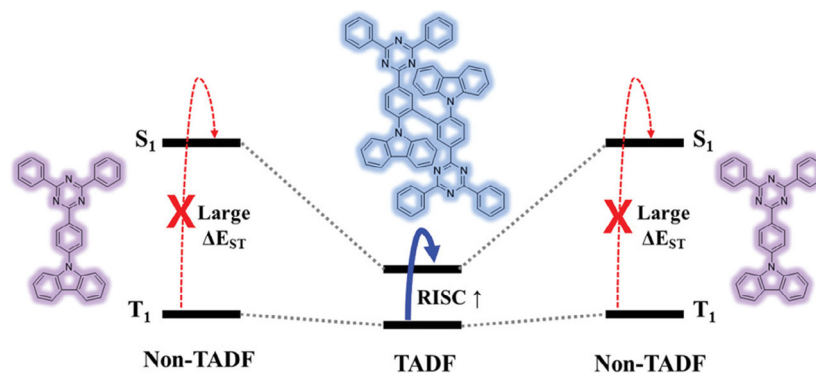


Figure 24. Design strategy for the TADF molecule TRZoCz. Reproduced with permission.^[48] Copyright 2020, Wiley-VCH.

The dimerization strategy (Figure 24) could also be used to convert a non-TADF emitter into a TADF emitter, as Lee et al.^[48] demonstrated by transforming the fluorescent emitter Cz-TRZ into a TADF emitters (TRZoCz and TRZotCz) by increasing the separation of the FMOs in the dimer structures. The highly twisted geometries in TRZoCz and TRZotCz lead to markedly smaller ΔE_{ST} (0.20 eV for TRZoCz, 0.06 eV for TRZotCz) compared to Cz-TRZ (0.36 eV). The Φ_{PL} of TRZoCz and TRZotCz are 96% and 98%, respectively, for the 10 wt% films in DPEPO. The PL spectra are red-shifted compared to that of Cz-TRZ due to the increased conjugation within their structures, the photophysics of the two compounds are also less sensitive to the doping concentration. The EQE_{max} of the TRZoCz and TRZotCz-based OLEDs are 27.8% and 26.6%, respectively, at CIE coordinates of (0.15, 0.32) and (0.20, 0.51), respectively. It is noteworthy that the emission profiles of these two emitters are not as broad than mostly common TADF emitters (FWHM = 90–110 nm), with FWHM for TRZoCz (67 nm) and TRZotCz (74 nm). This is due to the restricted conformational motion available in these compounds. The photophysics and electrochemical characteristics of the aforementioned materials are summarized in Table 9. The representative device performance is summarized in Table 10.

7. Modification to the Phenylene Bridge

The degree of orbital overlap between the HOMO and LUMO is controlled not only by the choice of donor and acceptor but also

by the bridging unit that mediates the conjugation between the two. For example, the introduction of a methyl group or phenyl group onto the phenylene bridge affects one of the torsion angles, leading to a more twisted conformation and thus a smaller ΔE_{ST} , while the inclusion of more strongly electron-withdrawing groups such as nitrile or trifluoromethyl substituents also contributes to strengthening the electron-acceptor and localizing the electron density of the LUMO.

Buchwald et al.^[49] reported a series of TADF emitters (Figure 25) that incorporate a triptycene-fused carbazole donor *para*-linked to a diphenyltriazine acceptor via a arylene bridge. The dihedral angle between donor and the bridging arylene was manipulated by controlling the position and number of methyl substituents. Compared with TCZTRZ (λ_{PL} : 457 nm; Φ_{PL} : 40%; τ_d : 38 μ s; ΔE_{ST} : 0.27 eV; 15 wt% in DPEPO), the introduction of a methyl group on the arylene bridge at a position adjacent to TRZ in TCZTRZ(Me) (λ_{PL} : 444 nm; Φ_{PL} : 51%; τ_d : 58 μ s; ΔE_{ST} : 0.12 eV; 15 wt% in DPEPO) results in a higher Φ_{PL} along with a reduced ΔE_{ST} due to the increased angle (25.1°) between the arylene plane and the TRZ plane despite the identical angle (51.5°) between the plane of triptycene-fused carbazole and the arylene plane. Placement of the methyl group close to the donor elicits a similar outcome. Emitter TCZTRZ(Me) (λ_{PL} : 451 nm; Φ_{PL} : 32%; τ_d : 51 μ s; 15 wt% in DPEPO; ΔE_{ST} : 0.16 eV) also possesses a twisted structure with the torsion angle increased from 51.5° in TCZTRZ to 69.5° in TCZTRZ(Me). The ΔE_{ST} of TCZTRZ(Me) is smaller as well at 0.16 eV; however, at a cost of a lower Φ_{PL} of 32%. The addition of a second methyl group on the arylene bridge in

Table 9. Summary of photophysical and electrochemical properties.

Emitter	Solution $\lambda_{PL}/\Phi_{PL}/\tau_d$ (medium) [nm/%/ μ s]	Solid State $\lambda_{PL}/\Phi_{PL}/\tau_d$ (medium) [nm/%/ μ s]	ΔE_{ST} [eV]	HOMO [eV]	LUMO [eV]	Ref.
mCBPTrz-1	-/-/(THF)	472/95/5.65 (10 wt% in DPEPO)	0.20	-6.11	-3.32	[46]
mCBPTrz-2	-/-/(THF)	482/74/3.21 (10 wt% in DPEPO)	0.19	-6.01	-3.22	[46]
p2Cz2Trz	-/-/--	\approx 505/86.3/16.6 (10 wt% in DPEPO)	0.18	-5.96	-4.16	[47]
m2Cz2Trz	-/-/--	\approx 510/95.6/12.2 (10 wt% in DPEPO)	0.09	-5.92	-3.33	[47]
DTRZ-Di	506/-/2.48 (PhMe)	521/83/1.47 (25 wt% in TCTA:Bepp2)	0.03	-5.68	-2.98	[35]
TRZoCz	\approx 450/-/(PhMe)	-/96/20 (10% in DPEPO)	0.20	-6.03	-3.30	[48]
TRZotCz	\approx 480/-/(PhMe)	-/98/25 (10% in DPEPO)	0.06	-5.9	-3.17	[48]

Table 10. Summary of device structures and performance.

Emitter	Device Structure	EL _{max} [nm]	CIE	V _{on} [V]	EQE/PE/CE ^{a)} [%/lm W ⁻¹ /cd A ⁻¹]	EQE _{100/1000} [cd] [m] ⁻²	Ref.
mCBPTrz-1	ITO/PEDOT:PSS/TAPC/mCP/DPEPO: mCBPTrz-1/TSPO1/TPBi/LiF/Al	503	(0.23, 0.52)	–	20.8/–/–	≈19.0/≈11.0	[46]
mCBPTrz-2	ITO/PEDOT:PSS/TAPC/mCP/DPEPO: mCBPTrz-2/TSPO1/TPBi/LiF/Al	521	(0.31, 0.59)	–	9.3/–/–	≈9.0/≈7.0	[46]
p2Cz2Trz	ITO/PEDOT:PSS/TAPC/mCP/DPEPO:30% p2Cz2Trz/TSPO1/TPBi/LiF/Al	534	(0.39, 0.58)	–	12.5/–/–	≈12.0/≈8.0	[47]
m2Cz2Trz	ITO/PEDOT:PSS/TAPC/mCP/DPEPO:30% m2Cz2Trz/TSPO1/TPBi/LiF/Al	493	(0.20, 0.47)	–	18.5/–/–	≈18.0/≈16.0	[47]
DTRZ-Di	ITO/HATCN/NPB/TAPC/TCTA:Bepp2:25% TADF emitter/TmPyPB/LiF/A	526	(0.32, 0.58)	–	26.2/80.2/73.9	≈25.0/≈22.0	[35]
TRzCz	ITO/(PEDOT:PSS)/(TAPC/mCP/DPEPO: 20% emitter/TSPO1/TPBi/LiF/A	478–484	(0.15, 0.32)	–	27.8/–/–	≈25.0/≈14.0	[48]
TRzotCz	ITO/PEDOT:PSS/TAPC/mCP/DPEPO:20% emitter/TSPO1/TPBi/LiF/A	497–501	(0.20, 0.51),	–	26.6/–/–	≈26.0/≈18.0	[48]

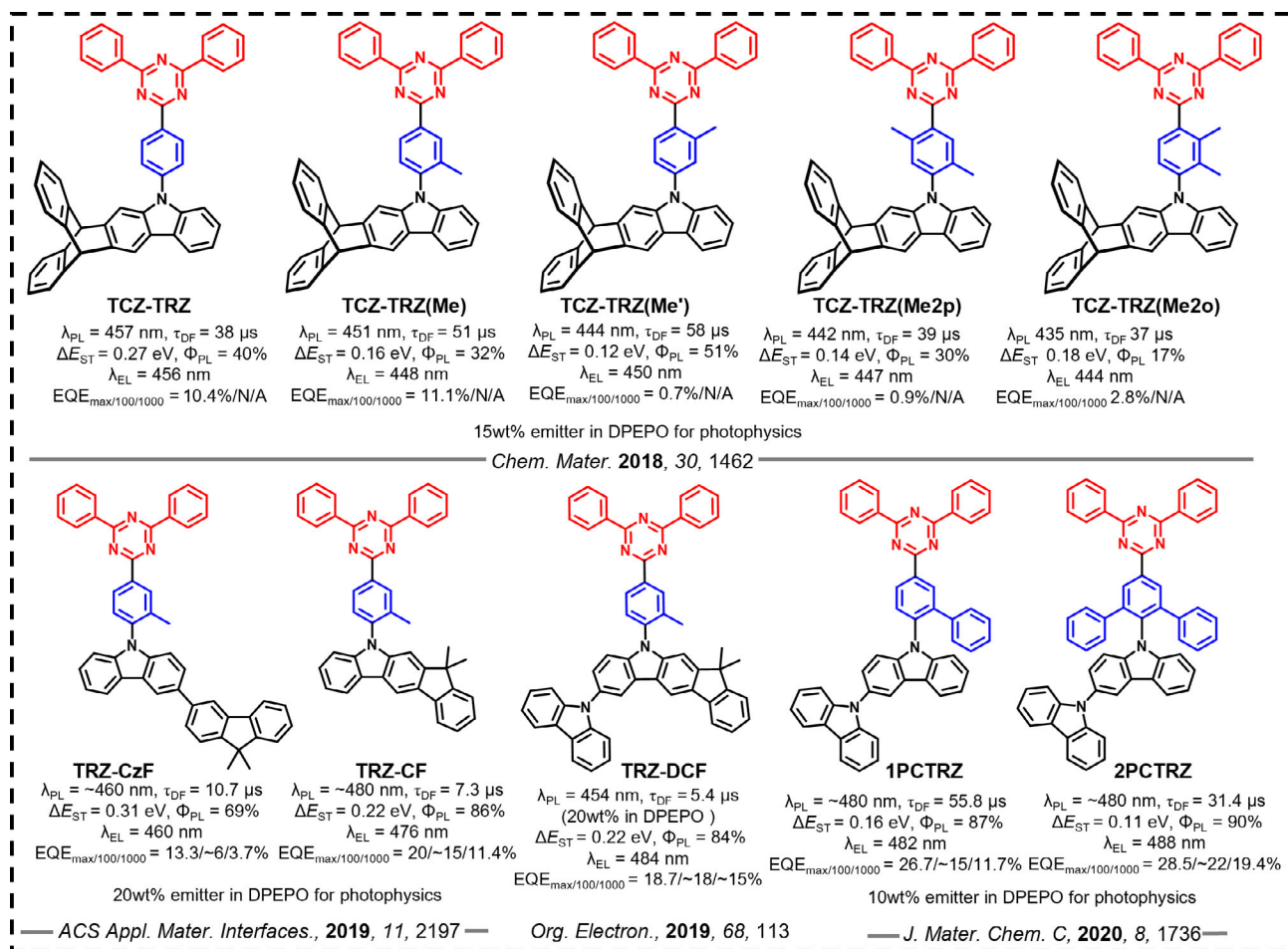


Figure 25. Molecular structures and properties of TRZ based TADF emitters with modification to the phenylene bridge.

TCZTRZ(Me2p) (λ_{PL} : 442 nm; Φ_{PL} : 30%; τ_d : 39 μs (15 wt% in DPEPO); ΔE_{ST} : 0.14 eV) and **TCZTRZ(Me2o)** (λ_{PL} : 435 nm; Φ_{PL} : 17%; τ_d : 37 μs (15 wt% in DPEPO); ΔE_{ST} : 0.18 eV) results

in compounds showing a blue-shifted emission, shorter τ_d and lower Φ_{PL} than **TCZTRZ(Me)**. The OLEDs employing **TCZTRZ** [λ_{EL} : 456 nm; CIE = (0.16, 0.14)] and **TCZTRZ(Me)** [λ_{EL} : 448 nm;

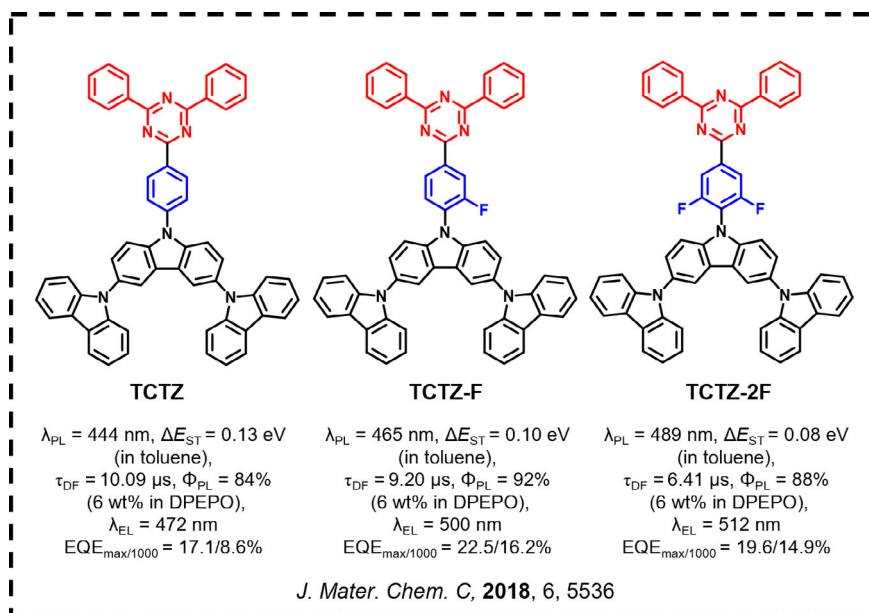


Figure 26. Molecular structures and properties of TRZ-based TADF emitters with fluorine-substitution on the phenylene bridge.

CIE = (0.17, 0.18)] showed EQE_{max} of 10.4 and 11.1%, respectively, while the devices using **TCZTRZ(Me)**, **TCZTRZ(Me2p)** and **TCZTRZ(Me2o)** as emitters showed much lower EQE_{max} values of 0.7%, 0.9% and 2.8%, respectively. The author attributed the inferior performance of those devices to the weak absorption, low Φ_{PL} s, and rapid degradation of the emitters under electrical excitation.

Liao et al.^[50] reported two blue TADF materials **TRZ-CF** (λ_{PL} : $\approx 480 \text{ nm}$; Φ_{PL} : 85.9%; τ_{d} : 7.34 μs ; ΔE_{ST} : 0.22 eV; 20 wt% in DPEPO) and **TRZ-CzF** (λ_{PL} : $\approx 460 \text{ nm}$; Φ_{PL} : 68.6%; τ_{d} : 10.68 μs ; ΔE_{ST} : 0.31 eV; 20 wt% in DPEPO) that likewise incorporate a methyl group on the arylene bridge at a position *ortho* to the donor (**Figure 25**), resembling the structure of **TCZTRZ(Me)**. However, the increased oscillator strength caused by the enhanced conjugation of the donors results in a higher Φ_{PL} in these two compounds compared to **TCZTRZ(Me)**, but at a cost of larger ΔE_{ST} , indicating that the methyl group is not sufficiently bulky to induce a highly twisted structure that can result in the required separation of the FMOs. Despite the red-shifted PL spectra, the OLEDs still exhibited blue emission with λ_{EL} at 476 and 460 nm and EQE_{max} of 20% and 13.3% for the devices with **TRZ-CF** and **TRZ-CzF**, respectively. Strengthening the donor by incorporating a distal carbazole served to red-shift the emission in **TRZ-DCF** (Φ_{PL} : 84%; τ_{d} : 5.43 μs ; 20 wt% in DPEPO) while the other photophysical properties remain unchanged.^[51] Compared to the OLED with **TRZ-CF** [λ_{EL} : 476 nm; CIE = (0.17, 0.27)], a slightly lower EQE_{max} of 18.7% was obtained for the sky-blue device with **TRZ-DCF** [λ_{EL} : 484 nm; CIE = (0.20, 0.33)].

The use of a phenyl substituent on the arylene bridge was explored by Lee et al.^[52] to modulate the conformation of the emitter. A cross-comparison of the photophysical properties of **1PCTRZ** (Φ_{PL} : 87%; τ_{d} : 55.8 μs ; ΔE_{ST} : 0.16 eV; 10 wt% in DPEPO) and **2PCTRZ** (Φ_{PL} : 90%; τ_{d} : 31.4 μs ; ΔE_{ST} : 0.11 eV;

10 wt% in DPEPO) reveals how *ortho*-disubstitution leads to a more twisted conformation (dihedral angle for **1PCTRZ** of 60.2° is smaller than that of **2PCTRZ** of 68.2°), which translates into a smaller ΔE_{ST} and a shorter τ_{d} , but without negatively impacting Φ_{PL} . However, the donor group adopts a less twisted conformation than those of **TCZTRZ(Me)**, **TCZTRZ(Me2p)** and **TCZTRZ(Me2o)**, all of which contain methyl substituents. This suggests that the phenyl group is effectively less bulky than the methyl substituent. High EQE_{max} values were obtained for the OLEDs with **1PCTRZ** [$\text{EQE}_{\text{max}} = 26.7\%$; λ_{EL} : 476 nm; CIE = (0.17, 0.27)] and **2PCTRZ** [$\text{EQE}_{\text{max}} = 28.5\%$; λ_{EL} : 488 nm; CIE = (0.18, 0.35)].

Liao et al. have also explored the use of fluorine atom decoration of the phenylene bridge^[53] in order to explore their influence on the photophysical properties of the emitters. They found that fluoro-substitution can reduce the ΔE_{ST} as a result of an increased dihedral angle between the bridge and the donor by cross-comparing **TCTZ** (Φ_{PL} : 84%; τ_{d} : 10.09 μs ; ΔE_{ST} : 0.13 eV; 6 wt% in DPEPO), **TCTZ-F** (Φ_{PL} : 92%; τ_{d} : 9.20 μs ; ΔE_{ST} : 0.10 eV; 6 wt% in DPEPO) and **TCTZ-2F** (Φ_{PL} : 88%; τ_{d} : 6.41 μs ; ΔE_{ST} : 0.08 eV; 6 wt% in DPEPO), as shown in **Figure 26**. The calculated dihedral angles of the ground-state optimized structures between the tercarbazole donor with the phenylene bridge increase slightly from 53.2°, 56.7° to 57.3° with increasing number of fluorine atoms. The minor changes to the dihedral angle are consistent with the small volume of the fluorine atoms. The strongly inductively withdrawing character of fluorine is responsible for the progressive stabilization of the S_1 state from 3.06, 2.96, to 2.90 eV for **TCTZ**, **TCTZ-F** and **TCTZ-2F**, respectively, while the triplet energies remain almost the same at 2.87, 2.86 to 2.85 eV, respectively. It is interesting to observe that **TCTZ-F** has the best balance between a small ΔE_{ST} and reasonably high oscillator strength, which is manifested in the highest Φ_{PL} of the three compounds. The best EQE_{max} was

achieved for the TCTZ-F-based device [$E_{QE,max} = 22.5\%$; $\lambda_{EL} = 500$ nm; CIE = (0.24, 0.43)] compared to the devices with TCTZ [$E_{QE,max} = 17.1\%$; $\lambda_{EL} = 472$ nm; CIE = (0.16, 0.24)] and TCTZ-2F [$E_{QE,max} = 19.6\%$; $\lambda_{EL} = 512$ nm; CIE = (0.27, 0.46)].

Isosteric trifluoromethyl groups have also been introduced onto the arylene bridge in a series of blue TADF emitters: TRZCz-Me, TRZCz-Me-1, TRZCz-DMe, TRZCz-CF₃, TRZCz-CF₃-1, TRZBuCz-CF₃, and TRZBuCz-CF₃-1, as shown in Figure 27.^[54] Only TRZCz-CF₃ ($\lambda_{PL} = 465$ nm; $\Phi_{PL} = 27.8\%$; $\tau_d = 5.62$ μ s in 5 wt% in mCP; $\Delta E_{ST} = 0.05$ eV) and TRZBuCz-CF₃ ($\lambda_{PL} = 476$ nm; $\Phi_{PL} = 72\%$; $\tau_d = 6.3$ μ s in 5 wt% in mCP; $\Delta E_{ST} = 0.02$ eV), with the trifluoromethyl group located adjacent to the carbazole donor, exhibit TADF. By comparison, TRZCz-Me ($\lambda_{PL} = 435$ nm; $\Phi_{PL} = 57.5\%$; in 10 wt% in mCP; $\Delta E_{ST} = 0.36$ eV) and TRZCz-DMe ($\lambda_{PL} = 434$ nm; $\Phi_{PL} = 31.8\%$; in 10 wt% in mCP; $\Delta E_{ST} = 0.35$ eV) with methyl groups similarly *ortho*-disposed to carbazole are not TADF emitters, while similar analogs TRZ-CF and TRZ-CzF with different donor structures to the above work demonstrated TADF. The Φ_{PL} was not completely dependent on the position of substituent groups on the bridge, for example, as evidenced by the large deviation between TRZCz-CF₃-1 ($\Phi_{PL} = 48\%$) and TRZBuCz-CF₃-1 ($\Phi_{PL} = 99\%$), the latter of which also contains a more strongly electron-donating 3,6-ditert-butylcarbazole donor. The blue OLEDs fabricated with TRZCz-CF₃ and TRZBuCz-CF₃ achieved $E_{QE,max}$ of 9.4% and 14.2% with CIE coordinates of (0.19, 0.23) and (0.18, 0.29), respectively.

Another strong electron-withdrawing group, CN, was used in lieu of the trifluoromethyl groups in a series of emitters reported by Hong et al. (Figure 27).^[55] Compared to TRZCz-CF₃, CzCNTRZ ($\lambda_{PL} = 458$ nm; $\Phi_{PL} = 46\%$; $\tau_d = 47.9$ μ s; $\Delta E_{ST} = 0.21$ eV; 10 wt% in DPEPO) shows a similar emission maximum and improved Φ_{PL} but at the cost of a larger ΔE_{ST} of 0.21 eV. The similar emission was attributed to the identical electron-withdrawing ability of the two electron-withdrawing groups; however, the larger ΔE_{ST} is indicative of a smaller steric bulk from the CN substituent. Thanks to the higher Φ_{PL} , the $E_{QE,max}$ of the CzCNTRZ-based device reached 13.9%. Similar to the PL spectrum, the CzCNTRZ device showed blue ($\lambda_{EL} = 461$ nm) emission with CIE coordinates of (0.15, 0.16), which resembles the emission profile of the TRZCz-CF₃ device ($\lambda_{EL} = 464$ nm).

Hong et al.^[56] also examined the effect of incorporation of a CN unit acting as a secondary electron acceptor on the TADF properties (Figure 27). The addition of the nitrile intensified the CT character of the emitters due to the enhanced acceptor strength, evidenced by the red-shifted emission spectrum. Compared to TRZBFCz ($\Phi_{PL} = 99.8\%$; $\tau_d = 26.3$ μ s in 10 wt% in DPEPO; $\Delta E_{ST} = 0.27$ eV), the ΔE_{ST} is reduced yet the Φ_{PL} is maintained at 100% in TRZCNBFCz ($\Phi_{PL} = 100\%$; $\tau_d = 9.4$ μ s in 10 wt% in DPEPO; $\Delta E_{ST} = 0.13$ eV), enabling a high $E_{QE,max}$ of 26.6% in the sky-blue TADF OLED ($\lambda_{EL} = 481$ nm). However, the addition of two CN substituents in TRZ2CNBFCz resulted in both a lower Φ_{PL} of 62% and a smaller ΔE_{ST} of 0.1 eV ($\Phi_{PL} = 62\%$; $\tau_d = 3.1$ μ s in

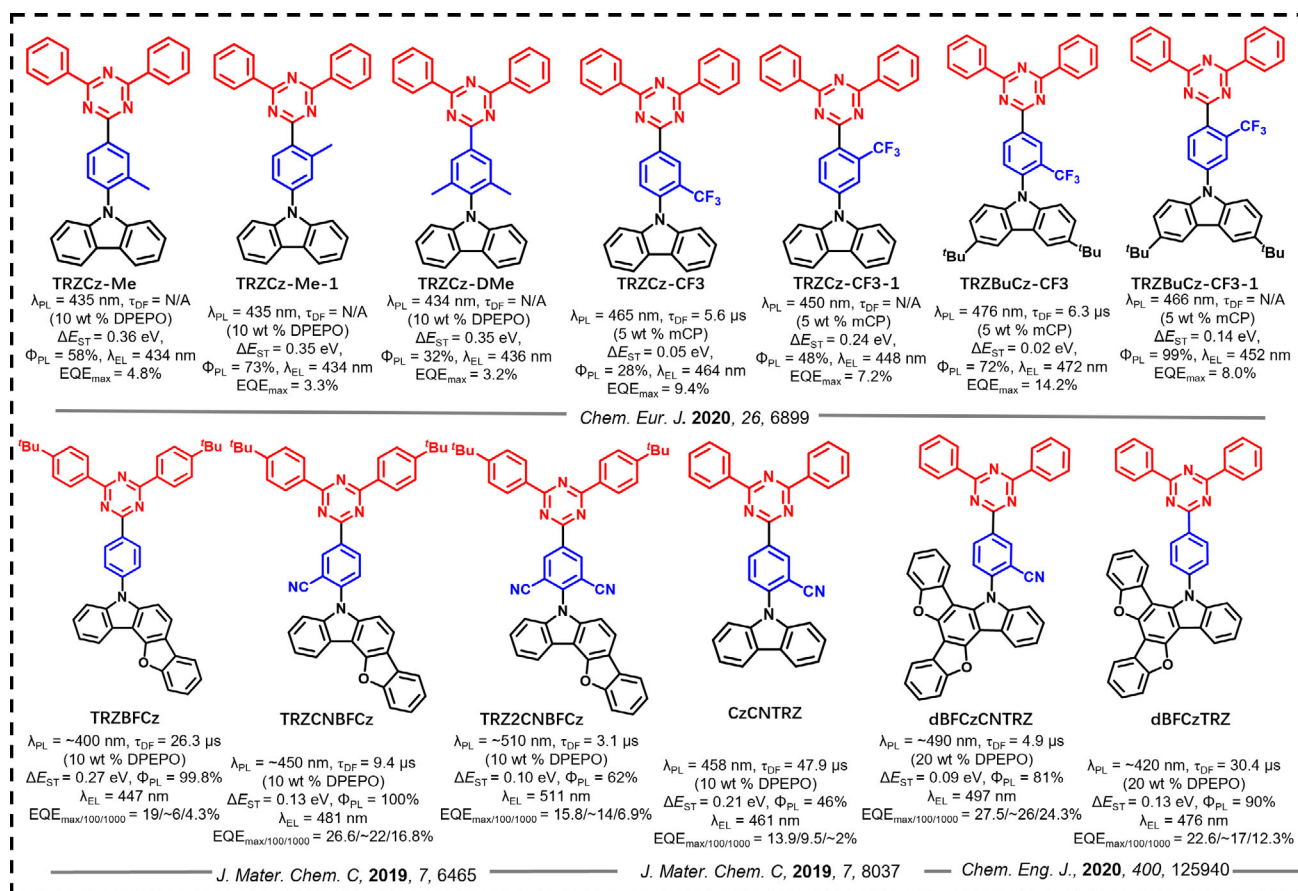


Figure 27. Molecular structures and properties of TRZ-based TADF emitters with modification to the phenylene bridge.

10 wt% in DPEPO; ΔE_{ST} : 0.1 eV), producing a green device (λ_{EL} : 511 nm) with a lower EQE_{max} of 15.8%. The OLED with the control compound **TRZBFCz** that does not have any CN groups on the arylene bridge showed an EQE_{max} of 19% and a λ_{EL} of 447 nm with color coordinates of (0.15, 0.09).

Lee et al.^[57] reported **dBFCzTRZ** (λ_{PL} : 420 nm; Φ_{PL} : 90%; τ_d : 30.4 μ s; ΔE_{ST} : 0.13 eV; 20 wt% in DPEPO) and **dBFCzCNTRZ** (λ_{PL} : 490 nm; Φ_{PL} : 81%; τ_d : 4.9 μ s; ΔE_{ST} : 0.09 eV; 20 wt% in DPEPO) that each employ a more conjugated donor and where the only difference between the two comes from the inclusion of the CN group on the phenylene bridge in **dBFCzCNTRZ** (Figure 27). Calculations showed that the HOMOs of both **dBFCzTRZ** (−5.25 eV) and **dBFCzCNTRZ** (−5.40 eV) are mainly localized on the donor moiety, while the LUMOs of **dBFCzTRZ** (−2.78 eV) and **dBFCzCNTRZ** (−3.06 eV) are distributed on both the arylene linker and the triazine acceptor. The CN unit in **dBFCzCNTRZ** promotes a stabilization of both the HOMO and LUMO levels, but the LUMO more pronouncedly. The dihedral angles between the donor moiety and the arylene bridge in **dBFCzCNTRZ** and **dBFCzTRZ** are similar at 75.1° and 71.1°, respectively, indicating the negligible steric influence from

the nitrile. The S_1/T_1 energies of **dBFCzCNTRZ** (2.97/2.88 eV) are both more stabilized than those of **dBFCzTRZ** (3.15/3.02 eV). Despite the similar ΔE_{ST} , the τ_d for **dBFCzCNTRZ** is much faster at 4.9 μ s compared to 30.4 μ s for **dBFCzTRZ**. There is a small sacrifice in Φ_{PL} of 81% for **dBFCzCNTRZ** compared to 90% for **dBFCzTRZ**. The OLEDs based on **dBFCzCNTRZ** and **dBFCzTRZ** demonstrated high EQE_{max} of 27.5% and 22.6%, respectively. **dBFCzCNTRZ** with the lower Φ_{PL} , however, produced a higher efficiency device which may be attributed to the better electron mobility resulting from the presence of the nitrile group. The operational lifetime (LT_{80}), defined as the lifetime of the device to reach 80% of its initial luminance, of the **dBFCzCNTRZ** device [λ_{EL} : 497 nm; LT_{80} : \approx 36 h; CIE = (0.22, 0.47)] was over three times longer than that of the **dBFCzTRZ** device [λ_{EL} : 476 nm; LT_{80} : \approx 11 h; CIE = (0.16, 0.27)]. The high k_{RISC} of the **dBFCzCNTRZ** emitter contributed to the enhanced device lifetime by suppressing triplet exciton triggered degradation mechanisms. The photophysics and electrochemical characteristics of the aforementioned materials are summarized in Table 11, and representative device performance is summarized in Table 12.

Table 11. Summary of photophysical and electrochemical properties.

Emitter	Solution $\lambda_{PL}/\Phi_{PL}/\tau_d$ (medium) [nm/%/ μ s]	Solid State $\lambda_{PL}/\Phi_{PL}/\tau_d$ (medium) [nm/%/ μ s]	ΔE_{ST} [eV]	HOMO [eV]	LUMO [eV]	Ref.
TCZ–TRZ	432/77/– (PhMe)	457/40/38 (15 wt% in DPEPO)	0.27	−5.64	−2.57	[112]
TCZ–TRZ(Me)	431/60/– (PhMe)	451/32/51 (15 wt% in DPEPO)	0.16	−5.64	−2.54	[112]
TCZ–TRZ(Me')	429/80/– (PhMe)	444/51/58 (15 wt% in DPEPO)	0.12	−5.60	−2.52	[112]
TCZ–TRZ(Me2p)	427/46/– (PhMe)	442/30/39 (15 wt% in DPEPO)	0.14	−5.62	−2.46	[112]
TCZ–TRZ(Me2o)	427/47/– (PhMe)	435/17/37 (15 wt% in DPEPO)	0.18	−5.59	−2.33	[112]
TRZ–CF	452/–/– (PhMe)	\approx 480/85.9/7.34 (20 wt% in DPEPO)	0.22	−5.34	−2.37	[50]
TRZ–CzF	445/–/– (PhMe)	\approx 460/68.6/10.68 (20 wt% in DPEPO)	0.31	−5.47	−2.42	[50]
TRZ–DCF	454/–/– (PhMe)	–/84/5.43 (20 wt% in DPEPO)	0.22	−5.36	−2.34	[51]
1PCTrz	–/–/–	–/87/55.8 (10 wt% in DPEPO)	0.16	−5.49	−2.51	[52]
2PCTrz	–/–/–	–/90/31.4 (10 wt% in DPEPO)	0.11	−5.50	−2.45	[52]
TCTZ	444/–/– (PhMe)	–/84/10.09 (6 wt% in DPEPO)	0.13	−5.68	−2.27	[53]
TCTZ–F	465/–/– (PhMe)	–/92/9.20 (6 wt% in DPEPO)	0.10	−5.68	−2.40	[53]
TCTZ–2 F	489/–/– (PhMe)	–/88/6.41 (6 wt% in DPEPO)	0.08	−5.68	−2.51	[53]
TrzCz–Me	414/–/– (PhMe)	435/57.5/– (10 wt% in DPEPO)	0.36	−5.66	−2.92	[54]
TrzCz–Me–1	414/–/– (PhMe)	435/73/– (10 wt% in DPEPO)	0.35	−5.64	−2.94	[54]
TrzCz–Dme	414/–/– (PhMe)	434/31.8/– (10 wt% in DPEPO)	0.35	−5.66	−2.90	[54]
TrzCz–CF3	457/–/– (PhMe)	465/27.8/5.62 (5 wt% in mCP)	0.05	−5.76	−3.10	[54]
TrzCz–CF3–1	443/–/– (PhMe)	450/48.1/– (5 wt% in mCP)	0.24	−5.73	−3.05	[54]
TrzBuCz–CF3	476/–/– (PhMe)	476/72/6.3 (5 wt% in mCP)	0.02	−5.61	−3.12	[54]
TrzBuCz–CF3–1	466/–/– (PhMe)	466/99/– (5 wt% in mCP)	0.14	−5.60	−3.06	[54]
TrzBFCz	\approx 400/–/– (THF)	–/99.8/26.3 (10 wt% in DPEPO)	0.27	−6.04	−3.21	[56]
TrzCNBFCz	\approx 450/–/– (THF)	–/100/9.4 (10 wt% in DPEPO)	0.13	−6.16	−3.41	[56]
Trz2CNBFCz	\approx 510/–/– (THF)	–/62/3.1 (10 wt% in DPEPO)	0.10	−6.37	−4.08	[56]
CzCNTrz	–/–/–	458/46/47.9 (10 wt% in DPEPO)	0.21	−6.27	−3.24	[55]
dBFCzCNTRz	–/–/–	–/0.81/4.9 (20 wt% in DPEPO)	0.09	−6.17	−3.06	[57]
dBFCzTrz	–/–/–	–/0.9/30.4 (20 wt% in DPEPO)	0.13	−6.17	−2.78	[57]

Table 12. Summary of device structures and performance.

Emitter	Device Structure	EL _{max} [nm]	CIE	V _{on} [V]	EQE/PE/CE ^(a) [%/lm W ⁻¹ /cd A ⁻¹]	EQE _{100/1000} [cd] [m] ⁻²	Ref.
TCZ–TRZ	ITO/HAT–CN/NPB/mCP/DPEPO:15 wt%emitter/ PPF/PPF:Liq/Liq/Al	456	(0.159, 0.142)	3.8	10.4/–/11.6	N/A	[112]
TCZ–TRZ(Me)	ITO/HAT–CN/NPB/mCP/DPEPO:15 wt%emitter/ PPF/PPF:Liq/Liq/Al	448	(0.170, 0.179)	4	11.1/–/12.8	N/A	[112]
TCZ–TRZ(Me')	ITO/HAT–CN/NPB/mCP/DPEPO:15 wt%emitter/ PPF/PPF:Liq/Liq/Al	450	(0.203, 0.229)	4.4	0.7/–/1.0	N/A	[112]
TCZ–TRZ(Me2p)	ITO/HAT–CN/NPB/mCP/DPEPO:15 wt%emitter/ PPF/PPF:Liq/Liq/Al	447	(0.197, 0.214)	5	0.9/–/1.0	N/A	[112]
TCZ–TRZ(Me2o)	ITO/HAT–CN/NPB/mCP/DPEPO:15 wt%emitter/ PPF/PPF:Liq/Liq/Al	444	(0.228, 0.289)	4.6	2.8/–/2.7	N/A	[112]
TRZ–CF	ITO/HATCN/TAPC/TCTA/mCP/DPEPO: 20 wt% TRZ–CF/DPEPO/TmPyPB/Liq/Al	476	(0.17, 0.27)	2.9	20/28/36	≈15/11.4	[50]
TRZ–CzF	ITO/HATCN/TAPC/TCTA/mCP/DPEPO:20 wt% TRZ–CzF/DPEPO/TmPyPB/Liq/Al	460	(0.15, 0.16)	3.5	13.3/10.7/16.5	≈6.0/3.7	[50]
TRZ–DCF	ITO/HAT–CN/TAPC/mCP/DPEPO: TRZ–DCF 20%/DPEPO/TmPyPB/Liq/Al	484	(0.20, 0.33)	–	18.7/30.5/39	≈18.0/≈15	[51]
1PCTrz	ITO/PEDOT:PSS/TAPC/mCP/ DPEPO:20% /TSPO1/ TPBi/LiF/Al	482	(0.17, 0.30)	–	26.7/–	≈15.0/11.7	[52]
2PCTrz	ITO/PEDOT:PSS/TAPC/mCP/ DPEPO:20% /TSPO1/ TPBi/LiF/Al	488	(0.18, 0.35)	–	28.5/–	≈22.0/19.4	[52]
TCTZ	ITO/HAT–CN/TAPC/mCP/DPEPO:6% TCTZ/3TPYMB/Liq/Al	472	(0.16, 0.24)	4.5	17.1/19.7/28.0	–/8.6	[53]
TCTZ–F	ITO/HAT–CN/TAPC/mCP/DPEPO:6% TCTZ–F/3TPYMB/Liq/Al	500	(0.24, 0.43)	4.4	22.5/40.8/56.5	–/16.2	[53]
TCTZ–2 F	ITO/HAT–CN/TAPC/mCP/DPEPO:6% TCTZ–2 F/3TPYMB/Liq/Al	512	(0.27, 0.46)	4.7	19.6/35.1/52.5	–/14.9	[53]
TrzCz–Me	ITO/PEDOT:PSS/NPB/mCP/TCTA/DPEPO:10% emi/TmPyPB/ LiF/Al	434	(0.16, 0.08)	4.3	4.8/2.51/3.44	N/A	[54]
TrzCz–Me–1	ITO/PEDOT:PSS/NPB/mCP/TCTA/DPEPO:10% emi/TmPyPB/ LiF/Al	434	(0.16, 0.08)	4.8	3.3/1.65/2.52	N/A	[54]
TrzCz–Dme	ITO/PEDOT:PSS/NPB/mCP/TCTA/DPEPO:10% emi/TmPyPB/ LiF/Al	436	(0.16, 0.09)	4.3	3.19/1.85/2.48	N/A	[54]
TrzCz–CF3	ITO/PEDOT:PSS/NPB/mCP/TCTA/DPEPO:10% emi/TmPyPB/ LiF/Al	464	(0.19, 0.23)	3.9	9.4/12.83/15.92	N/A	[54]
TrzCz–CF3–1	ITO/PEDOT:PSS/NPB/mCP/TCTA/DPEPO:10% emi/TmPyPB/ LiF/Al	448	(0.17, 0.15)	3.9	7.17/12.72/15.8	N/A	[54]
TrzBuCz–CF3	ITO/PEDOT:PSS/NPB/mCP/TCTA/DPEPO:10% emi/TmPyPB/ LiF/Al	472	(0.18, 0.29)	4.1	14.22/19.5/26.7	N/A	[54]
TrzBuCz–CF3–1	ITO/PEDOT:PSS/NPB/mCP/TCTA/DPEPO:10% emi/TmPyPB/ LiF/Al	452	(0.17, 0.16)	3.9	7.97/14.39/17.88	N/A	[54]
TrzBFCz	ITO/PEDOT:PSS/TAPC/mCP/DPEPO:10%TrzBFCz/ TSPO1/TPBi/LiF/Al	447	(0.15, 0.09)	8.1	19/–/–	≈6.0/4.3	[56]
TrzCNBFCz	ITO/PEDOT:PSS/TAPC/mCP/DPEPO:20%TrzBFCz/ TSPO1/TPBi/LiF/Al	481	(0.17, 0.31)	6.5	26.6/–/–	≈22.0/16.8	[56]
Trz2CNBFCz	ITO/PEDOT:PSS/TAPC/mCP/DPEPO:10%TrzBFCz/ TSPO1/TPBi/LiF/Al	511	(0.27, 0.52)	9	15.8/–/–	≈14/6.9	[56]
CzCNTrz	ITO/PEDOT:PSS/TAPC/mCP/EML (25 nm:10 wt%)/ TSPO1/TPBi/LiF/Al	461	(0.15, 0.16)	–	13.9/18.3/18.3	9.5/≈2.0	[55]
dBFCzCNTrz	ITO/PEDOT:PSS/TAPC/mCP/DPEPO:emitters/ TSPO1/TPBi/LiF/Al	497	(0.22, 0.47)	5.2	27.5/–/–	≈26.0/24.3	[57]
dBFCzTrz	ITO/PEDOT:PSS/TAPC/mCP/DPEPO:emitters/ TSPO1/TPBi/LiF/Al	476	(0.16, 0.27)	5.6	22.6/–/–	≈17.0/12.3	[57]

8. Functionalization of the Triazine

Lee et al.^[58] developed a blue TADF emitter, **mtCzTRZ** (λ_{PL} : 469 nm; Φ_{PL} : 65%; τ_{d} : 118.6 μs in 1 wt% in PS; ΔE_{ST} : 0.06 eV), by attaching a *para*-methoxy group to one of the phenyl rings of the TRZ acceptor, which was designed to blue shift the emission compared to **tCzTRZ** by weakening its electron-withdrawing capacity (Figure 28). The control compound, **tCzTRZ** (λ_{PL} : 469 nm; Φ_{PL} : 67%; τ_{d} : 89.4 μs in 1 wt% in PS; ΔE_{ST} : 0.05 eV), showed identical PL and similar photophysical properties to that of **mtCzTRZ**, indicating that there is negligible influence of the photophysical properties due to the presence of the methoxy group on the TRZ acceptor. However, the modification resulted in an improvement in the device performance. The solution-processed OLED with **mtCzTRZ** dispersed into the (5-(*tert*-butyl)-2-(4-(*tert*-butyl)phenoxy)phenyl)diphenylphosphine oxide (POBBPE)^[59] host as the emitting layer, a more soluble analog of DPEPO, showed an EQE_{max} of 16.1% at λ_{EL} of 461 nm and CIE coordinates of (0.16, 0.20). By contrast, the device with **tCzTRZ** only afforded an EQE_{max} of 12.5% at similar though slightly red-shifted color coordinates [λ_{EL} : 467 nm; CIE = (0.16, 0.24)].

FTRZTCz (Φ_{PL} : 85%; τ_{d} : 5.91 μs 10 wt% in DPEPO; ΔE_{ST} : 0.22 eV), also developed by Lee et al.,^[60] is an emitter containing a triazine acceptor with an inductively electron-withdrawing *para*-fluoro group onto one of the phenyl rings of the TRZ (Figure 28). 3,6-Di-*tert*-butylcarbazole groups connected at the *ortho* positions of the other two phenyl rings complete the donor-acceptor structure. Their placement was to prevent intermolecular interactions, a similar strategy to that used in **o-CzTRZ** (Figure 4). **FTRZTCz** showed a PL spectrum in toluene with the maximum at 450 nm, which though not directly comparable is similar to the PL maximum of **o-CzTRZ** (λ_{PL} 455 nm, 5 wt% in mCP) in mCP matrix. The missing information related to the compound without the fluoro group makes it difficult to conclude how much the fluoro substituent contributes to the shift of the PL given the similar donor-*ortho*-acceptor skeleton. However, it is still possible to infer the influence of the fluoro group by

comparing the properties of the compound with the previously reported molecule **o-CzTRZ**, which only has one *ortho*-connected carbazole. The red-shifted EL for the device with **FTRZTCz** [λ_{EL} : 496 nm, CIE coordinates = (0.20, 0.45)] compared to that with **o-CzTRZ** [λ_{EL} : 470 nm, CIE = (0.15, 0.22)] reveals the presence of a stronger electron-accepting triazine derivative in **FTRZTCz** compared to **o-CzTRZ**.

Xu et al.^[61] employed diphenylphosphine oxide (PO) as secondary acceptors within a series of D–A–A-type TADF emitters with the collective name of **xtBCznPO3-nTPTZ** ($x = o, m,$ and p , corresponding to placement of the diphenylphosphine oxide at the *ortho*-, *meta*-, and *para*-positions; and $n = 1$ and 2 , corresponding to the number of diphenylphosphine oxide acceptors), in which tBCz is 3,6-di-*tert*-butylcarbazole, and TPTZ is triphenyltriazine (aka TRZ) as shown in Figure 29. The incorporation of the electron-withdrawing PO group serves to stabilize the excited states and to enhance the CT character, leading to a greater localization of the FMO distributions. By virtue of this design strategy, **ptBCzPO2TPTZ** (λ_{PL} : 494 nm; Φ_{PL} : 96%; in 10 wt% in DPEPO; ΔE_{ST} : 0.01 eV) as the best example among this series, has almost unity Φ_{PL} (96%) and very efficient RISC efficiency, Φ_{RISC} , of 98% and k_{RISC} of $5.42 \times 10^4 \text{ s}^{-1}$. These properties established the basis for the high-performance OLED, which showed an EQE_{max} of 28.9% at λ_{EL} of 492 nm, corresponding to CIE coordinates of (0.18, 0.42). It is worth noting that the analog **p-CzTRZ** (Figure 4) without the PO groups does not show any TADF properties due to its too large ΔE_{ST} of 0.36 eV in 10 wt% in DPEPO. The other derivatives in this work showed moderate Φ_{PL} s ranging from 38% to 74%. The photophysics and electrochemical data of the aforementioned materials are summarized in Table 13, and representative device performance is summarized in Table 14.

9. Intramolecular Through Space Charge Transfer (TSCT) of Triazine Based TADF Emitters

The prior examples have implicated an S_1 state that has CT character and that the charge transfer process is mediated by

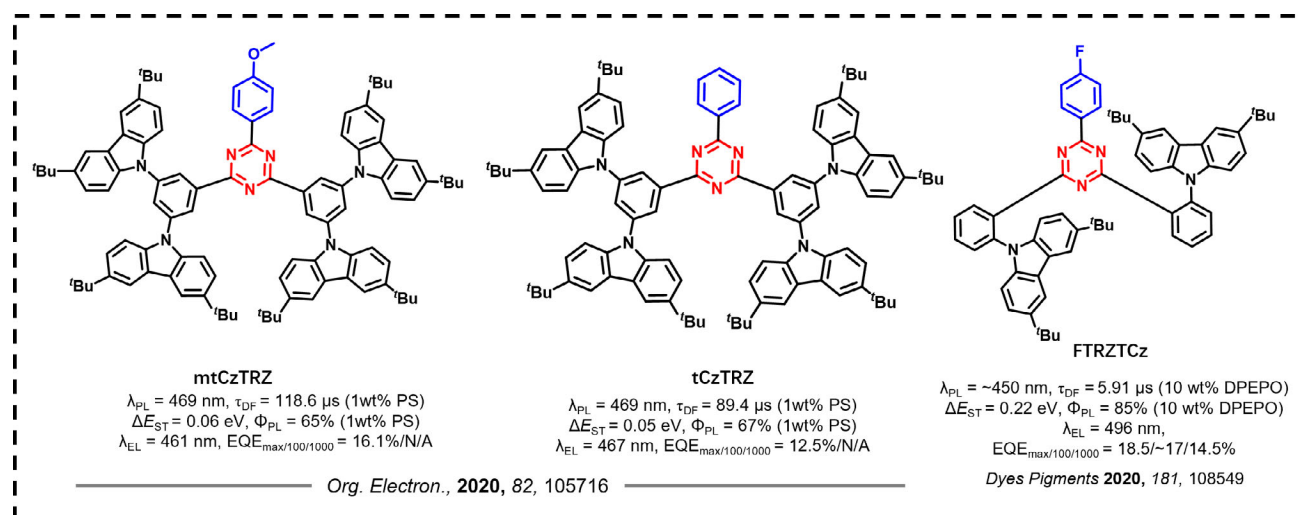


Figure 28. Molecular structures and properties of TADF emitters based on functionalized TRZ groups.

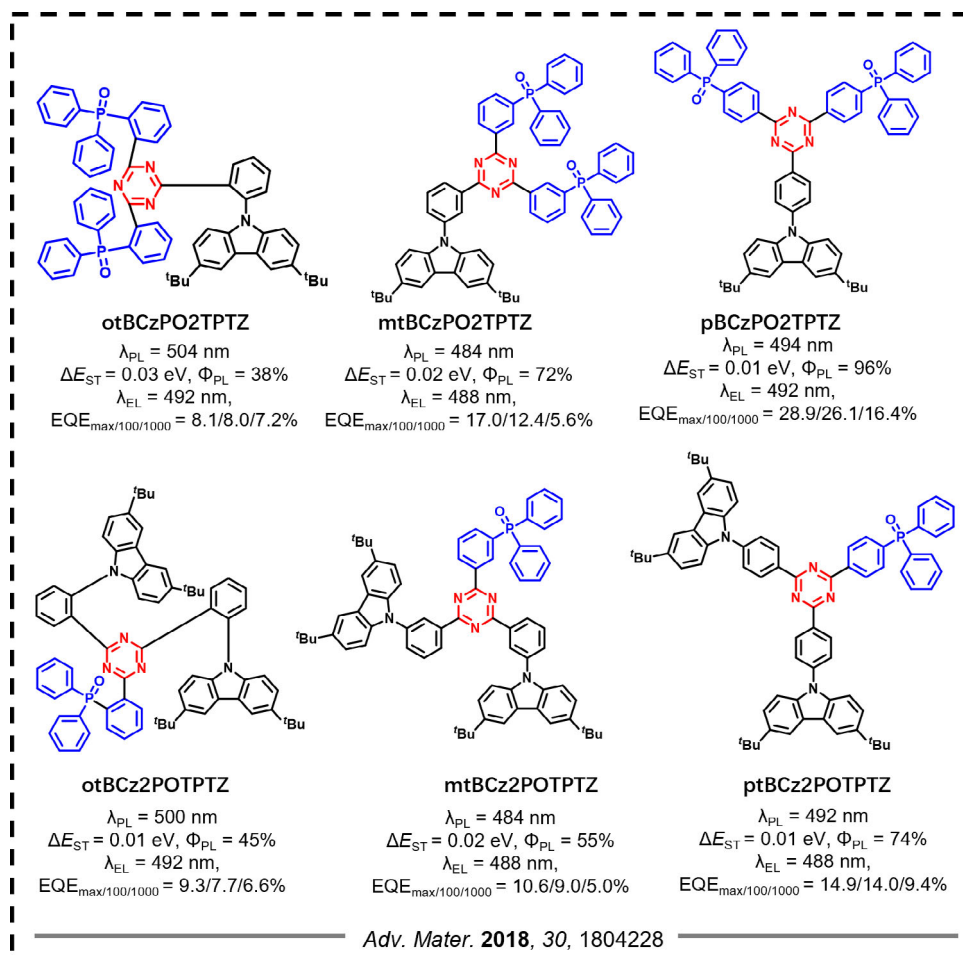


Figure 29. Molecular structures and properties of TADF emitters based on diphenylphosphine oxide (PO) functionalized triazine.

Table 13. Summary of photophysical and electrochemical properties.

Emitter	Solution $\lambda_{PL}/\Phi_{PL}/\tau_d$ (medium) [nm/%/ μs]	Solid State $\lambda_{PL}/\Phi_{PL}/\tau_d$ (medium) [nm/%/ μs]	ΔE_{ST} [eV]	HOMO [eV]	LUMO [eV]	Ref.
mtCzTrz	469/—/(PhMe)	—/65.1/118.6(1 wt% in PS)	0.06	−6.08	−3.41	[58]
tCzTrz	469/—/(PhMe)	—/66.6/89.4(1 wt% in PS)	0.05	−6.09	−3.43	[58]
ptBCzPO2TPTZ	506/—/(CHCl3)	494/96/—(10 wt% in DPEPO)	0.01	−6.05	−3.60	[61]
otBCzPO2TPTZ	518/—/(CHCl3)	504/38/—(10 wt% in DPEPO)	0.03	−6.04	−3.48	[61]
mtBCzPO2TPTZ	512/—/(CHCl3)	484/72/—(10 wt% in DPEPO)	0.02	−6.08	−3.60	[61]
ptBCzPO2TPTZ	506/—/(CHCl3)	494/96/—(10 wt% in DPEPO)	0.01	−6.05	−3.60	[61]
otBCz2POTPTZ	514/—/(CHCl3)	50 045/—(10 wt% in DPEPO)	0.01	−6.05	−3.53	[61]
mtBCz2POTPTZ	514/—/(CHCl3)	48 455/—(10 wt% in DPEPO)	0.02	−6.08	−3.58	[61]
ptBCz2POTPTZ	496/—/(CHCl3)	49 274/—(10 wt% in DPEPO)	0.01	−6.04	−3.50	[61]
FTrzTCz	≈450/—/(PhMe)	—/85/5.91(10% in DPEPO)	0.22	−6.13	−3.42	[60]

a π -conjugated bridging moiety. This type of CT is termed TBCT.^[62] There exists a second CT process that is mediated by π -stacking of the donor and acceptor units, termed through-space charge transfer (TSCT). Distinct from most of the TBCT emitters that feature strong electron coupling through

covalent bonds, TSCT emitters possess weaker electronic interaction between donors and acceptors due to the relatively smaller overlap of the FMOs in these systems. The degree of electronic coupling is controlled by the distance and the relative angles between the donor and acceptor groups. For example, an

Table 14. Summary of device structures and performance.

Emitter	Device Structure	EL _{max} [nm]	CIE	V _{on} [V]	EQE/PE/CE ^{a)} [%/lm W ⁻¹ /cd A ⁻¹]	EQE _{100/1000} [cd] [m] ⁻²	Ref.
mtCzTrz	ITO/PEDOT:PSS/PVK/POBBPE:20 wt% mtCzTrz //TSPO1/LiF/Al	461	0.16, 0.20	7.6	16.1/9.2/25	N/A	[58]
tCzTrz	ITO/PEDOT:PSS/PVK/POBBPE:20 wt% tCzTrz //TSPO1/LiF/Al	467	0.16, 0.24	8	12.5/7.9/21.4	N/A	[58]
ptBCzPO ₂ TPTZ	ITO/MoO ₃ /mCP/80 wt% ptBCzPO ₂ TPTZ: DPEPO/pTPOTZ/LiF/Al	≈488	(0.18, 0.42)	–	28.9/79.3/73.2	26.1/16.4	[61]
otBCzPO ₂ TPTZ	ITO/MoO ₃ /mCP/80 wt% otBCzPO ₂ TPTZ: DPEPO/pTPOTZ/LiF/Al	492	(0.21, 0.46)	3.6	8.1/15.8/21.9	8.0/7.2	[61]
mtBCzPO ₂ TPTZ	ITO/MoO ₃ /mCP/80 wt% mtBCzPO ₂ TPTZ: DPEPO/pTPOTZ/LiF/Al	488	(0.18, 0.36)	3.2	17/34.6/39.7	12.4/5.6	[61]
ptBCzPO ₂ TPTZ	ITO/MoO ₃ /mCP/80 wt% ptBCzPO ₂ TPTZ: DPEPO/pTPOTZ/LiF/Al	492	(0.18, 0.42)	2.9	28.9/79.3/73.2	26.1/16.4	[61]
otBCz ₂ POTPTZ	ITO/MoO ₃ /mCP/80 wt% otBCz ₂ POTPTZ: DPEPO/pTPOTZ/LiF/Al	492	(0.20, 0.44)	2.9	9.3/26.5/24.5	7.7/6.6	[61]
mtBCz ₂ POTPTZ	ITO/MoO ₃ /mCP/80 wt% mtBCz ₂ POTPTZ: DPEPO/pTPOTZ/LiF/Al	488	(0.18, 0.37)	3	10.6/22.7/24.9	9.0/5.0	[61]
ptBCz ₂ POTPTZ	ITO/MoO ₃ /mCP/80 wt% ptBCz ₂ POTPTZ: DPEPO/pTPOTZ/LiF/Al	488	(0.17, 0.32)	2.9	14.9/31.7/31.9	14.0/9.4	[61]
FTzTCz	ITO/PEDOT:PSS/TAPC/mCP/DPEPO:20% FTzTCz/TSPO1/TPBi/LiF/Al	496	(0.20, 0.45)	–	18.5/–/–	≈17.0/14.5	[60]

ortho-substitution pattern between the donor and acceptor moieties leads to sterically congested, co-facially aligned donor and acceptor groups in the molecule, inducing either a $\pi\cdots\pi^*$ type (as in the **B-oTC** emitter) or an $n\cdots\pi^*$ type (as in **TRZ-oCz**) interaction. The conformationally restricted structures result in limited change in the geometry of the emitter in the excited states and small reorganization energies, reflected in the narrower emission profiles of these compounds.

Swager et al.^[63] reported a series of TADF emitters possessing a TSCT state. As shown in **Figure 29**, the design of **XPT**, **XCT**, and **XtBuCT** is based on a xanthene scaffold with a donor and an acceptor co-facially aligned at a well-defined distance. These compounds possess very small ΔE_{ST} values as evidenced by DFT calculation (**Figure 30**), and the close alignment between the donor and acceptor groups restricts motion in the solid state, resulting in aggregation induced delayed fluorescence (AIDF) as exemplified by the increase in Φ_{PL} from dilute toluene to 10 wt% DPEPO films of **XPT** and **XtBuCT** [**XPT** (Φ_{PL} : 7.7% in toluene, Φ_{PL} : 66% in 10 wt% in DPEPO), and **XtBuCT** (Φ_{PL} : 6.0% in toluene, Φ_{PL} : 35% in 10 wt% in DPEPO)]. The strength of the electron donor directly impacted the corresponding emission color of the emitters as evidenced by the PL maximum shifting from 419 nm in **XCT** to 451 nm in **XPT** and 562 nm in **XtBuCT**. The OLED with **XPT** showed a 10% EQE_{max} with λ_{EL} at 586 nm while **XtBuCT**-based device exhibited a 4% EQE_{max} (limited by its lower Φ_{PL}) with λ_{EL} at 488 nm.

Lee et al.^[64] found that *ortho*-linked donor and acceptor compounds showed superior TADF properties to those where the donor was either *meta*- or *para*-disposed. The authors compared the optoelectronic properties of **oBFCzTRZ**, **mBFCzTRZ**, and **pBFCzTRZ**, which are based on *ortho*-, *meta*-, and *para*-linked diphenyltriazine and benzofurocarbazole groups (**Figure 31**). It

is noteworthy that the ΔE_{ST} of **oBFCzTRZ** is only 0.002 eV, while those of **mBFCzTRZ** and **pBFCzTRZ** are 0.191 and 0.302 eV, respectively, revealing the much weaker electronic coupling within the former. Moreover, **oBFCzTRZ** (Φ_{PL} : 97.9%; τ_d : 5.4 μ s in 10 wt% in DPEPO) also possessed a shorter delayed lifetime, and higher Φ_{PL} than **mBFCzTRZ** (Φ_{PL} : 31.1%; τ_d : 29.6 μ s in 10 wt% in DPEPO) and **pBFCzTRZ** (Φ_{PL} : 85.3%; τ_d : 31.2 μ s in 10 wt% in DPEPO), reflective of the more efficient RISC process in the former. The higher Φ_{PL} is likely due to the suppression of nonradiative decay due to the more conformationally restricted structure in **oBFCzTRZ**. Blue-emitting devices with **oBFCzTRZ** (λ_{EL} = 477 nm) > **mBFCzTRZ** (λ_{EL} = 473 nm) > **pBFCzTRZ** (λ_{EL} = 465 nm) showed EQE_{max} of 20.4% [λ_{EL} : 477 nm; CIE = (0.18, 0.31)], 13.2% [λ_{EL} : 473 nm; CIE = (0.17, 0.25)], and 16.7% [λ_{EL} : 465 nm; CIE = (0.15, 0.18)], respectively. Importantly, **oBFCzTRZ**-based device showed the least amount of efficiency roll-off.

Expanding on the *ortho*-disposed donor–acceptor platform, Lee et al.^[65] reported green TADF emitters **DPA-o-TRZ** and **MPA-o-TRZ** (**Figure 31**), which incorporated a diphenylamine group whose electron donating ability is stronger than benzofurocarbazole as in **oBFCzTRZ**. Thus, both **DPA-o-TRZ** and **MPA-o-TRZ** exhibited red-shifted PL with λ_{PL} at around 500 and 530 nm, respectively. Similar to the other TSCT emitters, **DPA-o-TRZ** and **MPA-o-TRZ** also have very small ΔE_{ST} values of 0.03 and 0.01 eV, respectively, and comparatively short delayed lifetimes of 1.62 μ s and 1.08 μ s, respectively. The OLEDs based on **DPA-o-TRZ** [λ_{EL} : 497 nm; CIE = (0.21, 0.45)] and **MPA-o-TRZ** [λ_{EL} : 532 nm; CIE = (0.35, 0.58)] showed EQE_{max} of 17.2% and 16.3%.

Using DFT calculations, Bredas et al.^[66] investigated the origins of the TSCT in a number of TADF emitters (**Figure 32**). Two pathways for TSCT were identified:

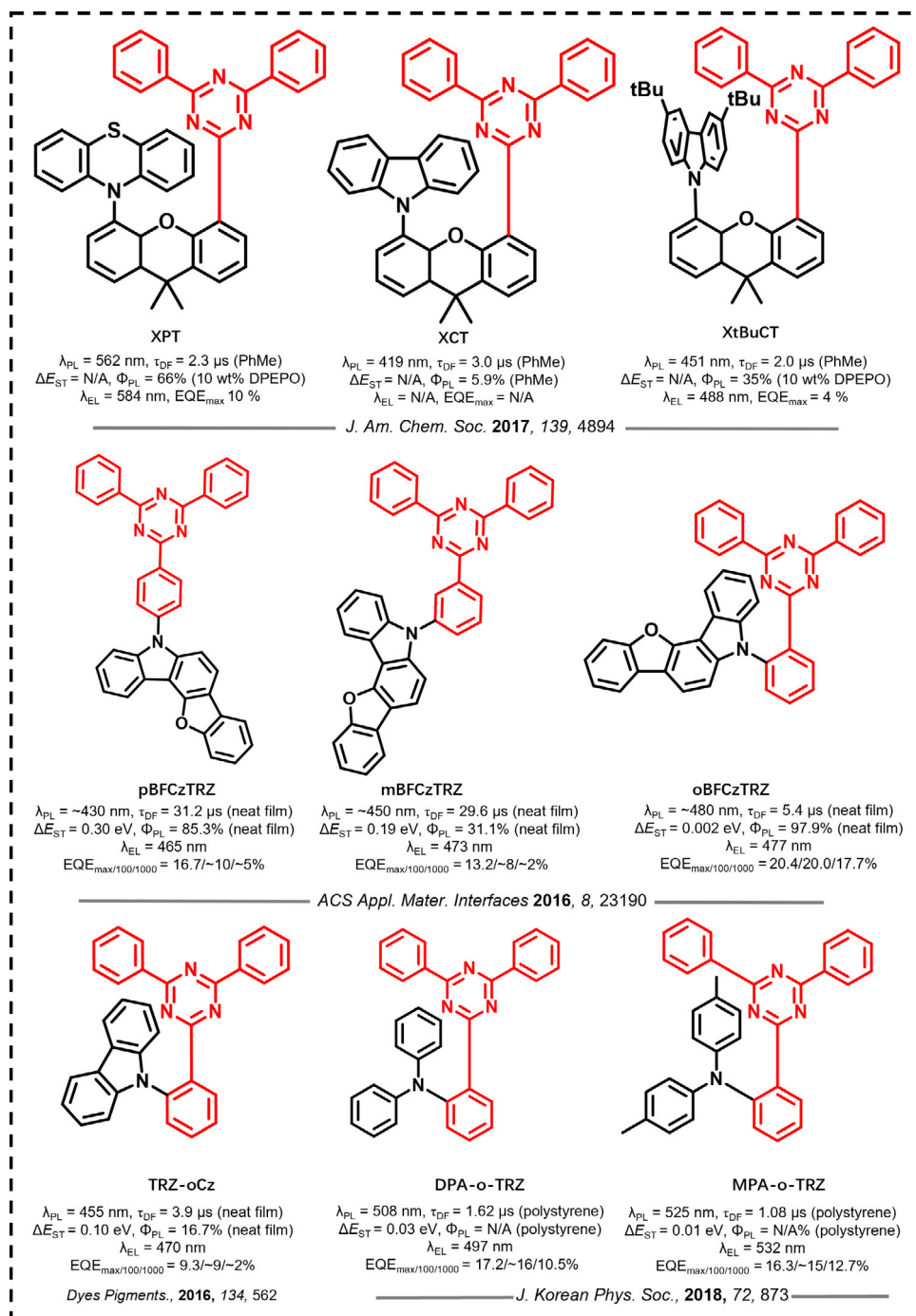


Figure 30. HOMO and LUMO orbital distributions and calculated bandgaps, singlet (S_1), triplet (T_1) energy levels, and oscillator strengths (f) for XPT, XCT, and XtBuCT based on TD-DFT at the B3LYP functional and 6-31 G* basis set. Reproduced with permission.^[63] Copyright 2017, American Chemical Society.

intramolecular $\pi \cdots \pi$ and $n \cdots \pi$ noncovalent interactions. The mechanism of the $\pi \cdots \pi$ interaction is the one that is operational for XPT, XCT, and XtBuCT.^[63] However, in the cases of TRZ-oCz^[17] and TRZ-oBFCz, the computations indicated a very close packing between one of the nitrogen atoms of the triazine ring with the carbazole plane, which the authors asserted triggered noncovalent interactions between the lone-pair electrons of this

triazine nitrogen atom and the carbazole π electrons. The $n \rightarrow \pi^*$ interactions were identified as critical for enhancing the singlet–triplet spin–orbit coupling, and as a result, greatly facilitating the RISC process.

Further examples based on an *ortho*-connection strategy include the incorporation of a dibenzofuran as the bridge in BCzTRZDBF, TCzTRZDBF, and IDCzTRZDBF (Figure 33)

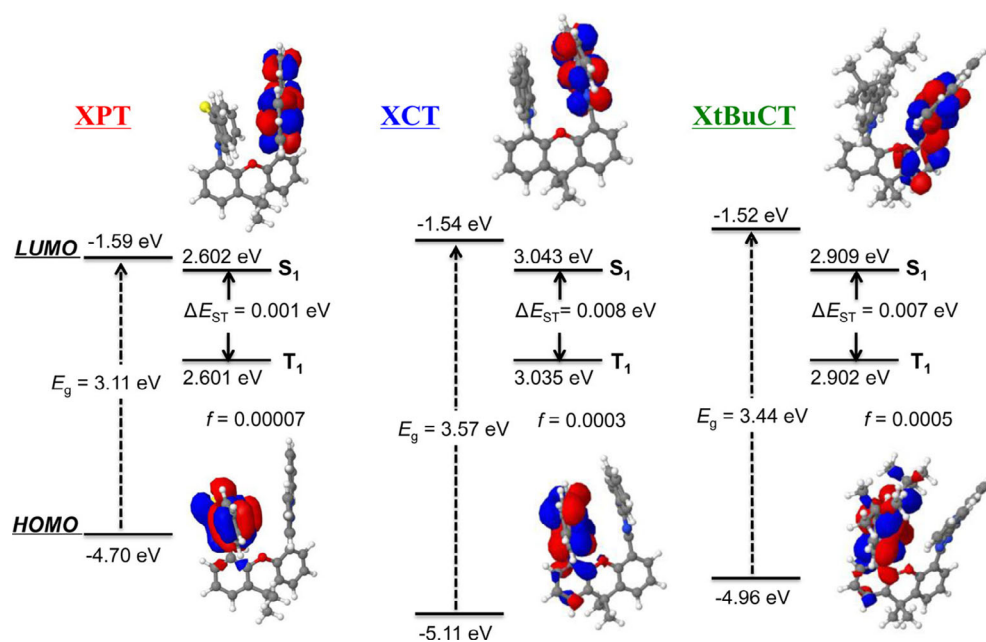


Figure 31. Molecular structures and properties of TADF emitters based on TSCT mechanism.

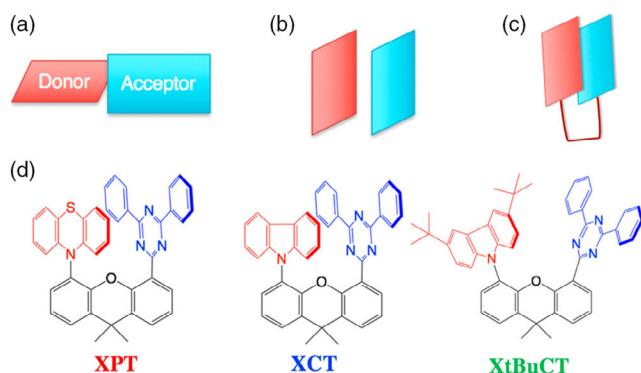


Figure 32. Molecular structures of the TSCT molecules based on intramolecular $\pi\cdots\pi$ $n\cdots\pi$ noncovalent interactions. Reproduced with permission.^[66] Copyright 2019, American Chemical Society.

where substitution next to the oxygen of the dibenzofuran induced a large conformational distortion.^[67] This, coupled with the *ortho*-connection between the donor and acceptor, leads to shortened delayed lifetimes and small ΔE_{ST} , both of which were ascribed to the TSCT character of the emissive excited state. **BCzTRZDBF**, **TCzTRZDBF**, and **IDCzTRZDBF** possess small ΔE_{ST} of less than 0.1 eV yet with high Φ_{PL} of 82.4, 86.3, and 85.4%, respectively, as 5 wt% in mCBPTRZ films. The best device was obtained with **TCzTRZDBF** as the emitter and showed an EQE_{max} of 23.5% with CIE coordinates of (0.27, 0.57) and FWHM of 80 nm. Like **TCzTRZDBF**, another analog **BCzTRZDBF**, with a less bulky dendritic donor, also exhibited a similar EQE_{max} of 20.1% and comparable CIE coordinates of (0.24, 0.52) and FWHM of 84 nm. However, the device with **IDCzTRZDBF** showed a much worse performance with an EQE_{max} of only 12.2%, a CIE coordinates of (0.22, 0.48) and FWHM of 81 nm. Based on the fact that **IDCzTRZDBF** has a

Φ_{PL} of 85.4%, the unexpected lower efficiency may be attributed to the unoptimized device configuration for **IDCzTRZDBF** which has the largest HOMO-LUMO gap and the deepest HOMO level among the three compounds.

TADF molecules based on *ortho*-disposed donors and acceptors were shown by Bredas and co-workers to contain emissive excited states that comprise both TBCT and TSCT character. Yang et al.^[68] reported a series of highly twisted emitters, **SF34oTz**, **SF23oTz** and **SF12oTz**, containing indolin-fused spiro-bifluorene donors (Figure 33). According to the DFT computations, the ratios of TBCT/TSCT were initially calculated by integrating the transition density localized on/not on the phenylene bridge. Among them, **SF34oTz** (Φ_{PL} : 65% in 10 wt% DPEPO) showed a dominant TSCT (96.8% as suggested by TD-DFT calculations) and a relative larger ΔE_{ST} of 0.29 eV, whereas **SF23oTz** (Φ_{PL} : 86% in 10 wt% in DPEPO; ΔE_{ST} : 0.08 eV) and **SF12oTz** (Φ_{PL} : 92% in 10 wt% in DPEPO; ΔE_{ST} : 0.05 eV) exhibit higher TBCT contributions, with the ratio increasing to 21% and 32%, respectively. The higher TBCT contribution in **SF12oTz** leads to much higher ratio of delayed fluorescence (79.1% vs 39.2%) compared with **SF23oTz**, which the authors asserted was due to the more effective channel of TBCT over TSCT to realize charge transfer from donors to the acceptor. However, the largest ΔE_{ST} of 0.29 eV for **SF34oTz** in the series does not align with the expectation that a compound with a greater TSCT contribution should have the smallest ΔE_{ST} in theory. Among the three emitters, the OLED with **SF12oTz** performed the best, showing an EQE_{max} of 22.4% [λ_{EL} : 496 nm; CIE = (0.23, 0.47)]. The devices with **SF23oTz** [λ_{EL} : 484 nm; CIE = (0.19, 0.35)] and **SF34oTz** [λ_{EL} : 482 nm; CIE = (0.18, 0.37)] showed EQE_{max} of 19.6% and 14.6%, respectively. The trend in device efficiencies align with that of the Φ_{PL} .

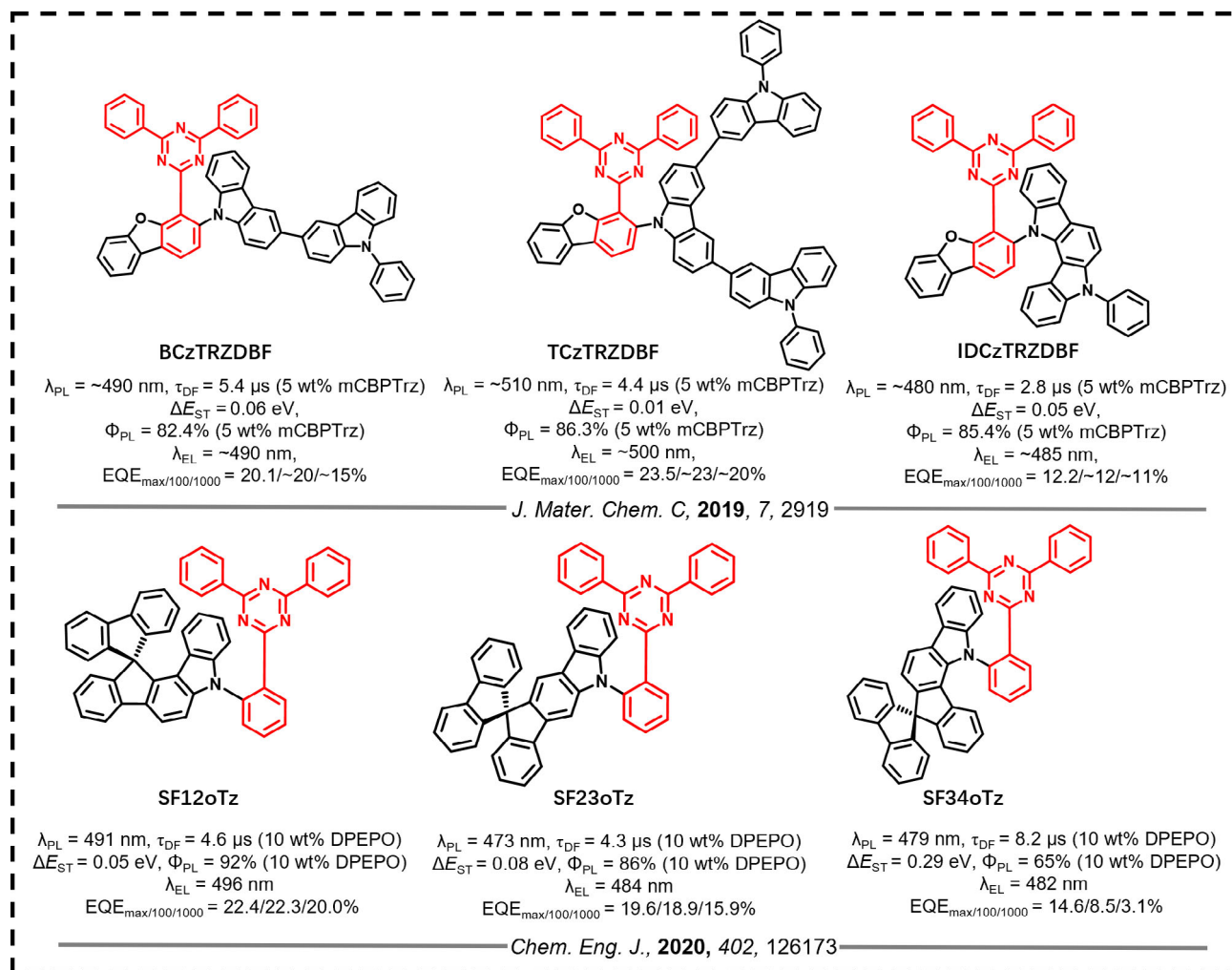


Figure 33. Molecular structures and properties of TADF emitters based on TSCT mechanism.

Many OLEDs that contain TADF compounds that emit from an excited state containing some TSCT character still suffer from low device performance.^[63] Recently, Kaji et al.^[69] and Liao et al.^[70] elucidated the importance of the relative orientation of donor and acceptor groups on the electronic coupling between the two in TSCT compounds that influences also the magnitude of the nonradiative decay. Similar to the other TSCT molecules discussed in this section, **DM-B** (Φ_{PL} : 96% in 20 wt% in DPEPO; ΔE_{ST} : 0.17 eV) and **DM-Bm** (Φ_{PL} : 92% in 20 wt% in DPEPO; ΔE_{ST} : -0.08 eV) were designed by connecting the donor and acceptor units via a rigid fluorene linker thereby confining them into a closely packed coplanar configuration (Figure 34). **DM-G** (Φ_{PL} : 88% in 20 wt% in DPEPO; ΔE_{ST} : -0.11 eV) features a diphenyltriazine acceptor instead of triphenyltriazine in **DM-B** and **DM-Bm**. By contrast, the authors also developed a more flexible control compound **DM-X** (Φ_{PL} : 32% in 20 wt% in DPEPO; ΔE_{ST} : 0.03 eV), which differs from **DM-G** as it contains less rotationally constrained 1,2-phenylene bridge instead of the rigid fluorene linker. Another control compound **DM-Z** (Φ_{PL} : 23% in 20 wt% in DPEPO; ΔE_{ST} : 0.54 eV) has also been designed to analyze the effect of increasing the D/A separation by placing the

donor and acceptor units on the opposite sides of the rigid fluorene linker. Despite their similar absorption and emission spectra, the Φ_{PL} values of the rigid **DM-B**, **DM-Bm**, and **DM-G** are remarkably higher than those of the flexible control compounds, which further validated the design strategy on the suppression of intramolecular vibrations and rotations. The ΔE_{ST} values are 0.17, -0.08, -0.11, 0.03, and 0.54 eV for **DM-B**, **DM-Bm**, **DM-G**, **DM-X**, and **DM-Z**, respectively. The negative ΔE_{ST} of **DM-Bm** and **DM-G** were attributed by the authors to different molecular geometries in their respective fully relaxed singlet and triplet states. Another analog **DM-Me-B** (Φ_{PL} : 73% in 30 wt% in DPEPO; ΔE_{ST} : 0.25 eV) was also developed by replacing the phenyl group onto the donor unit of **DM-B** with a methyl group.^[71] In contrast to **DM-B** (Φ_{PL} : 96%), the slight structural change contributes to a reduction of the Φ_{PL} to 73% although **DM-Me-B** still maintains similar TADF properties. OLEDs based on **DM-B** (50 wt% in DPEPO) achieved an EQE_{max} of 27.4%, with only minor efficiency roll-off at a luminance of 1,000 cd m⁻² where the $EQE_{1000} = 24.4\%$. The EQE_{max} of the devices based on **DM-Bm** (30 wt% in DPEPO) and **DM-G** (20 wt% in DPEPO) are 21.7% and 18.5%, respectively, which are

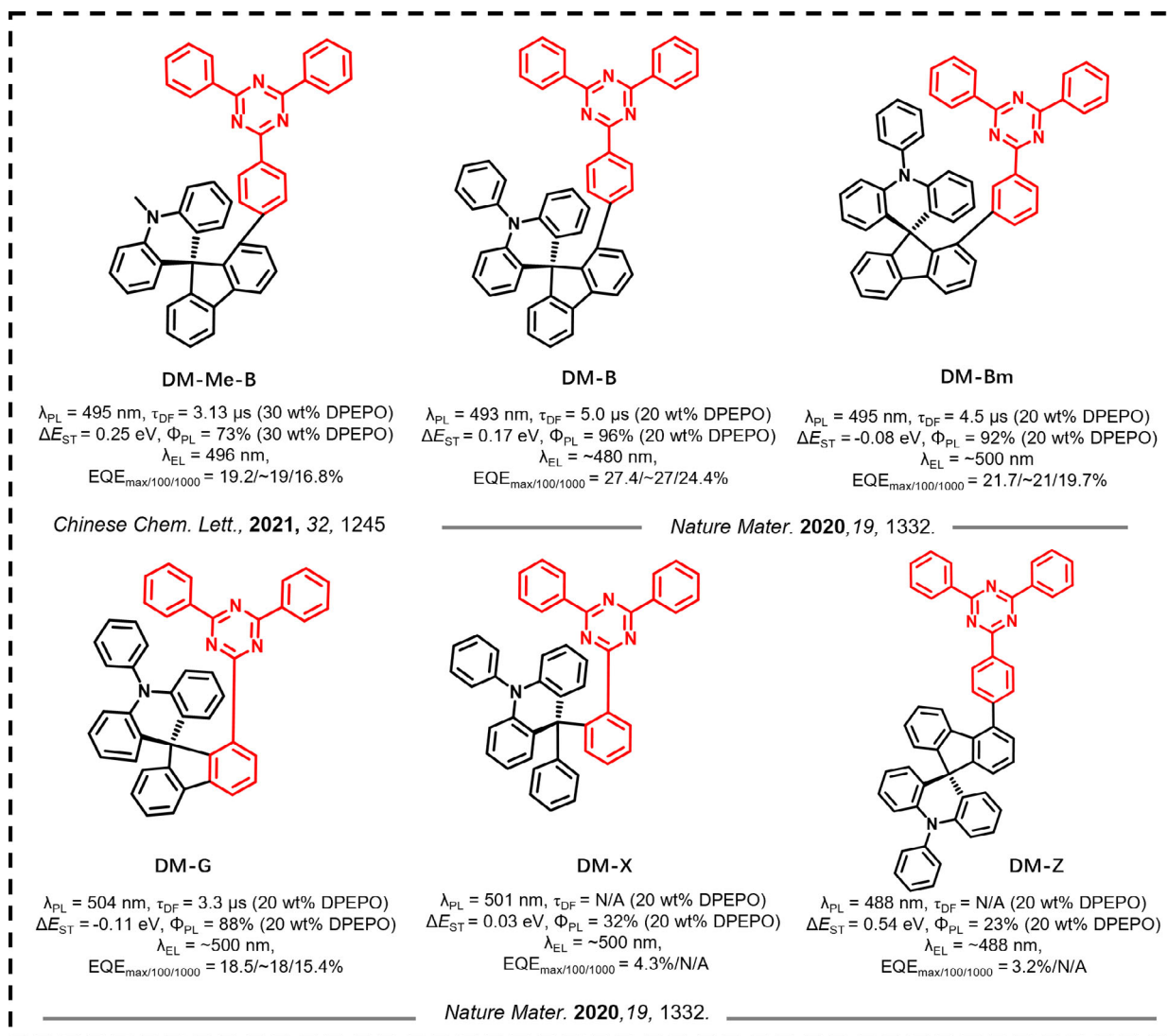


Figure 34. Molecular structures and properties of TADF emitters based on TSCT mechanism.

proportional to the Φ_{PL} of these emitters. In contrast, the devices based on the more flexible and less electronically coupled **DM-X** (20 wt% in DPEPO) and **DM-Z** (30 wt% in DPEPO) exhibit considerably lower maximum efficiencies of 4.3% and 3.2%, respectively.

Kaji et al.^[69] reported a TSCT compound **TpAT-tFFO** (Figure 35) based on the design strategy of controlling the distance and relative orientation between the adjacent tilted donor and acceptor moieties attached via the triptycene (Tp) scaffold. According to the DFT calculations, there is an increase in the energy levels of 1CT and 3CT states with increasing distance between the donor and acceptor (Figure 36b top). By contrast, the 3LE state only shows a weak dependence on the donor-acceptor distance. RISC is mediated by the intervening 3LE state between the 1CT and 3CT states, and the high k_{RISC} of $1.2 \times 10^7 \text{ s}^{-1}$ is ensured by the energy level matching of the three states. Importantly, the authors showed by DFT calculations that tilted face-to-face orientation between the donor and acceptor

greatly enhances the SOC between the 1CT and 3LE states, which is not the case for the coplanar conformation. **TpAT-tFFO** exhibited strong sky-blue emission with a λ_{PL} of 485 nm. The Φ_{PL} in toluene markedly increased from 1.8% to 84% after 30 min of Ar bubbling, while the Φ_{PL} of the film 25 wt% doped into the mCBP host and for the neat film were determined to be 76% and 71%, respectively. A device using an optimized doping concentration of 25 wt% showed an EQE_{max} of 19.2%. A gentle efficiency roll-off was obtained with EQEs of 19.1% and 18.1% at 100 cd m^{-2} and $1,000 \text{ cd m}^{-2}$, respectively; moreover, EQE of 14.4% and 11.6% were retained even at high luminance of $10,000 \text{ cd m}^{-2}$ and $20,000 \text{ cd m}^{-2}$.

Monkman et al.^[72] developed two unsymmetric donor-acceptor (D-D'-A) type emitters, **Ph₃TRZCzTPA** and **Ph₂TRZCzTPA** (Figure 35), where the co-facial overlap between D and A is controlled by the introduction of a weak (rigid) carbazole donor bridge (D'). According to the crystallographic data, the pendant (spacer) aryl rings are highly twisted from

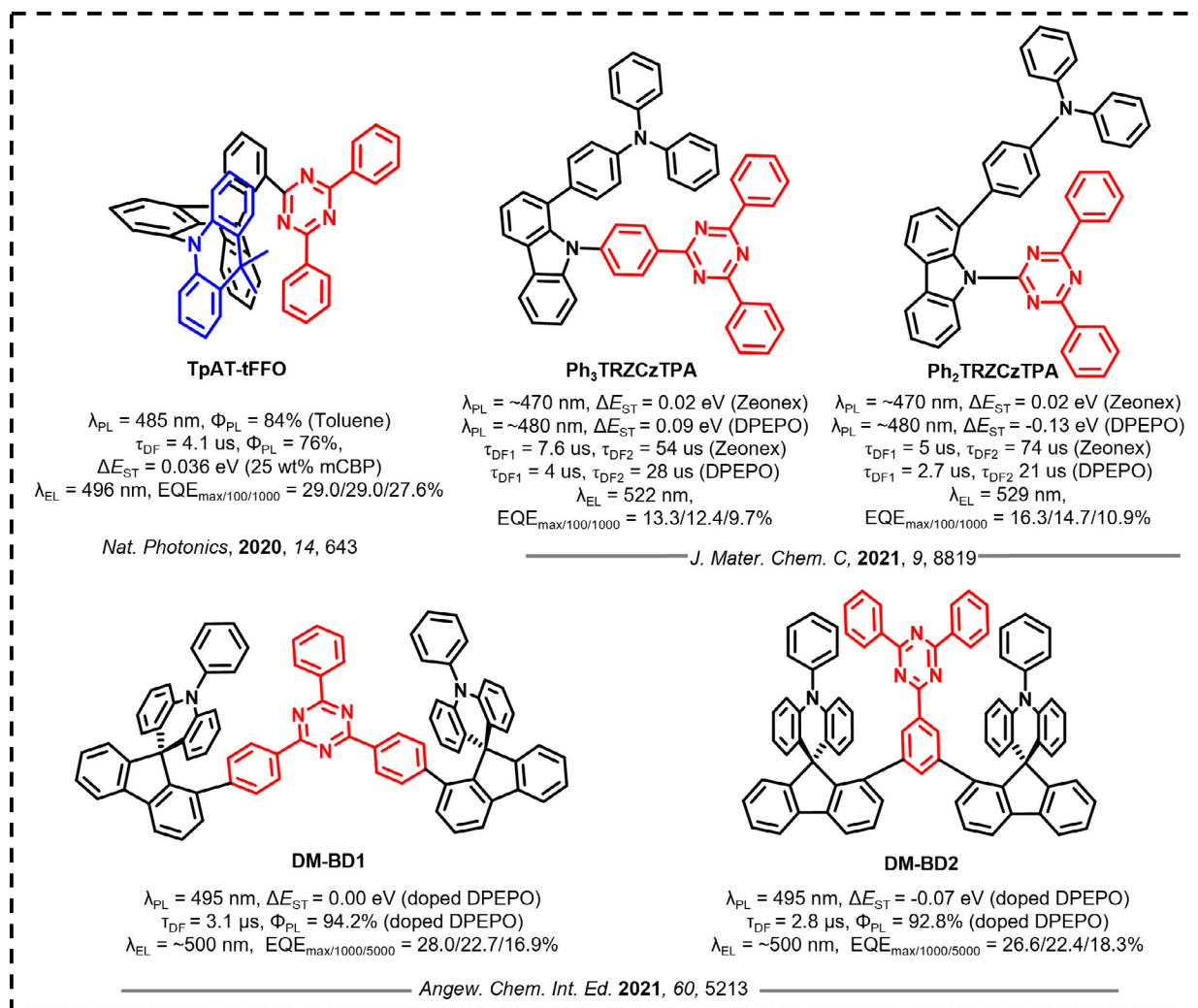


Figure 35. Molecular structures and properties of TADF emitters based on TSCT triazine motifs.

the carbazole bridge (*D'*) due to congested steric interactions. The short distances between the donor and acceptor enable the through space interaction. By comparing with the emission at 492 nm from the exciplex between TPA and TRZ in toluene, the identical emission observed from **Ph₃TRZCzTPA** and **Ph₂TRZCzTPA** indicates that the CT emission in both comes from a through-space intramolecular TRZ-TPA CT excited state. No contribution from a through-bond, TRZ—weak *D'* CT pair was observed. Both **Ph₃TRZCzTPA** and **Ph₂TRZCzTPA** have the same small ΔE_{ST} of 20 meV in Zeonex matrix. However, **Ph₂TRZCzTPA** has a faster k_{RISC} than **Ph₃TRZCzTPA**, which is ascribed to the more optimal tilted co-facial orientation of *D* and *A* forming the through-space CT state, which the authors contend is critical in controlling SOC and thus the RISC rate, as proposed by Kaji et al.^[69] The EQE_{max} values of the devices based on **Ph₃TRZCzTPA** (20 wt% in 26DCzPPy) and **Ph₂TRZCzTPA** (12 wt% in CBP) are 13.3% and 16.3%, respectively, which correlate with the relative RISC rates of the materials.

The π -stacked scaffold has also been expanded to spatially confine donor/acceptor/donor (D/A/D) motifs.^[73] Similar to the monomer analogs of **DM-B** and **DM-Bm**,^[70] **DM-BD1** and **DM-BD2** also rely on spatially confined donor-acceptor interaction but with two donors within one molecule in a sandwich-like structure (Figure 35). The single-crystal structures of **DM-BD1** and **DM-BD2** are shown in Figure 37. The additional donor is asserted to be helpful in realizing a more parallel D/A alignment, which results in a small ΔE_{ST} (0.00 eV for **DM-BD1** and -0.07 eV for **DM-BD2**) and fast k_{RISC} ($2.9 \times 10^5 \text{ s}^{-1}$ for **DM-BD1** and $3.1 \times 10^5 \text{ s}^{-1}$ for **DM-BD2**). The torsion angles between the donor and acceptor moieties were determined to be 30° for **DM-BD1** and 25° for **DM-BD2** from the crystal structures, where the not quite co-facial orientation has been demonstrated by Kaji et al.^[69] to be critical to turn on spin-orbit coupling and facilitate RISC. Interestingly, both compounds showed broad, structureless CT emission that are almost identical to those in solution, with a λ_{PL} of 495 nm. The Φ_{PL} of **DM-BD1** (10 wt% doped in DPEPO matrix) and **DM-BD2** (10 wt% doped in DPEPO matrix)

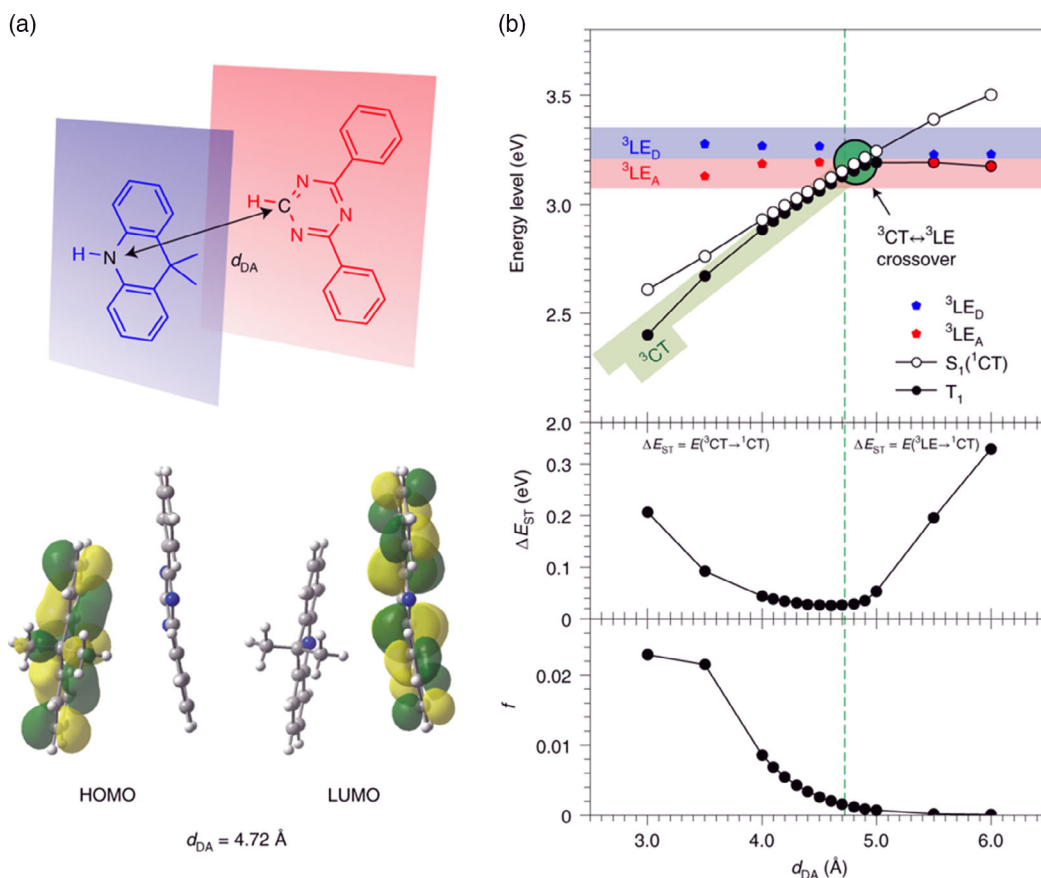


Figure 36. a) Structures of the donor (blue) and acceptor (red) segments (top). The donor and acceptor have a tilted ($\approx 10^\circ$) face-to-face alignment and are spatially separated at a certain distance, d_{DA} . HOMO and LUMO with d_{DA} of 4.72 Å (bottom). b) DFT-calculated energy levels of S_1 , T_1 , 3LE_D , and 3LE_A (top), ΔE_{ST} (middle) and f (bottom) as a function of d_{DA} , where 3LE_D and 3LE_A denote the 3LE states on the donor and acceptor segments, respectively. The vertical green dashed line indicates $d_{DA} = 4.72$ Å, which corresponds to d_{DA} of a DFT-optimized structure for TpAT-tFFO at the ground state. The blue, red, and green shaded regions highlight the energy levels of the 3LE_D , 3LE_A , and 3CT states, respectively. Reproduced with permission.^[69] Copyright 2020, Nature Portfolio.

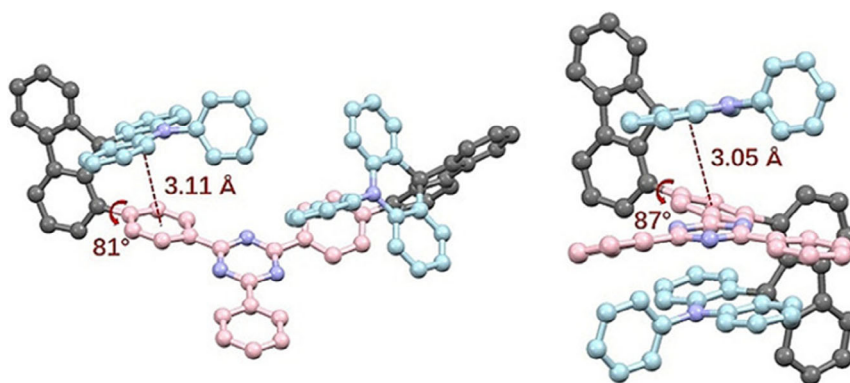


Figure 37. Single-crystal structures (hydrogen atoms are omitted) of DM-BD1 (left) and DM-BD2 (right). Reproduced with permission.^[73] Copyright 2021, Wiley-VCH.

were determined to be 94.2% and 92.8%, respectively. The near unity Φ_{PL} provides evidence of the effectiveness of this strategy to suppress nonradiative loss mechanisms. The best OLEDs contained a 30 wt% emitter and showed EQE_{max} of 28.0% and 26.6%, respectively, for devices with DM-BD1 and DM-BD2,

corresponding to CIE coordinates of (0.21, 0.47) and (0.20, 0.46), respectively.

To enhance the D–A electronic interactions by adjusting the D–A distance, Zhang et al.^[74] employed a xanthene bridge in two TSCT TADF emitters, mCz-Xo-TRZ and dCz-Xo-TRZ

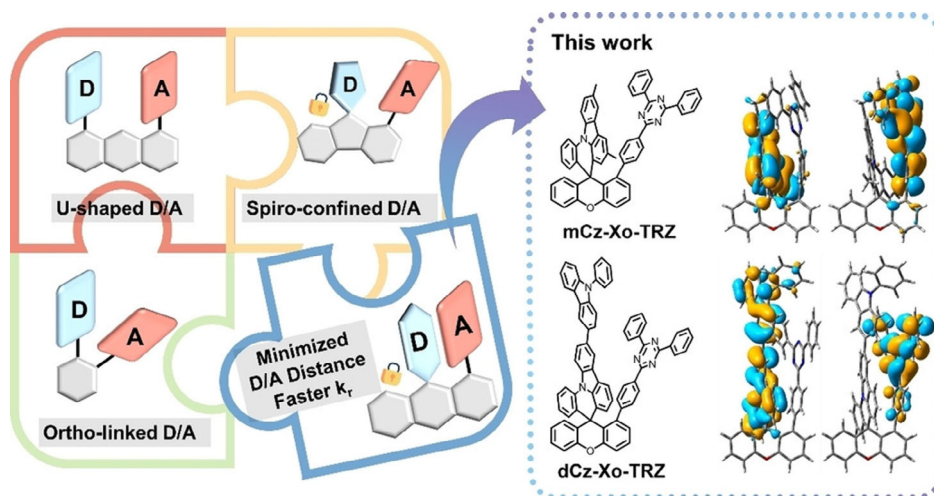


Figure 38. TSCT-TADF molecules with different types of donor–acceptor alignments and chemical structures of **mCz-Xo-TRZ** and **dCz-Xo-TRZ** with their HOMO/LUMO distribution. Reproduced with permission.^[74] Copyright 2022, Wiley-VCH.

(Figure 38), that possess space-confined face-to-face D–A alignment and minimized D–A distance down to 2.7–2.8 Å, which is shorter than twice the van der Waals radius of a carbon atom (1.7 Å). As a result, the greatly strengthened electronic interaction between D and A leads to fast k_r of 9.9 and $8.7 \times 10^6 \text{ s}^{-1}$ for **mCz-Xo-TRZ** and **dCz-Xo-TRZ**, respectively. The stronger donor in **dCz-Xo-TRZ** versus **mCz-Xo-TRZ** leads to a red-shift of the PL spectrum in toluene (from 454 to 461 nm) and the 30 wt% doped film in bis(diphenylphosphiny)l-dibenzofuran (PPF) matrix (from 469 to 482 nm). The Φ_{PL} values of 90% and 92% for **mCz-Xo-TRZ** and **dCz-Xo-TRZ**, respectively, are high; however, the k_{RISC} values are $3.0 \times 10^5 \text{ s}^{-1}$ and $3.3 \times 10^5 \text{ s}^{-1}$, respectively, which are significantly slower than that of **TpAT-tFFO** ($1.2 \times 10^7 \text{ s}^{-1}$). The blue OLEDs showed broad emission with λ_{EL} of 477 and 464 nm for devices with **dCz-Xo-TRZ** and **mCz-Xo-TRZ**, corresponding to the CIE coordinates of (0.16, 0.29) and (0.15, 0.20), respectively. The EQE_{max} of 27.8% for the device with **dCz-Xo-TRZ** and 21.0% for the device with **mCz-Xo-TRZ** showed only modest efficiency roll-off where the EQE values remained at 24.0% and 17.1% at a luminance of 1000 cd m^{-2} .

Zysman-Colman and co-workers recently reported a systematic study that documented explicitly in the PL spectrum emission from a TSCT in the compound **TPA-ace-TRZ**^[75] (Figure 39). This work provides a direct evidence that the TSCT plays a major role in the communication between the donor and acceptor. The photophysical studies in toluene of **TPA-ace-TRZ** show two characteristic lifetimes corresponding to the fast-decaying through-bond CT (TBCT) state ($\tau_{\text{PL}} = 9.6 \text{ ns}$) and longer lived TSCT state ($\tau_{\text{PL}} = 51 \text{ ns}$). The existence of the two different CT states was ascribed to rapid decay from the initially populated TBCT state (with moderate D–A dihedral angles of 48° between the TPA and ace units and 57° between the ace and TRZ units) to the more stable TSCT state. The Φ_{PL} of **TPA-ace-TRZ** was measured to be only 17%, which is due to the weak electronic communication between the donor and acceptor through the ace bridge (the ace unit is orthogonal and electronically decoupled from both

D and A groups). It was found the the lowest-energy triplet state resides on the ace bridge, which also leads to a large ΔE_{ST} of 0.48 eV (determined in 1 wt% ZEONEX film). The weak electronic communication makes it difficult for the triplet harvesting through the spin-vibronic coupling mechanism because the potentially mediating local triplet state resides on the ace bridge, which is orthogonal to both D and A and thus cannot efficiently couple to the TSCT state. Therefore, even though **TPA-ace-TRZ** possesses a strong TSCT state, it can hardly produce TADF because of the lack of coupling to a mediating LE triplet state. This study reveals the intimate interplay that the bridging ace group has on mediating both the TBCT state and the TSCT state.

Wang et al.^[76] incorporated TSCT states in the design of two star-shaped TADF emitters, containing DMAC (**Ac3TRZ3**) or a dendritic teracridan (**TAc3TRZ3**) as donors and TRZ as acceptors about a hexaphenylbenzene scaffold (Figure 40). Because of the

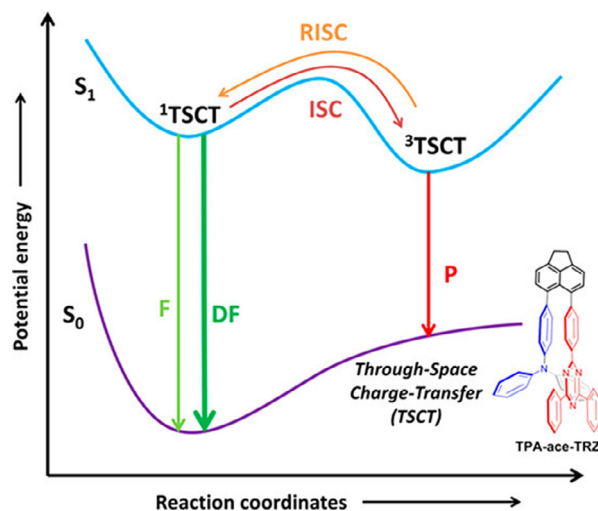


Figure 39. Molecular structure of **TPA-ace-TRZ** and schematic diagram of the potential energy involved in the S_0 and S_1 states. Reproduced with permission.^[75] Copyright 2021, American Chemical Society.

steric hindrance inherent in the structure both molecules adopt a propeller-shaped conformation in which the peripheral aromatic units are almost perpendicular to the central phenyl ring. As a result of the strong TSCT character coupled with the weak TBCT character due to the physical separation of donors and acceptors, both molecules show small ΔE_{ST} values of 0.04 eV for **TAc3TRZ3** and -0.08 eV for **Ac3TRZ3**. The negative ΔE_{ST} is likely due to different molecular geometries in the fully relaxed singlet and triplet states as also identified in **DM-Bm** and **DM-G**. Compared to **Ac3TRZ3** [Φ_{PL} : 54% 10 wt% in Ac6 (control compound contains six acridan donors)], **TAc3TRZ3**, containing the stronger dendritic donor, shows a higher Φ_{PL} of 63% (10 wt% in Ac6). The authors ascribed this higher photoluminescence quantum yield to the more efficient charge transfer in **TAc3TRZ3** mediated by the spatial π - π interactions. The use of the stronger dendritic donors also leads to a red-shift of the emission spectrum from λ_{PL} of 486 nm for **Ac3TRZ3** to λ_{PL} of 508 nm for **TAc3TRZ3**. The nondoped OLEDs showed EQE_{max} of 3.5% and 3.1% for the devices with **Ac3TRZ3** [λ_{EL} : 492 nm; CIE = (0.22, 0.42)] and **TAc3TRZ3** [λ_{EL} : 503 nm; CIE = (0.25, 0.47)], respectively. However, the doped devices showed improved EQE_{max} of 11.0% and 14.2% for the devices with **Ac3TRZ3** [λ_{EL} : 520 nm; CIE = (0.30, 0.54)] and **TAc3TRZ3** [λ_{EL} : 538 nm; CIE = (0.22, 0.48)], respectively.

Wang et al.^[77] also prepared a series of blue TADF polymers that exploit only TSCT to electronically couple donor and acceptor moieties (Figure 41). The polymers use a nonconjugated

polyethylene backbone, 9,9-dimethyl-10-phenyl-acridan (**Ac**) or 9,9-bis(1,3-di-*tert*-butylphenyl)-10-phenyl-acridan (**TBAc**) as the donor pendant and TRZ as the acceptor pendant. In this design, D and A units are not directly electronically decoupled, but are spatially close to each other, allowing through-space, rather than the TBCT processes to occur. The TSCT character observed from the Ac-based polymer results in both a small ΔE_{ST} of 0.019 eV and moderate Φ_{PL} of 60% in the neat film. In comparison, the **TBAc**-based polymers only exhibited fast prompt fluorescence emission without TSCT contribution because the steric 1,3-dibutylphenyl groups separate the electron-donating acridan unit from the electron-accepting triazine unit, which weakens the TSCT transition. The device with a polymer consisting of 95 mol% Ac and 5 mol% TRZ content demonstrated the best device performance with CIE coordinates of (0.18, 0.27) and an EQE_{max} of 12.1%. The optoelectronic properties of the aforementioned materials are summarized in Table 15, and the device performance metrics are summarized in Table 16.

10. Chiral TADF Emitters Containing Triazine

Circularly polarized luminescence (CPL) materials have attracted great attention due to their potential applications in optical data storage,^[78] chirality sensing,^[79] organic electronic devices,^[80] and bio imaging.^[81] In 1997, Meijer et al.^[82] developed the first example of a circularly polarized OLED (CP-OLED). Since then, many chiral emitters have been explored, including chiral polymers,^[83]

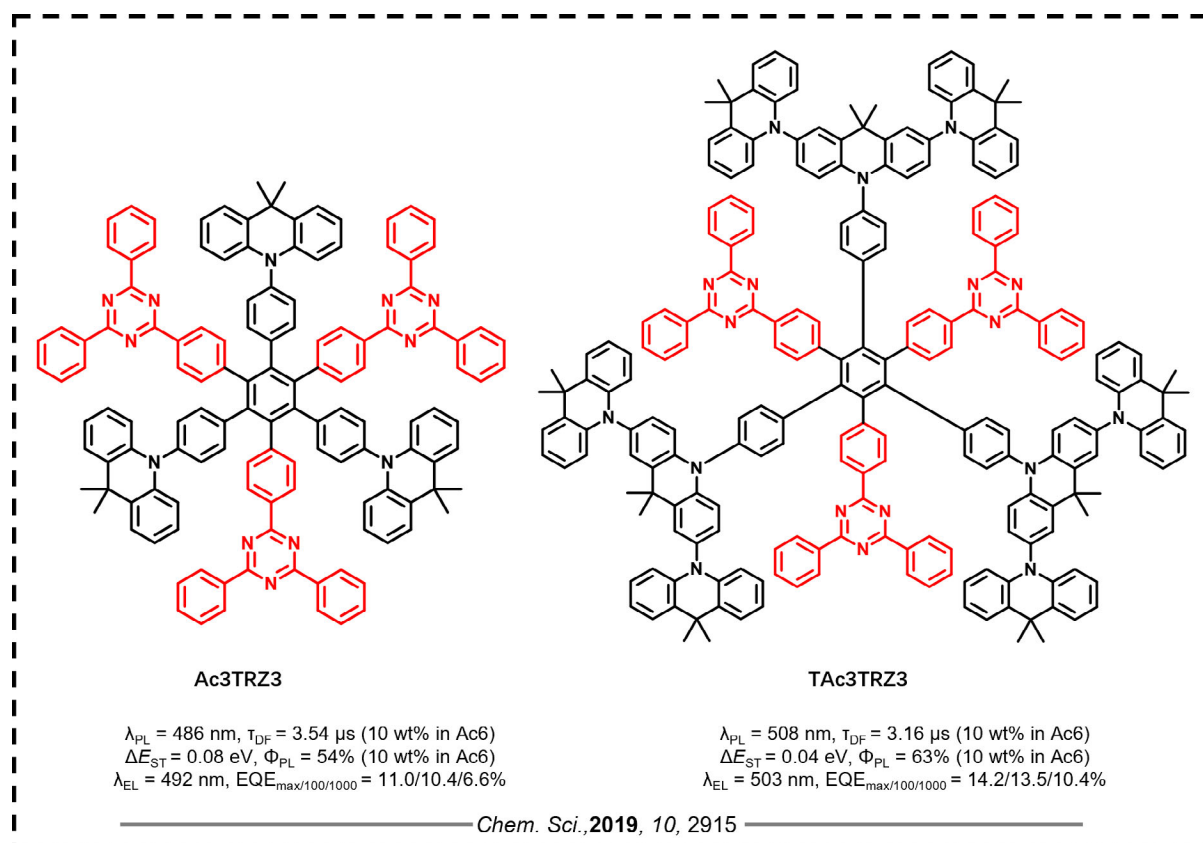


Figure 40. Molecular structures and properties of TADF dendrimer emitters based on TSCT hexaarylbenzene motifs.

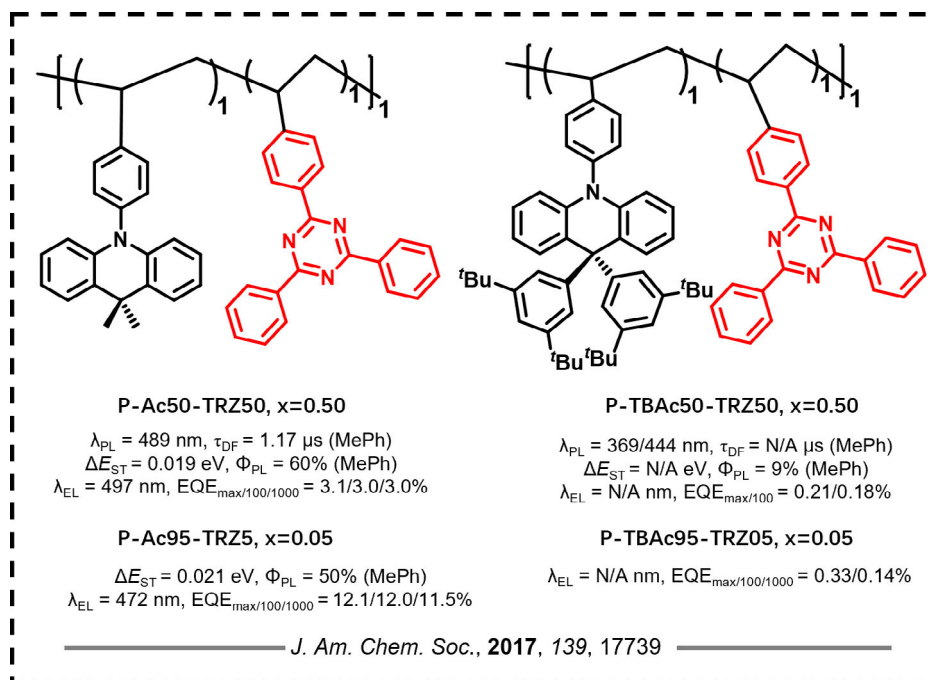


Figure 41. Molecular structures and properties of TADF polymer emitters with nonconjugated backbone and TSCT effect.

chiral phosphorescent complexes,^[84] and chiral TADF small molecules.^[85] Of the latter, there are a few examples of chiral TADF emitters incorporating a triazine acceptor.

In 2019, Zysman-Colman and co-workers^[15] introduced the carbazolophane (Czp) donor unit (indolo[2.2]paracyclophane) for the design of chiral TADF emitters, **R_p-CzpPhTrz** and **S_p-CzpPhTrz** (Figure 42). The bulky carbazolophane donor unit increased the torsion between the donor and the phenylene bridge compared to the control compound **CzPhTrz** (same structure as **CzTRZ** discussed in Section 2). As discussed above, **CzPhTrz** was known to be a non-TADF compound; however, the larger torsion between the donor and the bridge in **CzpPhTrz** leads to a decreased ΔE_{ST} of 0.16 eV, which contributes to the turn on of the TADF. **rac-CzpPhTrz** is a sky-blue emitter with λ_{PL} of 482 nm, and high Φ_{PL} of 69% in 10 wt% doped DPEPO films. The chiroptical properties of the enantiomers **R_p-CzpPhTrz** and **S_p-CzpPhTrz** reveal mirror image circular dichroism (CD) and CPL, with g_{lum} values of 5×10^{-3} / -7×10^{-3} , respectively. Sky blue-emitting OLEDs were fabricated with an EQE_{max} of 17% and associated CIE coordinates of (0.17, 0.25).

Zheng et al.^[86] reported a pair of chiral TADF emitters (Figure 42), **R_p-5** and **S_p-5**, by combining a TRZ acceptor with a chiral donor group (PXZp). PXZp is a phenoxazine derivative containing an annulated [2.2]paracyclophane (pCp) skeleton which has ever been demonstrated as an efficient unit enabling a blue chiral TADF emitters by Zysman-Colman and co-workers in 2019.^[15] Similar to their analog **PXZ-TRZ** (λ_{PL} : 540 nm; Φ_{PL} : 66%; τ_d : 1.1 μ s in 8 wt% mCPCN; ΔE_{ST} : 0.017 eV), **R_p-5** and **S_p-5** exhibited broad PL with λ_{PL} of 548 nm (in toluene), 539 nm (in neat film), and 527 nm (in 10 wt% CBP film). A moderate Φ_{PL} of 60% as well as a small ΔE_{ST} of 0.03 (in 10 wt% CBP film)

resemble the photophysical properties of **PXZ-TRZ**, indicating the weak influence from the pCp on the TADF properties. The dissymmetry values, g_{lum} , of **R_p-5** and **S_p-5** (Figure 43) are -2.4×10^{-3} / $+3.3 \times 10^{-3}$ and -2.3×10^{-3} / $+2.7 \times 10^{-3}$ in toluene (1×10^{-5} mol L⁻¹) and neat films, respectively, which are typical values from organic emitters. Solution-processed CP-OLEDs showed EQE_{max} of 7.8%/7.1% and g_{EL} of $+1.4 \times 10^{-3}$ / -2.0×10^{-3} . Although the nondoped devices based on **S_p-5** / **R_p-5** possessed lower EQE_{max} of 2.5%/1.8%; however, the g_{EL} improved modestly to $+4.3 \times 10^{-3}$ / -4.6×10^{-3} .

A pair of triptycene-based enantiomers, **(S,S)/(R,R)-TpAc-TRZ**,^[87] were developed containing a triptycene-fused diacridine chiral donor (S,S)/(R,R)-TpAc (Figure 42). The compounds can be recognized as the combination of two well-known **DMAC-TRZ** TADF emitters through a nonconjugate 3D triptycene bridge. Therefore, the excellent TADF properties of **DMAC-TRZ** are still maintained for the enantiomers, especially the suppression of concentration quenching in their neat films. The **(S,S)-TpAc-TRZ** neat film (λ_{PL} : 541 nm; Φ_{PL} : 85%; τ_d : 1.1 μ s; ΔE_{ST} : 0.03 eV) showed photophysical properties reminiscent to those of the **DMAC-TRZ** in neat film (λ_{PL} : 500 nm; Φ_{PL} : 83%; τ_d : 3.6 μ s; ΔE_{ST} : 0.05 eV), except for the 41 nm red-shift in the PL. The circular dichroism (CD) spectra of **(S,S)-(+)-TpAc-TRZ** and **(R,R)-(-)-TpAc-TRZ** exhibited clear mirror-image relationship with alternating positive and negative cotton effects (Figure 44). The g_{PL} values are $+1.9 \times 10^{-3}$ for **(S,S)-(+)-TpAc-TRZ** and -1.8×10^{-3} for **(R,R)-(-)-TpAc-TRZ** in neat films. Due to the high molecular weight of the emitters, only solution-processed OLEDs were fabricated, with an EQE_{max} of 25.5% (λ_{EL} : 534 nm). However, a significant efficiency roll-off was observed and the EQE decreased to 1.6% at a luminance of 1000 cd m⁻².

Table 15. Summary of photophysical and electrochemical properties.

Emitter	Solution $\lambda_{\text{PL}}/\Phi_{\text{PL}}/\tau_{\text{d}}$ (medium) [nm/%/ μs]	Solid State $\lambda_{\text{PL}}/\Phi_{\text{PL}}/\tau_{\text{d}}$ (medium) [nm/%/ μs]	ΔE_{ST} [eV]	HOMO [eV]	LUMO [eV]	Ref.
XPT	562/7.7/2.3(PhMe)	-/66/- (10 wt% in DPEPO)	-	-4.99	-2.22	[63]
XCT	419/5.9/3.0(PhMe)	-/-/-	-	-5.58	-2.39	[63]
XtBuCT	451/6/2.0(PhMe)	-35/- (10 wt% in DPEPO)	-	-5.49	-2.33	[63]
oBFCzTRZ	\approx 480/-/- (PhMe)	-/97.9/5.4 (in neat film)	0.002	-6.10	-3.40	[64]
mBFCzTRZ	\approx 450/-/- (PhMe)	-/31.1/29.6 (in neat film)	0.19	-6.10	-3.30	[64]
pBFCzTRZ	\approx 430/-/- (PhMe)	-/85.3/31.2 (in neat film)	0.30	-6.10	-3.20	[64]
oBFCzTRZ	-/-/-	-/100/- (8 wt% in DPEPO)	-	-	-	[64]
DPA-o-TRZ	-/-/-	-/-/1.62(mCP)	0.03	-5.84	-3.25	[65]
MPA-o-TRZ	-/-/-	-/-/1.08(mCP)	0.01	-5.7	-3.26	[65]
BCzTRZDBF	-/-/-	\approx 490/83.4/5.4(5 wt% in mCBPTRZ)	0.06	-5.85	-3.34	[67]
TCzTRZDBF	-/-/-	\approx 510/86.3/4.4(5 wt% in mCBPTRZ)	0.01	-5.87	-3.43	[67]
IDCzTRZDBF	-/-/-	\approx 480/85.4/2.8(5 wt% in mCBPTRZ)	0.05	-5.88	-3.34	[67]
SF12oTz	-/-/-	491/92/4.6(10 wt% in DPEPO)	0.05	-5.58	-2.92	[68]
SF23oTz	-/-/-	473/86/4.3(10 wt% in DPEPO)	0.08	-5.6	-2.87	[68]
SF34oTz	-/-/-	479/65/8.2(10 wt% in DPEPO)	0.29	-5.71	-2.88	[68]
DM-Me-B	-/- (PhMe)	495/73/3.1(30 wt% in DPEPO)	0.25	-5.29	-2.88	[71]
DM-B	-/-/- (PhMe)	493/96/5.0(20 wt% in DPEPO)	0.17	-	-	[70]
DM-Bm	-/-/- (PhMe)	495/92/4.5(20 wt% in DPEPO)	-0.08	-	-	[70]
DM-G	-/-/- (PhMe)	504/88/3.3(20 wt% in DPEPO)	-0.11	-	-	[70]
DM-X	-/-/- (PhMe)	504/32/- (20 wt% in DPEPO)	0.03	-	-	[70]
DM-Z	-/-/- (PhMe)	488/23/- (20 wt% in DPEPO)	0.54	-	-	[70]
Ac3TRZ3	486/-/- (PhMe)	-/54/3.5(10 wt% in Ac6)	0.08	-5.28	-2.96	[76]
TAc3TRZ3	508/-/- (PhMe)	-/63/3.2(10 wt% in Ac6)	0.04	-5.10	-2.94	[76]
P-Ac50-TRZ50	489/60/1.2(PhMe)	-/-/-	0.02	-5.26	-2.68	[77]
P-TBAc50-TRZ50	444/9/- (PhMe)	-/-/-	-	-5.30	-2.64	[77]

Similar to g_{PL} , the g_{EL} values reached to $+1.5 \times 10^{-3}$ for the (S,S)-(+)-TpAc-TRZ-based device and -2.0×10^{-3} for (R,R)-(-)-TpAc-TRZ-based device.

Chen et al.^[88] reported a pair of macrocyclic TADF enantiomers (+)-(R,R)-MC and (-)-(S,S)-MC linking chiral octahydrobinaphthol units with a DMAC-TRZ derivative (Figure 42). The four-unit nonconjugated macrocycle consisting of two donors and two acceptors shows TADF. Similar to DMAC-TRZ, the enantiomers (+)-(R,R)-MC and (-)-(S,S)-MC showed a small ΔE_{ST} of 0.067 eV, a short τ_{d} of 1.5 μs , suppressed concentration quenching in neat films and Φ_{PL} of 79.7% (25 wt% (+)-(R,R)-MC: CBP). The $|g_{\text{PL}}|$ of 2.2×10^{-3} in solution (Figure 45) and mirror image CD spectra are typical for chiral TADF emitters. The solution-processed CP-OLEDs (25 wt% (+)-(R,R)-MC/ (-)-(S,S)-MC: CBP) displayed EQE_{max} of 17.1%/15.5% and g_{EL} of $1.5 \times 10^{-3}/-1.7 \times 10^{-3}$.

Based on the molecule structure of DM-B, Jiang et al. reported two chiral derivatives SFST and SFOT (Figure 46),^[89] which contain asymmetric donors with either PTZ or PXZ attached onto the spiro-skeleton linkage. Similar to DM-B, both SFST (λ_{PL} : 512 nm; Φ_{PL} : 53.1%; τ_{d} : 6.78 μs ; ΔE_{ST} : 0.052 eV; 30 wt% in mCBP) and SFOT (λ_{PL} : 512 nm; Φ_{PL} : 89.0%; τ_{d} : 7.98 μs ;

ΔE_{ST} : 0.053 eV; 30 wt% in mCBP) are TSCT emitters where the donor and acceptor are aligned in a near co-facial manner. The difference between SFST and SFOT is based on the heteroatoms contained within the donor. As shown in Figure 47, the CD spectra of (R)-SFST/(S)-SFST and (R)-SFOT/(S)-SFOT show the typical mirror-image feature of enantiomeric molecules. The dissymmetry values g_{lum} of (S)-SFOT/(R)-SFOT in toluene are 2.2×10^{-3} and -2.0×10^{-3} , respectively. Interestingly, the g_{lum} values of (S)-SFST/(R)-SFST are almost twice those of (S)-SFOT/(R)-SFOT, at 3.4×10^{-3} and -4.0×10^{-3} , respectively. This change can be attributed to the more distorted structure of SFST due to the presence of the larger sulfur atom. The CPEL signals of the CP-OLEDs, g_{EL} , are 1.30×10^{-3} and 1.0×10^{-3} for the devices with (S)-SFST and (S)-SFOT, respectively.

Based on the same design strategy and structurally similar to SFST and SFOT, another analog SDMAC (Figure 48) has also been reported by Jiang et al.^[90] SDMAC also shows CPL emission, as well as aggregation-induced emission enhancement (AIEE), solvatochromic, and piezochromic luminescence. It is reasonable to speculate that the analogs SFST and SFOT can also possess these same multistimulus response properties because

Table 16. Summary of device structures and performances.

Emitter	Device Structure	EL _{max} [nm]	CIE	V _{on} [V]	EQE/PE/CE ^{a)} [%/lm W ⁻¹ /cd A ⁻¹]	EQE _{100/1000} [cd] [m] ⁻²	Ref.
XPT	ITO/TAPC/DPEPO: 10% emitter/DPEPO/ TmPyPb/LiF/Al	584	–	≈3.2	10/–/–	–/–	[63]
XtBuCT	ITO/TAPC/DPEPO: 10% emitter/DPEPO/ TmPyPb/LiF/Al	488	–	≈4.0	4/–/–	–/–	[63]
oBFCzTRZ	ITO/PEDOT:PSS/TAPC/mCP/DPEPO:20% oBFCzTRZ/TSPO1/TPBi/LiF/Al	477	(0.18, 0.31)	–	20.4/–/–	20.0/17.4	[64]
mBFCzTRZ	ITO/PEDOT:PSS/TAPC/mCP/DPEPO:20% mBFCzTRZ/TSPO1/TPBi/LiF/Al	473	(0.17, 0.25)	–	13.2/–/–	≈8.0/≈2.0	[64]
pBFCzTRZ	ITO/PEDOT:PSS/TAPC/mCP/DPEPO:20% pBFCzTRZ/TSPO1/TPBi/LiF/Al	465	(0.15, 0.18)	–	16.7/–/–	≈10.0/≈5.0	[64]
DPA–o–TRZ	ITO/PEDOT:PSS/TAPC/mCP/mCP:TSPO1: 5% emitter/TSPO1/LiF/Al	497	(0.21, 0.45)	≈4.2	17.2/34.5/45	≈16.0/10.5	[65]
MPA–o–TRZ	ITO/PEDOT:PSS/TAPC/mCP/mCP:TSPO1: 5% emitter/TSPO1/LiF/Al	532	(0.35, 0.58)	≈4.2	16.3/41.9/54.7	≈15.0/12.7	[65]
BCzTRZDBF	ITO/DNTPD/BPBPA/PCzAC/mCBPTRZ:5 wt% BCzTRZDBF/DBFTRZ/ZADN/LiF/Al	≈490	(0.24, 0.52)	–	20.1/35.1/59.6	≈20.0/≈15.0	[67]
TCzTRZDBF	ITO/DNTPD/BPBPA/PCzAC/mCBPTRZ:5 wt% TCzTRZDBF/DBFTRZ/ZADN/LiF/Al	≈500	(0.27, 0.57)	–	23.5/44.7/74.8	≈23.0/≈20.0	[67]
IDCzTRZDBF	ITO/DNTPD/BPBPA/PCzAC/mCBPTRZ:5 wt% IDCzTRZDBF/DBFTRZ/ZADN/LiF/Al	≈485	(0.22, 0.48)	–	12.2/19.3/33.6	≈12.0/≈11.0	[67]
SF12oTz	ITO/MoO ₃ /TAPC/mCP/DPEPO: 20% SF12oTz/ DPEPO/TmPyPB/LiF/Al	496	(0.23, 0.47)	2.9	22.4/59.1/60.4	22.3/20.0	[68]
SF23oTz	ITO/MoO ₃ /TAPC/mCP/DPEPO: 20% SF23oTz/ DPEPO/TmPyPB/LiF/Al	484	(0.19, 0.35)	3.2	19.6/45.5/46.9	18.9/15.9	[68]
SF34oTz	ITO/MoO ₃ /TAPC/mCP/DPEPO: 20% SF34oTz/ DPEPO/TmPyPB/LiF/Al	482	0.18, 0.37	3.2	14.6/31/31.4	8.5/3.1	[68]
DM–Me–B	ITO/HAT–CN/TAPC/TCTA/mCP/DPEPO:30% emitters/DPEPO/TmPyPB/Liq/Al	500	(0.26, 0.48)	–	19.2/–/–	≈19.0/16.8	[71]
DM–B	ITO/HAT–CN/TAPC/TCTA/mCP/DPEPO:50% emitters/DPEPO/TmPyPB/Liq/Al	≈488	(0.20, 0.44)	2.8	27.4/68.1/–	≈27.0/24.4	[70]
DM–Bm	ITO/HAT–CN/TAPC/TCTA/mCP/DPEPO:30% emitters/DPEPO/TmPyPB/Liq/Al	≈500	(0.22, 0.48)	2.6	21.7/62.7/–	≈21.0/19.7	[70]
DM–G	ITO/HAT–CN/TAPC/TCTA/mCP/DPEPO:20% emitters/DPEPO/TmPyPB/Liq/Al	≈500	(0.24, 0.50)	3	18.5/47.5/–	≈18.0/15.4	[70]
DM–X	ITO/HAT–CN/TAPC/TCTA/mCP/DPEPO:20% emitters/DPEPO/TmPyPB/Liq/Al	≈500	(0.23, 0.45)	3.4	4.3/10.2/–	–/–	[70]
DM–Z	ITO/HAT–CN/TAPC/TCTA/mCP/DPEPO:30% emitters/DPEPO/TmPyPB/Liq/Al	≈488	(0.19, 0.35)	3.9	3.2/5.1/–	–/–	[70]
Ac3TRZ3	ITO/PEDOT:PSS/Ac6: 10 wt% Ac3TRZ3/TSPO1/ TmPyPB/LiF/Al	492	(0.22, 0.42)	2.9	11/–/30.3	10.4/6.6	[76]
TAc3TRZ3	ITO/PEDOT:PSS/Ac6: 10 wt% TAc3TRZ3/ TSPO1/TmPyPB/LiF/Al	503	(0.25, 0.47)	2.9	14.2/–/40.6	13.5/10.4	[76]
P–Ac50–TRZ50	ITO/PEDOT:PSS/EML/TSPO1/TmPyPB/LiF/Al	497	0.222, 0.428	3.4	3.1/–/8.5	3.0/3.0	[77]
P–Ac95–TRZ05	ITO/PEDOT:PSS/polymer/TSPO1/TmPyPB/LiF/Al	472	0.176, 0.269	3.2	12.1/–/24.8	12.0/11.5	[77]
P–TBAc50–TRZ50	ITO/PEDOT:PSS/polymer/TSPO1/TmPyPB/LiF/Al	453	0.235, 0.243	3.8	0.21/–/0.6	0.18/–	[77]
P–TBAc95–TRZ05	ITO/PEDOT:PSS/polymer/TSPO1/TmPyPB/LiF/Al	445	0.207, 0.196	5.8	0.33/–/0.51	0.14/–	[77]

of their similar molecule framework. **SDMAC** has a smaller ΔE_{ST} of 0.034 eV than that of **SFST** and **SFOT**, which is evidenced by the shortest delayed emission lifetime of 4.17 μ s in contrast to

6.78 μ s and 7.98 μ s for **SFST** and **SFOT**, respectively. The Φ_{PL} is 90% in a doped film containing 30 wt% **SDMAC** in 2,8-bis(diphenylphosphoryl)dibenzo[b,d]furan (PPF). Both the CD and

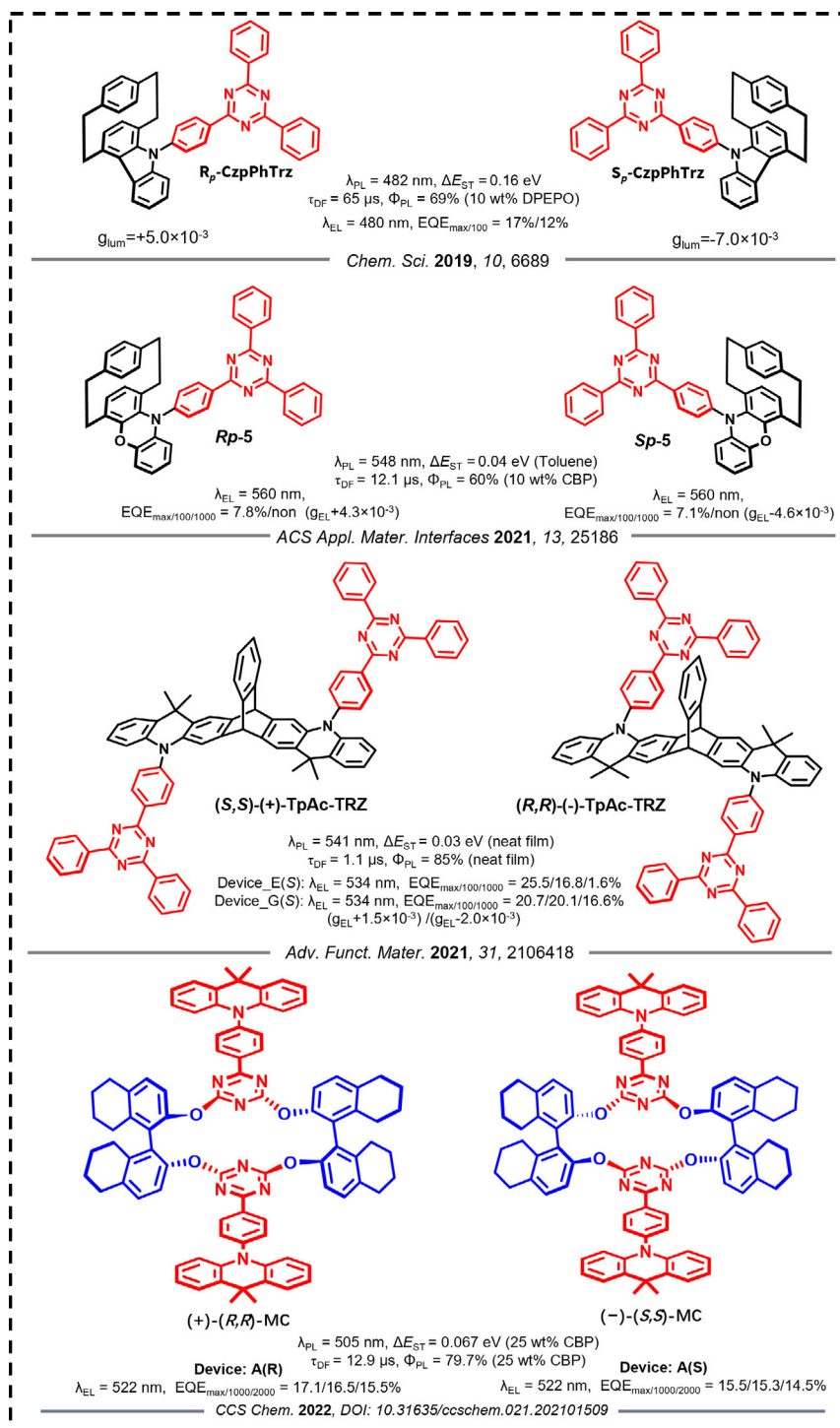


Figure 42. Molecular structures and properties of chiral TADF emitters based on triazine.

CPL spectra of the enantiomers (*R*)-SDMAC and (*S*)-SDMAC measured in dilute dichloromethane solutions (10^{-5} M) exhibit mirror symmetry. The g_{lum} values of (*R*)-SDMAC and (*S*)-SDMAC are -1.19×10^{-3} and $+1.39 \times 10^{-3}$, respectively, while the CP-OLEDs showed relatively lower g_{EL} values than g_{lum} of -8.43×10^{-4} and $+9.80 \times 10^{-4}$ for (*R*)-SDMAC and

(*S*)-SDMAC, respectively. The OLED device (30 wt% of SDMAC doped into PPF) was also optimized by adjusting the thickness of the electron injection layer (TmPyPB) from 25 nm to 40 nm. An EQE_{max} of 28.4% was achieved at 35 nm thickness of the EIL, and it remained as high as 24.5% at 100 cd m^{-2} ; however, the EQE then dropped by 40% to 17.1% at 1000 cd m^{-2} (Table 17 and 18).

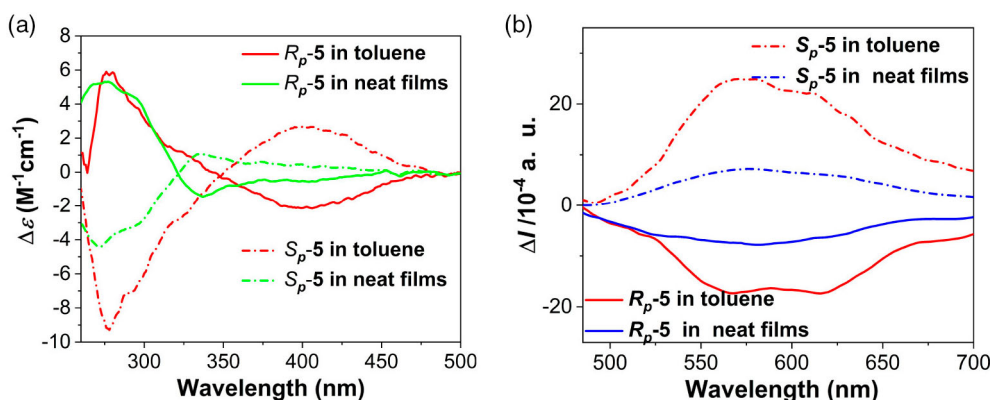


Figure 43. a) CD and b) CPL spectra of S_p-5/R_p-5 . Reproduced with permission.^[86] Copyright 2021, Wiley-VCH.

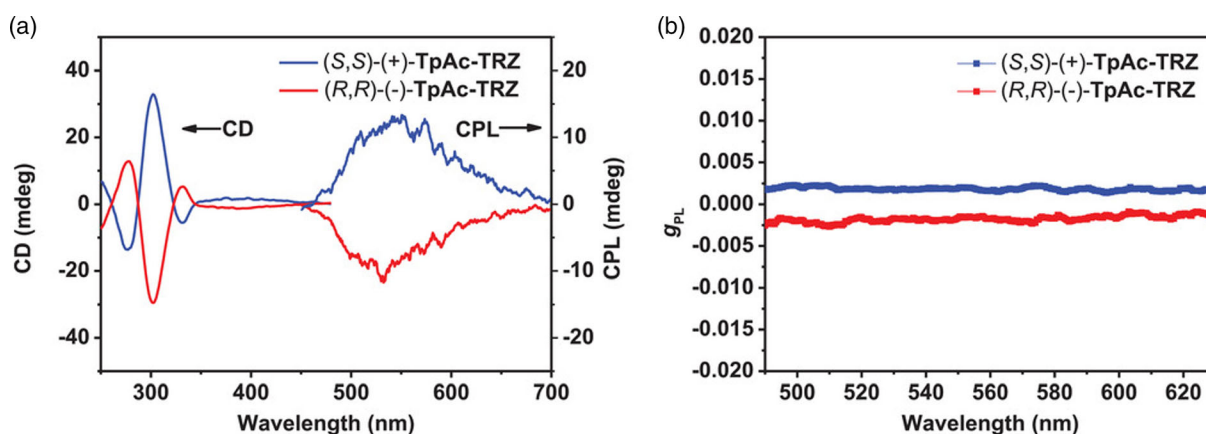


Figure 44. a) CD and CPL spectra of $(S,S)-/(R,R)-TpAc-TRZ$ in neat film states. b) g_{PL} versus wavelength curves of $(S,S)-/(R,R)-TpAc-TRZ$ in neat film states. Reproduced with permission.^[87] Copyright 2021, Wiley-VCH.

11. TADF Emitters Based on Triazine and Other Donors

In addition to carbazole, many alternative *N*-heterocycle donors have also been investigated as building blocks in triazine-based TADF emitters. 9,9-dimethyl-9,10-dihydroacridine (DMAC), 10 *H*-phenoxazine (PXZ), and 10 *H*-phenothiazine (PTZ) are the most popular six-membered *N*-heterocyclic donors used in the design of TADF emitters. The sequence of electron-donating strength typically follows $PTZ > PXZ > DMAC > carbazole$, with carbazole being the weakest donor. Unlike carbazole, the use of these larger *N*-heterocyclic donors generally produces a highly twisted conformation between the donor and the bridging units when they are *N*-bound because of the increased steric hindrance. As a result, the highly twisted conformation leads to a greater separation of the FMOs, which generally results in a small ΔE_{ST} .

Wu et al.^[91] reported what is now considered one of the most widely studied TADF emitters, **DMAC-TRZ** (λ_{PL} : 495 nm; Φ_{PL} : 90%; τ_d : 1.9 μ s; ΔE_{ST} : 0.05 eV; in 8 wt% mCPCN) as shown in **Figure 49**. **DMAC-TRZ** shows high Φ_{PL} (90%) in an 8 wt% mCPCN doped film, which is not much reduced in the neat film

(83%). The EQE_{max} of doped and non-doped device based on **DMAC-TRZ** were reported to be 26.5% and 20%, respectively, reflecting in part the differences in Φ_{PL} . Due to its good solubility, a solution-processed non-doped OLED showed only a slightly lower EQE_{max} of 17.6%. Hu et al.^[92] observed that photoexciting CT states can lead to a magneto-PL signal in the SOC regime, but not found when photoexciting LE states. This is the first experimental evidence that SOC is produced in CT states. Furthermore, they found that the **DMAC-TRZ**-based OLEDs demonstrated magneto-EL in the high field regime (> 10 mT).^[92] This high-field magneto-EL signal provides direct evidence to indicate that the SOC is indeed enhanced, in the absence of heavy elements, towards developing spin-dependent TADF in OLEDs. Compared with **DMAC-TRZ** (λ_{PL} : 495 nm; Φ_{PL} : 90%; τ_d : 1.9 μ s; ΔE_{ST} : 0.05 eV; in 8 wt% mCPCN), the emission spectrum of **PXZ-TRZ** (λ_{PL} : 540 nm; Φ_{PL} : 66%; τ_d : 1.1 μ s in 8 wt% mCPCN; ΔE_{ST} : 0.017 eV) is red-shifted by about 45 nm due to the enhanced electron-donating ability of the PXZ. Even though both compounds show similarly small ΔE_{ST} and relatively short delayed fluorescence lifetimes (τ_d : 1.1 μ s; ΔE_{ST} : 0.017 eV; 8 wt% **PXZ-TRZ** in mCPCN), the much lower Φ_{PL} of **PXZ-TRZ** (66% in 8 wt% mCPCN) indicates greater nonradiative decay, which

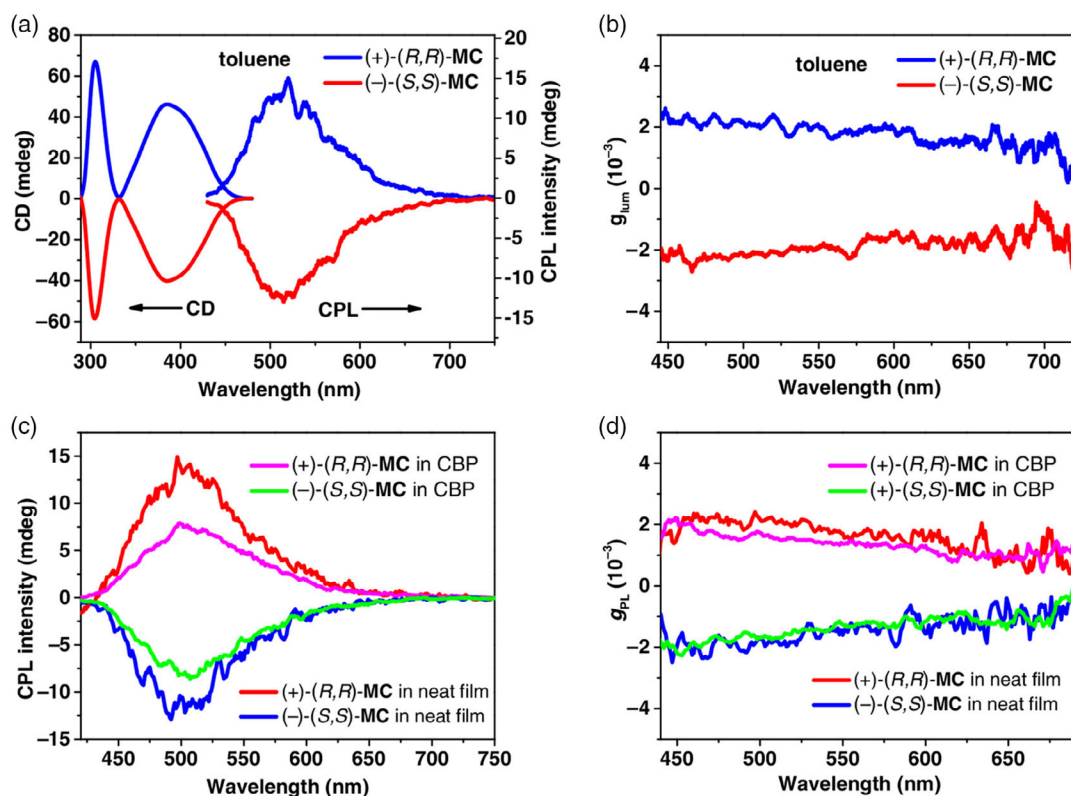


Figure 45. a) CD and CPL spectra and b) g_{PL} versus wavelength curves of (+)-(R,R)/(-)-(S,S)-MC in toluene ($c = 1 \times 10^{-4}$ M). c) CPL spectra and d) g_{PL} versus wavelength curves of (+)-(R,R)/(-)-(S,S)-MC in neat film and doped film (25 wt% macrocyclic enantiomers: CBP).

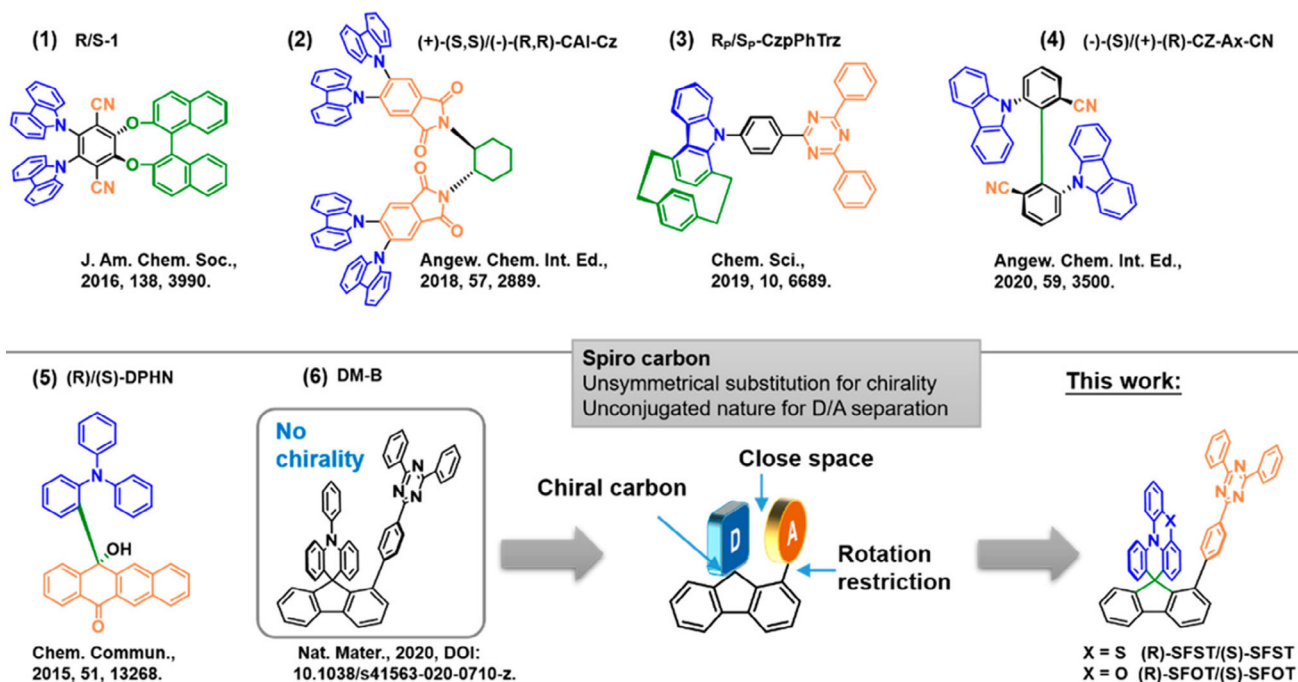


Figure 46. Representative CP-TADF molecular structures. Reproduced with permission.^[89] Copyright 2020, American Chemical Society.

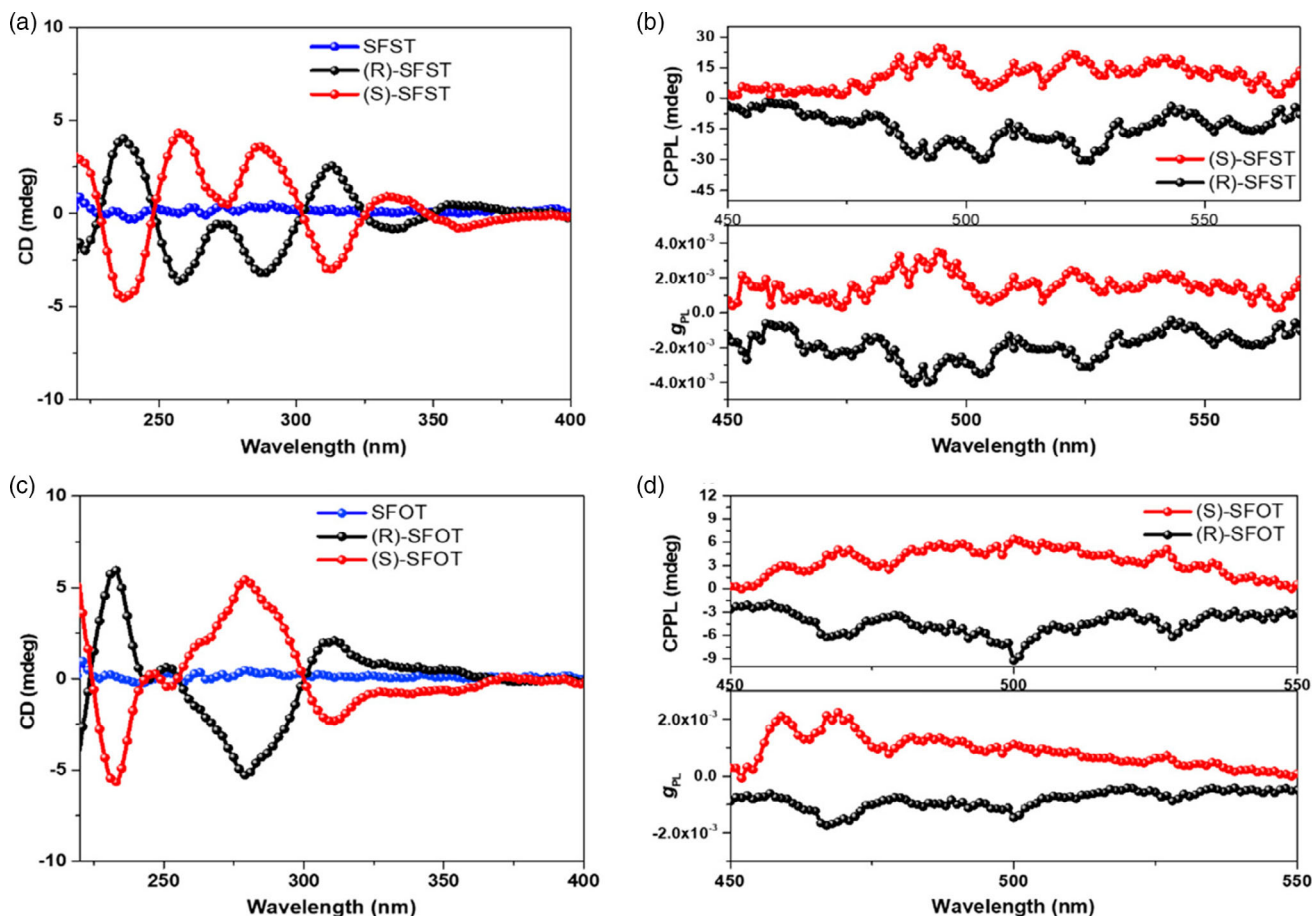
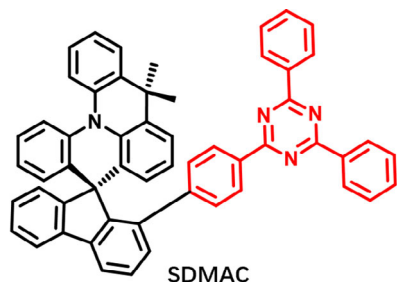


Figure 47. a,c) CD spectra of SFST, SFOT, (R)-SFST/(S)-SFST, and (R)-SFOT/(S)-SFOT. b,d) CPPL spectra of (S)-SFST/(R)-SFST and (S)-SFOT/(R)-SFOT. Reproduced with permission.^[89] Copyright 2020, American Chemical Society.



$\lambda_{PL} = 467 \text{ nm}$, $\Delta E_{ST} = 0.034 \text{ eV}$ (in toluene),
 $\tau_{DF} = 4.17 \text{ } \mu\text{s}$, $\Phi_{PL} = 90\%$ (30 wt% in PPF)
(R)-SDMAC: $g_{lum} = -1.19 \times 10^{-3}$ (in dichloromethane)
(S)-SDMAC: $g_{lum} = +1.39 \times 10^{-3}$ (in dichloromethane)
 $\lambda_{EL} = 492 \text{ nm}$, $EQE_{max/100/1000} = 28.4/24.5/17.1\%$
(35 nm of electron injection layer)

Angew. Chem. Int. Ed. **2022**, *61*, e202206861

Figure 48. Molecular structure and properties of SDMAC.

may be ascribed to the energy gap law.^[91] An OLED containing 6 wt% PXZ-TRZ doped in CBP as the emitter layer exhibited an EQE_{max} of 12.5% (λ_{EL} of 529 nm).^[93] The authors also demonstrated that the orientation of the TDM of PXZ-TRZ can be

modulated in mCBP by varying the temperature on the ITO glass holder during the deposition of the emitting layer. The horizontal orientation of the TDM of PXZ-TRZ can be enhanced by lowering the temperature of the ITO glass from 300 K to 200 K. As a result, the EQE_{max} is improved from 9.6% at 300 K to 11.9% at 200 K.^[94]

The use of PTZ as a donor introduces additional conformational dynamics due to the existence of two ground-state conformers resulting from puckering of the PTZ ring, each with their own associated ΔE_{ST} .^[95] PTZ-TRZ shows a slightly red shifted emission maximum (λ_{PL} : 562 nm; in toluene) and similar Φ_{PL} (65.8%; in 2 wt% mCBP) to those of its analog PXZ-TRZ (545 nm in toluene, Φ_{PL} 65.7%; 6 wt% in CBP),^[93] while the ΔE_{ST} (0.07 eV) of PTZ-TRZ is the largest amongst the three compounds: DMAC-TRZ, PXZ-TRZ, and PTZ-TRZ. The relatively similar electron-donating strength of the PXZ and PTZ groups in PXZ-TRZ and PTZ-TRZ translates to similar emission spectra and Φ_{PL} . The device containing PTZ-TRZ exhibited an EQE_{max} of 10.8%, which is also of similar performance to that of PTZ-TRZ-based OLED although the two reports^[93,95] used different hosts within the emissive layer. The EL spectrum shows two emission bands, one high-energy band at around 393 nm and a stronger broad band at 532 nm, resulting from the simultaneous emission from the two conformers.

Table 17. Summary of photophysical and electrochemical properties.

Emitter	Solution $\lambda_{PL}/\Phi_{PL}/\tau_d$ (medium) [nm/%/ μ s]	Solid State $\lambda_{PL}/\Phi_{PL}/\tau_d$ (medium) [nm/%/ μ s]	ΔE_{ST} [eV]	HOMO [eV]	LUMO [eV]	Ref.
CzpPhTrz	470/70/– (toluene)	482/69/65 (10 wt% DPEPO)	0.16	–5.80	–3.23	[15]
5	548/–/– (toluene)	527/60/12.1 (10 wt% CBP)	0.03	–4.11	–2.70	[86]
(S,S)–(+)-TpAc–TRZ	525/–/– (toluene)	541/85/1.1 (neat film)	0.03	–5.19	–2.55	[87]
(–)–(S,S)–MC	512/–/– (toluene)	505/80/12.9 (25 wt% CBP)	2.69	–5.38	–2.72	[88]
SFST	512/–/– (toluene)	–/53.1/6.78 (30 wt% mCBP)	0.05	–5.21	–2.92	[89]
SFOT	512/–/– (toluene)	–/89.0/7.98 (30 wt% mCBP)	0.05	–5.13	–2.91	[89]
SDMAC	468/47/– (toluene)	–/90/4.17 (30 wt% PPF)	0.03	–5.29	–2.66	[90]

Table 18. Summary of device structures and performance.

Emitter	Device Structure	EL_{max} [nm]	CIE	V_{on} [V]	$EQE/PE/CE^a$ [%/lm W ^{–1} /cd A ^{–1}]	$EQE_{100/1000}$ [cd] [m] ^{–2}	Ref.
Rp–5	ITO/PEDOT: PSS/10 wt% R _p –5:CBP/TPBi/ Ca/Ag	560	(0.42, 0.54)	4.2	7.8/–/23.8	–	[86]
Sp–5	ITO/PEDOT: PSS/10 wt% S _p –5:CBP/TPBi/ Ca/Ag	560	(0.43, 0.54)	4.2	7.1/–/21.6	–	[86]
(S,S)–(+)-TpAc–TRZ	ITO/PEDOT:PSS/(S,S)–(+)-TpAc–TRZ/ TPBi/LiF/Al	534	–	2.5	25.5/95.9/88.6	16.8/1.6	[87]
(+)- (R,R)–MC	ITO/PEDOT:PSS/CBP:25 wt% (+)–(R,R)/ MC/TPBi/LiF/Al	522	(0.28, 0.54)	3.8	17.1/37.0/53.7	–/16.5	[88]
(–)–(S,S)–MC	ITO/PEDOT:PSS/CBP:25 wt% (–)–(S,S)– MC/TPBi/LiF/Al	522	(0.28, 0.54)	3.5	15.5/34.9/48.8	–/15.3	[88]
SFST	ITO/HAT–CN/TAPC/TCTA/30 wt% SFST: mCBP /TmPyPB/Liq/Al	508	(–, –)	3.6	12.5/31.8/37.0	–/11.3	[89]
SFOT	ITO/HAT–CN/TAPC/TCTA/30 wt% SFOT: mCBP /TmPyPB/Liq/Al	508	(–, –)	4.0	23.1/53.6/68.0	–/21.3	[89]
SDMAC	ITO/HAT–CN/TAPC/TCTA/mCBP/30 wt% SDMAC: PPF/PPF/TmPyPB/Liq/Al	492	(0.18, 0.41)	3.4	28.4/35.5/60.0	24.5/17.1	[90]

3ACR-TRZ, an analog of **DMAC-TRZ** containing 3 donor groups, reported by Kaji et al.^[96] shows somewhat similar photophysical properties to **DMAC-TRZ**, with near unity Φ_{PL} (98%; in 16 wt% CBP) and a slightly red-shifted emission (λ_{PL} : 504 nm; in 16 wt% CBP). The small red-shift implies that there is only a weak influence on the stabilization of the singlet state by increasing the number of DMAC units. However, the multiple donors could further delocalize the distribution of HOMO, thus leading to a smaller ΔE_{ST} (0.015 eV). The solution-processed device showed an EQE_{max} of 18.6% at an emission of $\lambda_{EL} \approx 520$ nm. Analog compounds containing either trisubstituted PXZ or PTZ donor groups have also been reported.^[97] Similar evolution of the photophysical properties from the linear D–A compounds to the D₃-symmetric analogs was observed for **tri-PXZ-TRZ** (λ_{PL} : 568 nm; Φ_{PL} : 58% in 6 wt% mCP; τ_d : 1.10 μ s in toluene) and **TRZ3(Ph-PTZ)** (λ_{PL} : 575 nm in toluene; τ_d : 7.2 μ s in 2 wt% mCP).^[98] The OLEDs based on **TRZ3(Ph-PTZ)** shows yellowish-green electroluminescence with a $\lambda_{EL} \approx 550$ nm and exhibits a much higher EQE_{max} of 17.4% than those of the devices of the **tri-PXZ-TRZ**-based OLEDs (EQE_{max} : 13.3%, λ_{EL} : 553 nm). The Zysman–Colman group reported yellow-emitting OLEDs based on **tri-PXZ-TRZ** by doping the emitter into a bespoke host **4-mCBPy**, thus demonstrating an improved device performance

with an EQE_{max} of 19.4% and a dramatically reduced efficiency roll-off ($EQE = 16.0\%$ at a luminance of 10 000 cd m^{–2}).^[99]

i-DMAC-TRZ (λ_{PL} : 452 nm; Φ_{PL} : 55%; τ_d : 1840 μ s; ΔE_{ST} : 0.35 eV; in 3 wt% DPEPO) is a constitutional isomer of **DMAC-TRZ** but where the phenylene bridge is C-bound *para* to the nitrogen atom of the DMAC donor (**Figure 50**).^[100] Distinct from the highly twisted conformation of **DMAC-TRZ**, such a structural change results in a flattened conformation, leading to enhanced conjugation between the DMAC and TRZ, and hence a much larger ΔE_{ST} (0.35 eV) than that found for **DMAC-TRZ** (0.06 eV). Despite the emission spectrum being blue-shifted from **DMAC-TRZ** (λ_{PL} : 495 nm) to **i-DMAC-TRZ** (λ_{PL} : 452 nm), the Φ_{PL} is reduced by almost half. The device-based **i-DMAC-TRZ** (10 wt% in mCBP) presents a deep-blue emission with λ_{EL} at 450 nm and CIE coordinates of (0.15, 0.11) and an EQE_{max} of 10.9%.

DTPSAF (λ_{PL} : 459 nm; Φ_{PL} : 82%; in 10 wt% mCP) is the SpiroAC analog of **i-DMAC-TRZ**. When compared to **i-DMAC-TRZ**, **DTPSAF** has a similar λ_{PL} but has a higher Φ_{PL} due to the restricted rotational flexibility conferred by the rigid bulky SpiroAC group. Addition of methyl groups on the phenylene bridge of **DTPSAF** to generate **DTTSAF** further enhances the restriction of the rotation and produces a more twisted

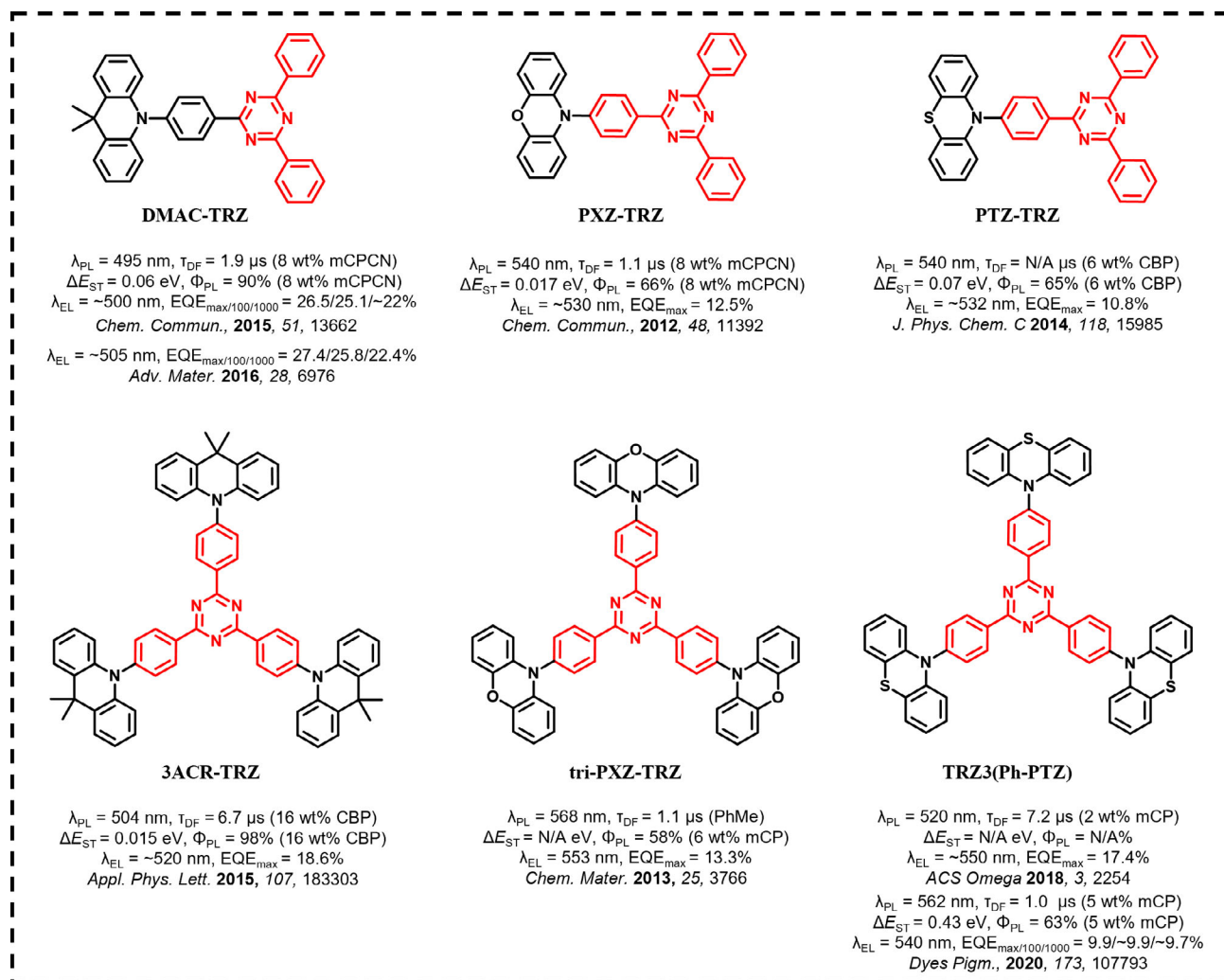


Figure 49. Molecular structures and properties of TADF emitters based on triazine and noncarbazole donors.

conformation, leading to a near unity Φ_{PL} and a 9 nm blue-shift in the emission for **DTTSAF** (λ_{PL} : 450 nm; Φ_{PL} : 100%; in 10 wt% mCP) and **DTXSAF** (λ_{PL} : 446 nm; Φ_{PL} : 98%; in 10 wt% mCP), which contain toluenyl and xylenyl bridges, respectively. Distinct to **i-DMAC-TRZ**, there is no reported TADF in these analogs, which based on DFT calculations can be ascribed to their too large ΔE_{ST} values. The EQEs of the **DTTSAF**- and **DTXSAF**-doped OLEDs (6.2 and 7.7%, respectively) were higher than that of the **DTPSAF**-doped device (5.7%) due to the higher Φ_{PL} values of **DTTSAF** (Φ_{PL} : 100%) and **DTXSAF** (Φ_{PL} : 98%) over that of **DTPSAF** (Φ_{PL} : 82%). **DTXSAF**-based OLEDs show the deepest blue emission with CIE coordinates of (0.15, 0.08) and λ_{EL} of 444 nm compared to those of **DTPSAF** (λ_{EL} of 460 nm) and **DTTSAF** (λ_{EL} of 448 nm).^[101]

Wu et al.^[102] reported two compounds **DPAC-TRZ** (λ_{PL} : 478 nm; Φ_{PL} : 82%; ΔE_{ST} : 0.133 eV; in 12 wt% mCPCN) and **SpiroAC-TRZ** (λ_{PL} : 480 nm; (Φ_{PL} : 100%; ΔE_{ST} : 0.072 eV; in 12 wt% mCPCN), both of which are derivatives of **DMAC-TRZ** but where the two methyl groups on the acridan are replaced by phenyl and 2,2'-biphenyl (spirobiphenyl),^[103]

respectively. In contrast to **DMAC-TRZ**, the structural modifications of the donor contribute to a blue-shift of the emission. The fluorescence (phosphorescence) spectra of **SpiroAC-TRZ**, **DPAC-TRZ**, and **DMAC-TRZ** in 12 wt% mCPCN films are structureless with λ_{PL} of 480 nm (483 nm), 478 nm (482 nm), and 495 nm (504 nm), respectively. Both compounds possess small ΔE_{ST} values though larger than that of **DMAC-TRZ**, thus leading to relatively short delayed lifetime (**DPAC-TRZ**: τ_d of 2.9 μs ; **SpiroAC-TRZ**: τ_d of 2.1 μs). **DPAC-TRZ** has a lower Φ_{PL} of 82% than **SpiroAC-TRZ** (Φ_{PL} : 100%), the latter of which is higher compared with **DMAC-TRZ** (λ_{PL} : 495 nm; Φ_{PL} : 90%; τ_d : 1.9 μs ; ΔE_{ST} : 0.05 eV; in 8 wt% mCPCN). **DPAC-TRZ** and **SpiroAC-TRZ** have TDMs that are highly horizontally oriented, with θ of 78%, 83% for **DPAC-TRZ** and **SpiroAC-TRZ**, respectively, in 12 wt% mCPCN, resulting in EQE_{max} of 25.8% and 36.7% in the respective devices. The device with **SpiroAC-TRZ** retains a high EQE_{1000} of 30.5% at a luminance of 1000 cd m^{-2} .

Replacement of the methyl groups on the acridan with a spiro adamantyl unit, as in **a-DMAC-TRZ** (λ_{PL} : 479 nm; Φ_{PL} : 86.1%; τ_d : 4.09 μs in 20 wt% DPEPO; ΔE_{ST} : 0.20 eV) results in a

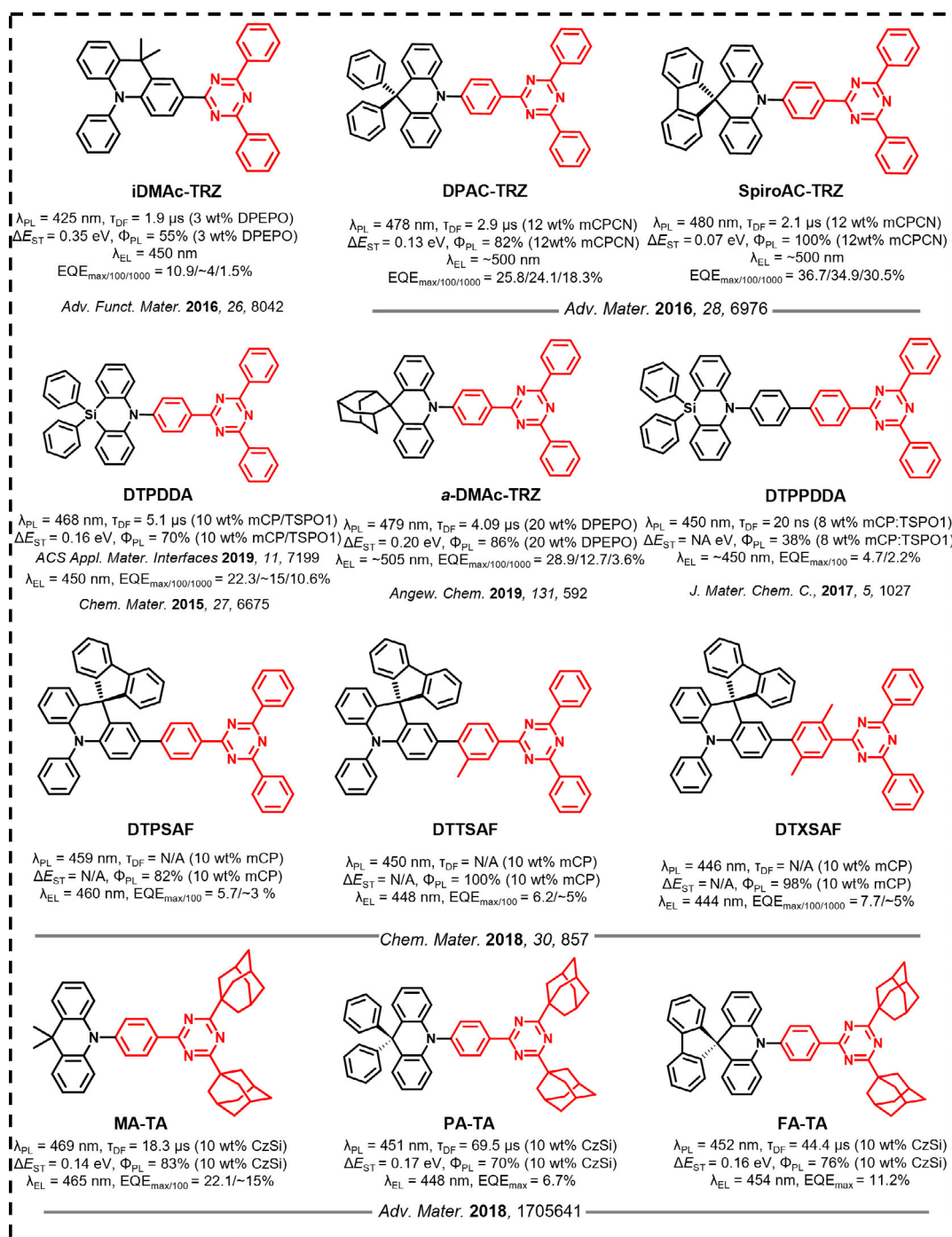


Figure 50. Molecular structures and properties of TADF emitters based on triazine and DMAC derivatives donors.

blue-shifted emission, but with otherwise comparable photo-physical properties to that of **DMAC-TRZ**^[91] (λ_{PL} : 495 nm; Φ_{PL} : 90%; τ_d : 1.9 μs ; ΔE_{ST} : 0.05 eV; in 8 wt% mCPCN). The introduction of the rigid and bulky adamantanyl moiety not only suppresses the geometry relaxation in the excited state but also induced the formation of quasi-axial conformer (QAC) and quasi-equatorial conformer (QEC) geometries corresponding to a shoulder emission peak at around 419 nm and a main

emission peak at around 479 nm in the PL spectrum, respectively. The ΔE_{ST} values of two conformers were confirmed separately by different excitation wavelength. With an excitation wavelength of 360 nm, the S_1 and T_1 energies of QAC were calculated to be 2.97 and 2.66 eV, demonstrating a large ΔE_{ST} of 0.31 eV. At an excitation wavelength of 420 nm, the S_1 and T_1 energy levels of **a-DMAC-TRZ** for QEC were calculated to be 2.79 and 2.59 eV, thus translating to a smaller ΔE_{ST} of

0.20 eV. Owing to the effect of the rigid molecular backbone and the degenerate alignment of ³LE of QAC and ³CT of QEC for efficient dual fluorescence emission, the resulting OLEDs achieved a high EQE_{max} of 28.9% at CIE coordinates of (0.18, 0.35).^[104]

Kaji et al.^[105] demonstrated that by replacing the distal phenyl groups attached to the triazine with adamantyl substituents, the acceptor becomes weaker, leading to a blue-shifted emission compared to **DMAC-TRZ**,^[91] **DPAC-TRZ**,^[102] and **SpiroAc-TRZ**.^[102] Solution-processed devices employing the emitters **FA-TA** (λ_{PL} : 452 nm in toluene; Φ_{PL} : 76%; τ_d : 44.4 μ s in 10 wt% CzSi; ΔE_{ST} : 0.16 eV), **MA-TA** (λ_{PL} : 469 nm in toluene; Φ_{PL} : 83%; τ_d : 18.3 μ s in 10 wt% CzSi; ΔE_{ST} : 0.14 eV), and **PA-TA** (λ_{PL} : 450 nm in toluene; Φ_{PL} : 70%; τ_d : 69.5 μ s in 10 wt% CzSi; ΔE_{ST} : 0.17 eV) exhibited EQE_{max} of 11.2% with CIE coordinates of (0.15, 0.13), 22.1% with CIE coordinates of (0.15, 0.19) and 6.7% with CIE coordinates of (0.15, 0.10), respectively, as shown in **Figure 50**. **MA-TA** represents one of the most efficient blue emitters for solution-processed OLEDs reported to date. However, the much poorer performance of the devices with **PA-TA** and **FA-TA** is likely in part due to the random orientation of the TDMs in the spin-coated films when compared to the highly horizontally oriented TDMs of **DPAC-TRZ** and **SpiroAc-TRZ** in evaporated 12 wt% mCPCN, although the emitters are similar in structure. The higher energy excited states of **PA-TA** and **FA-TA** also make it difficult to find suitable host materials or blocking layers in devices, which might be the reason for this poor performance.

Replacement of the spiro-carbon in **DPAC-TRZ**^[102] with a silicon atom results in the emitter **DTPDDA**.^[106] This compound

shows a 10 nm blue-shifted emission (λ_{PL} : 468 nm; Φ_{PL} : 70%; τ_d : 5.1 μ s in 10 wt% mCP/TSPO1; ΔE_{ST} : 0.16 eV) than **DPAC-TRZ** (λ_{PL} : 478 nm; Φ_{PL} : 82%; ΔE_{ST} : 0.13 eV; in 12 wt% mCPCN), yet both compounds have comparable ΔE_{ST} . However, the larger silicon atom radius makes **DTPDDA** more flexible, which adversely reduces its Φ_{PL} . A blue OLED with the CIE coordinates of 0.15, 0.20 showed an EQE_{max} of 22.3%; the EQE reduced to 10.6% at 1000 cd m⁻² when the emitter was doped in a mixed exciplex co-host system of mCP:TSPO1.

The addition of a second phenylene ring within the bridge in **DTPDDA** resulted in an increased spatial separation between the donor and acceptor, as well as an improved horizontal dipole ratio of the TDM. **DTPDDA** (λ_{PL} : 450 nm in toluene; Φ_{PL} : 38%; τ_d : 20 ns in 8 wt% mCP/TSPO1; ΔE_{ST} : 0.04 eV)^[107] showed a TDM θ value of 0.73 compared to that of **DTPDDA** (0.66: isotropic). However, the extremely short “delayed lifetime” of 20 ns clearly indicates that **DTPDDA** is not a TADF emitter. The biphenylene ring will adversely result in a lower local-excited triplet state energy than the energy of its lowest charge transfer triplet state (³LE < ³CT) because the former is sensitive to the enhanced conjugation while the latter is predominantly determined by the charge transfer strength. As a result, the upconversion of the triplet excitons become impossible due to its large barrier from the ³LE to the S₁ state. Although the ΔE_{ST} was determined to be as small as 0.04 eV, it does not align with this analysis. The triplet energy was determined according to the delayed fluorescence that, however, did not provide the delayed time for the measurement of phosphorescence. The OLED employing **DTPDDA** showed an EQE_{max} of 4.7% and deep blue emission at CIE

Table 19. Summary of photophysical and electrochemical properties.

Emitter	Solution $\lambda_{PL}/\Phi_{PL}/\tau_d$ (medium) [nm/%/ μ s]	Solid State $\lambda_{PL}/\Phi_{PL}/\tau_d$ (medium) [nm/%/ μ s]	ΔE_{ST} [eV]	HOMO [eV]	LUMO [eV]	Ref.
DMAC-TRZ	-/-/-	495/90/1.9(12 wt% in mCPCN)	0.06	-5.61	-3.12	[91]
PXZ-TRZ	-/29.5/0.676	540/66/1.1(8 wt% in mCPCN)	0.02	-5.50	-3.10	[91]
PTZ-TRZ	-/-/(PhMe)	540/65/- (6 wt% in CBP)	0.07	-5.50	-3.00	[95]
3ACR-TRZ	51 194-(PhMe)	504/98/6.7(16 wt% in CBP)	0.02	-	-	[96]
tri-PXZ-TRZ	568/-/1.101(PhMe)	-/58/- (6 wt% in mCP)	-	-5.70	-3.40	[97]
TRZ3(Ph-PTZ)	575/-/(PhMe)	520/-/7.2(2 wt% in mCP)	-	-	-	[99a]
i-DMAc-TRZ	432/53.4/(PhMe)	452/55/1840(3 wt% in DPEPO)	0.35	-	-	[100]
DPAC-TRZ	-/-/(-)	478/82/2.9(12 wt% in mCPCN)	0.13	-5.72	-3.12	[102]
SpiroAc-TRZ	-/-/(-)	480/100/2.1(12 wt% in mCPCN)	0.07	-5.70	-3.12	[102]
SpiroAc-TRZ	-/-/(-)	483/98/3.9(10 wt% in mCP/TSPO1)	0.07	-	-	[102]
DTPDDA	-/-/(-)	468/70/5.1(10 wt% in mCP/TSPO1)	0.16	-	-	[106]
DTPDDA	\approx 475/-/(PhMe)	-/-/(-)	-	-5.57	-2.80	[106]
a-DMAc-TRZ	479/-/(PhMe)	-/86.1/4.09(20 wt% in DPEPO)	-	-	-	[104]
DTPDDA	450/-/(PhMe)	-/38/20 ns (8 wt% in mCP : TSPO1)	-	-6.08	-2.83	[107]
DTPSAF	-/-/(PhMe)	459/82/- (10 wt% in mCP)	-	-5.51	-2.63	[101]
DTTSAF	-/-/(PhMe)	450/100/- (10 wt% in mCP)	-	-5.55	-2.56	[101]
DTXSAF	-/-/(PhMe)	446/98/- (10 wt% in mCP)	-	-5.52	-2.48	[101]
MA-TA	469/-/(PhMe)	-/83/18.3(10 wt% in CzSi)	0.14	-5.86	-2.96	[105]
FA-TA	452/-/(PhMe)	-/76/44.4(10 wt% in CzSi)	0.16	-5.91	-2.96	[105]
PA-TA	451/-/(PhMe)	-/70/69.5(10 wt% in CzSi)	0.17	-6.00	-2.99	[105]

Table 20. Summary of device structures and performance.

Emitter	Device Structure	EL _{max} [nm]	CIE	V _{on} [V]	EQE/PE/CE ^{a)} [%/lm W ⁻¹ /cd A ⁻¹]	EQE _{100/1000} [cd] [m] ⁻²	Ref.
DMAC–TRZ	ITO/PEDOT:PSS/TAPC/mCP/mCPCN: DMAC–TRZ 8 wt%/DPPS /3TPYMB/LiF/Al	≈500	–	3	26.5/65.6/66.8	25.1/≈22.0	[91]
DMAC–TRZ	ITO/MoO ₃ /TAPC/mCPCN: 12 wt% DMAC–TRZ/LiF/Al	≈505	–	3	27.4/80.8/77.1	25.8/22.4	[91]
PXZ–TRZ	ITO/α–NPD/6 wt% PXZ–TRZ: CBP/TPBi/LiF/Al	529	–	3.5	12.5/–/–	–/–	[91]
PTZ–TRZ	ITO/α–NPD/2 wt% PTZ– TRZ:mCBP/TPBi/LiF/Al	≈532	–	–	10.8/–/–	–/–	[95]
3ACR–TRZ	ITO/PEDOT:PSS/16 wt% 3ACR–TRZ:CBP/ BmPyPhB/Liq/Al	≈520	–	4.8	18.6/36.3/–	–/–	[96]
tri–PXZ–TRZ	ITO/α–NPD/6 wt%: mCBP/TPBi/LiF/Al	553	–	–	13.3/–/–	–/–	[97]
TRZ3(Ph–PTZ)	ITO /α–NPD/TCTA/mCP/5 wt% TRZ3(Ph–PTZ): mCBP/DPEPO /TPBi/LiF/Al	≈550	(0.23, 0.75)	4.2	17.4/17.4/58.6	–/–	[99a]
i–DMAc–TRZ	ITO/TAPC/10 wt% i–DMACTRZ: mCBP/ TmPyPB/LiF/Al	450	(0.15, 0.11)	–	10.9/–/–	≈4.0/1.5	[100]
DPAC–TRZ	ITO/MoO ₃ /TAPC/mCPCN:12 wt% DPAC–TRZ/LiF/Al	≈500	–	–	25.8/62.7/60	24.1/18.3	[102]
SpiroAC–TRZ	ITO/MoO ₃ /TAPC/mCPCN: 12 wt% SpiroAC–TRZ/LiF/Al	≈500	–	–	36.7/98.4/94	34.9/30.5	[102]
DTPDDA	ITO/4 wt% ReO ₃ :mCP/mCP/mCP:TSPO1:16 wt% DPTDDA(0.42:0.42:0.16 in wt%)/TSPO1/4 wt% Rb ₂ CO ₃ :TSPO1/Al	450	(0.149, 0.197)	3	22.3/30.4/35.6	≈15.0/10.6	[106]
a–DMAc–TRZ	ITO/TAPC/mCP/DPEPO:20 wt% a–DMAc–TRZ/DPEPO/TmPyPB)/LiF/Al	≈505	(0.18, 0.35)	3.3	28.9/–/63.7	12.7/3.6	[104]
DTPDDA	ITO/4 wt% ReO ₃ : mCP/mCP/mCP : TSPO1: emitter/TSPO1/4 wt% Rb ₂ CO ₃ : TSPO1/Al	≈450	(0.151, 0.087)	3.3	4.7/–/–	2.2/–	[107]
DTPSAF	ITO/6 wt% ReO ₃ :mCP/mCP/10 wt%:mCP/ TSPO1/6 wt% Rb ₂ CO ₃ :TSPO1/Al	460	(0.143, 0.131)	4.1	5.7/6.9/–	≈3.0/–	[101]
DTTSAF	ITO/6 wt% ReO ₃ :mCP/mCP/10 wt%:mCP/ TSPO1/6 wt% Rb ₂ CO ₃ :TSPO1/Al	448	(0.147, 0.096)	4.1	6.2/4.8/–	≈5.0/–	[101]
DTXSAF	ITO/6 wt% ReO ₃ :mCP/mCP/10 wt%:mCP/ TSPO1/6 wt% Rb ₂ CO ₃ :TSPO1/Al	444	(0.149, 0.082)	4.1	7.7/5.2/–	≈5.0/–	[101]
MA–TA	ITO/PEDOT:PSS/PVK/10 wt% MA–TA:CzSi/ TSPO1/TPBi/LiQ/Al	465	(0.15, 0.19)	5.1	22.1/–/–	≈15.0/–	[105]
FA–TA	ITO/PEDOT:PSS/PVK/10 wt% FA–TA:CzSi/ TSPO1/TPBi/LiQ/Al	452	(0.15, 0.13)	5.5	11.2/–/–	–/–	[105]
PA–TA	ITO/PEDOT:PSS/PVK/10 wt% PA–TA:CzSi/ TSPO1/TPBi/LiQ/Al	451	(0.15, 0.10)	5.5	6.7/–/–	–/–	[105]

coordinates of (0.15, 0.09).^[107] The optoelectronic characterization of the aforementioned materials is summarized in **Table 19**, and device performance metrics are summarized in **Table 20**.

12. Conclusions

The objective of this review is to provide a detailed overview of triazine-based TADF materials, to compare and contrast their optoelectronic properties and to report their performance as emitters in OLEDs. The emission properties of these TADF emitters were mainly modulated via the tuning of the donor

strength, modifying the substituents about the triazine, varying the nature of the D–A bridge and switching CT channels (intramolecular CT vs. through-space CT). The plethora of examples contained within this review reveals the versatility of triazine as an acceptor in the design of TADF emitters. By simply varying the strength and number of donors along with the structure of the bridging aryl groups, the emission spectrum can be easily tuned from deep blue through to yellow. The planar conformation adopted by the TRZ moiety can facilitate to the formation of intermolecular exciplexes or through space charge transfer interactions, which enriches the photo-physical behavior of these compounds and can contribute to enhancing k_{RISC} .

Despite the progress that has been made, the potential of triazine as a moiety in TADF emitter design still has not been fully realized. First, one of the major factors affecting the device lifetime of OLEDs is the stability of the emitter. TADF compounds containing a TRZ acceptor have already demonstrated some potential for improved device lifetimes over their analogs containing acceptors like benzophenone or diphenyl sulfone. TRZ has long been recognized as a chemically stable moiety in the design of epoxy resin,^[108] polymers,^[109] and covalent TRZ frameworks (CTFs);^[110] however, OLED stability studies based on TRZ-functionalized TADF emitters remain limited. Studies that probed the influence of intramolecular hydrogen bonding, glass transition temperatures, and charge mobility on the stability of TRZ-functionalized molecules and the impact on the device lifetime would be welcome.

The orientation of the TDM of the emitters, which impacts the light out-coupling efficiency of the device, is correlated with the EQE of the OLED. Due to the rigid and planar structure of TRZ linked to extended donors, a number of TRZ-based compounds have been documented to show preferential horizontal orientation of their TDM, leading to enhanced light outcoupling efficiency in the device, with $\text{EQE}_{\text{max}} > 30\%$. The parameters controlling the orientation of the TDM during thermal evaporation remain unclear,^[111] and this is clearly a design feature that can be exploited further.

Solution-processing techniques such as ink-jet printing are promising for producing large-area OLEDs, which remains challenging and expensive for thermal evaporation. More and more attention has been paid to the development of TRZ-containing TADF dendrimers and polymers as attractive classes of emitters suitable for solution-processed OLEDs. However, in contrast to the advances reported for small molecular weight TADF emitters that show high PLQY, horizontal orientation of their TDM, fast RISC rates, and examples of chiral analogs that show CPL, it remains challenging to develop TADF dendrimers and polymers inheriting these properties. Thus, the performance of solution-processed OLEDs containing TRZ-based macromolecules still lags behind small-molecule TRZ-based evaporated OLEDs.

Acknowledgements

D.S. acknowledges support from the Royal Academy of Engineering Enterprise Fellowship (EF2122-13106). This project has received funding from the European Union's Horizon 2020 research and innovation program under the Marie Skłodowska-Curie grant agreements No. 897098 (AIE-RTP-PLED). T.W. acknowledges support from the Marie Skłodowska-Curie Individual Fellowship. C.S. acknowledges support from the China Scholarship Council (201806890001). The authors thank the EPSRC (EP/P010482/1) for financial support.

Conflict of Interest

The authors declare no conflict of interest.

Keywords

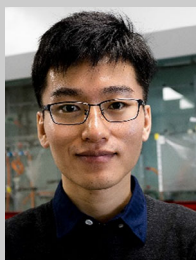
carbazole, emitters, organic light-emitting diodes (OLEDs), thermally activated delayed fluorescence (TADF), triazine

Received: July 8, 2022
Revised: September 6, 2022
Published online:

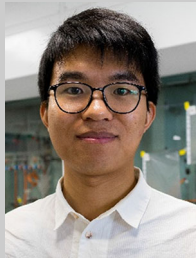
- [1] C. W. Tang, S. A. VanSlyke, *Appl. Phys. Lett.* **1987**, *51*, 913.
- [2] H. Uoyama, K. Goushi, K. Shizu, H. Nomura, C. Adachi, *Nature* **2012**, *492*, 234.
- [3] R. Mertens, *Kyulux announces first shipment of OLED TADF emitters to Wisechip*, <https://www.oled-info.com/kyulux-announces-first-shipment-oled-tadf-emitters-wisechip> (accessed: September 2022) **2020**.
- [4] Y.-L. Zhang, Q. Ran, Q. Wang, Y. Liu, C. Hänisch, S. Reineke, J. Fan, L.-S. Liao, *Adv. Mater.* **2019**, *31*, 1902368.
- [5] T.-L. Wu, M.-J. Huang, C.-C. Lin, P.-Y. Huang, T.-Y. Chou, R.-W. Chen-Cheng, H.-W. Lin, R.-S. Liu, C.-H. Cheng, *Nat. Photon.* **2018**, *12*, 235.
- [6] D. H. Ahn, S. W. Kim, H. Lee, I. J. Ko, D. Karthik, J. Y. Lee, J. H. Kwon, *Nat. Photon.* **2019**, *13*, 540.
- [7] Y. Kondo, K. Yoshiura, S. Kitera, H. Nishi, S. Oda, H. Gotoh, Y. Sasada, M. Yanai, T. Hatakeyama, *Nat. Photon.* **2019**, *13*, 678.
- [8] R. Fink, C. Frenz, M. Thelakkat, H.-W. Schmidt, *Macromolecules* **1997**, *30*, 8177.
- [9] Z.-F. An, R.-F. Chen, J. Yin, G.-H. Xie, H.-F. Shi, T. Tsuboi, W. Huang, *Chem. Eur. J.* **2011**, *17*, 10871.
- [10] K. Goushi, K. Yoshida, K. Sato, C. Adachi, *Nat. Photon.* **2012**, *6*, 253.
- [11] W.-Y. Hung, G.-C. Fang, S.-W. Lin, S.-H. Cheng, K.-T. Wong, T.-Y. Kuo, P.-T. Chou, *Sci. Rep.* **2014**, *4*, 5161.
- [12] F. Tenopala-Carmona, O. S. Lee, E. Crovini, A. M. Neferu, C. Murawski, Y. Olivier, E. Zysman-Colman, M. C. Gather, *Adv. Mater.* **2021**, *33*, 2100677.
- [13] B. Wex, B. R. Kaafarani, *J. Mater. Chem. C* **2017**, *5*, 8622.
- [14] S. Y. Byeon, J. Kim, D. R. Lee, S. H. Han, S. R. Forrest, J. Y. Lee, *Adv. Opt. Mater.* **2018**, *6*, 1701340.
- [15] N. Sharma, E. Spuling, C. M. Mattern, W. Li, O. Fuhr, Y. Tsuchiya, C. Adachi, S. Bräse, I. D. W. Samuel, E. Zysman-Colman, *Chem. Sci.* **2019**, *10*, 6689.
- [16] X. Chen, A. Khan, S.-N. Zou, Y. Li, Q.-S. Tian, C. Zhong, M.-K. Fung, Z.-Q. Jiang, L.-S. Liao, *J. Mater. Chem. C* **2021**, *9*, 4792.
- [17] J.-R. Cha, C. W. Lee, J. Y. Lee, M.-S. Gong, *Dyes Pigment.* **2016**, *134*, 562.
- [18] K. Shizu, Y. Sakai, H. Tanaka, S. Hirata, C. Adachi, H. Kaji, *ITE Trans. Media Technol. Appl.* **2015**, *3*, 108.
- [19] D. Liu, D. Li, H. Meng, Y. Wang, L. Wu, *J. Mater. Chem. C* **2019**, *7*, 12470.
- [20] M. Kim, S. K. Jeon, S.-H. Hwang, J. Y. Lee, *Adv. Mater.* **2015**, *27*, 2515.
- [21] C. S. Oh, D. D. S. Pereira, S. H. Han, H.-J. Park, H. F. Higginbotham, A. P. Monkman, J. Y. Lee, *ACS Appl. Mater. Interfaces* **2018**, *10*, 35420.
- [22] D. R. Lee, M. Kim, S. K. Jeon, S.-H. Hwang, C. W. Lee, J. Y. Lee, *Adv. Mater.* **2015**, *27*, 5861.
- [23] C. S. Oh, H. L. Lee, S. H. Han, J. Y. Lee, *Chem. Eur. J.* **2019**, *25*, 642.
- [24] L.-S. Cui, A. J. Gillett, S.-F. Zhang, H. Ye, Y. Liu, X.-K. Chen, Z.-S. Lin, E. W. Evans, W. K. Myers, T. K. Ronson, H. Nakanotani, S. Reineke, J.-L. Bredas, C. Adachi, R. H. Friend, *Nat. Photon.* **2020**, *14*, 636.
- [25] A. Endo, K. Sato, K. Yoshimura, T. Kai, A. Kawada, H. Miyazaki, C. Adachi, *Appl. Phys. Lett.* **2011**, *98*, 083302.
- [26] S. Youn Lee, T. Yasuda, H. Nomura, C. Adachi, *Appl. Phys. Lett.* **2012**, *101*, 093306.
- [27] D. H. Kim, K. Inada, L. Zhao, T. Komino, N. Matsumoto, J. C. Ribierre, C. Adachi, *J. Mater. Chem. C* **2017**, *5*, 1216.
- [28] K. Shizu, H. Noda, H. Tanaka, M. Taneda, M. Uejima, T. Sato, K. Tanaka, H. Kaji, C. Adachi, *J. Phys. Chem. C* **2015**, *119*, 26283.
- [29] T. Serevičius, T. Nakagawa, M.-C. Kuo, S.-H. Cheng, K.-T. Wong, C.-H. Chang, R. C. Kwong, S. Xia, C. Adachi, *Phys. Chem. Chem. Phys.* **2013**, *15*, 15850.

- [30] a) S.-Y. Kim, W.-I. Jeong, C. Mayr, Y.-S. Park, K.-H. Kim, J.-H. Lee, C.-K. Moon, W. Brütting, J.-J. Kim, *Adv. Funct. Mater.* **2013**, *23*, 3896; b) C. Mayr, S. Y. Lee, T. D. Schmidt, T. Yasuda, C. Adachi, W. Brütting, *Adv. Funct. Mater.* **2014**, *24*, 5232; c) T. D. Schmidt, L. J. Reichardt, A. F. Rausch, S. Wehrmeister, B. J. Scholz, C. Mayr, T. Wehlius, R. M. Ciarnáin, N. Danz, T. C. G. Reusch, W. Brütting, *Appl. Phys. Lett.* **2014**, *105*, 043302.
- [31] S. Xiang, X. Lv, S. Sun, Q. Zhang, Z. Huang, R. Guo, H. Gu, S. Liu, L. Wang, *J. Mater. Chem. C* **2018**, *6*, 5812.
- [32] H. Kaji, H. Suzuki, T. Fukushima, K. Shizu, K. Suzuki, S. Kubo, T. Komino, H. Oiwa, F. Suzuki, A. Wakamiya, Y. Murata, C. Adachi, *Nat. Commun.* **2015**, *6*, 8476.
- [33] C.-K. Moon, K. Suzuki, K. Shizu, C. Adachi, H. Kaji, J.-J. Kim, *Adv. Mater.* **2017**, *29*, 1606448.
- [34] J.-I. Nishide, H. Nakanotani, Y. Hiraga, C. Adachi, *Appl. Phys. Lett.* **2014**, *104*, 233304.
- [35] K. J. Kim, G. H. Kim, R. Lampande, D. H. Ahn, J. B. Im, J. S. Moon, J. K. Lee, J. Y. Lee, J. Y. Lee, J. H. Kwon, *J. Mater. Chem. C* **2018**, *6*, 1343.
- [36] X. Zeng, Y.-H. Huang, S. Gong, P. Li, W.-K. Lee, X. Xiao, Y. Zhang, C. Zhong, C.-C. Wu, C. Yang, *Mater. Horiz.* **2021**, *8*, 2286.
- [37] H. Arai, H. Sasabe, H. Tsuneyama, K. Kumada, J. Kido, *Chem. Eur. J.* **2021**, *27*, 10869.
- [38] K. Albrecht, K. Matsuoka, K. Fujita, K. Yamamoto, *Angew. Chem. Int. Ed.* **2015**, *54*, 5677.
- [39] K. Albrecht, K. Matsuoka, D. Yokoyama, Y. Sakai, A. Nakayama, K. Fujita, K. Yamamoto, *Chem. Comm.* **2017**, *53*, 2439.
- [40] K. Albrecht, K. Matsuoka, K. Fujita, K. Yamamoto, *Mater. Chem. Front.* **2018**, *2*, 1097.
- [41] D. Sun, E. Duda, X. Fan, R. Saxena, M. Zhang, S. Bagnich, X. Zhang, A. Köhler, E. Zysman-Colman, *Adv. Mater.* **2022**, *34*, 2110344.
- [42] D. Sun, R. Saxena, X. Fan, S. Athanasopoulos, E. Duda, M. Zhang, S. Bagnich, X. Zhang, E. Zysman-Colman, A. Köhler, *Adv. Sci.* **2022**, *9*, 2201470.
- [43] T. Matulaitis, N. Kostiv, J. V. Grazulevicius, L. Peciulyte, J. Simokaitiene, V. Jankauskas, B. Luszczynska, J. Ulanski, *Dyes Pigm.* **2016**, *127*, 45.
- [44] T. Matulaitis, P. Imbrasas, N. A. Kukhta, P. Baronas, T. Bučiūnas, D. Banevičius, K. Kazlauskas, J. V. Gražulevičius, S. Juršėnas, *J. Phys. Chem. C* **2017**, *121*, 23618.
- [45] X. Ban, W. Jiang, T. Lu, X. Jing, Q. Tang, S. Huang, K. Sun, B. Huang, B. Lin, Y. Sun, *J. Mater. Chem. C* **2016**, *4*, 8810.
- [46] H.-J. Park, S. H. Han, J. Y. Lee, *J. Mater. Chem. C* **2017**, *5*, 12143.
- [47] D. R. Lee, S. H. Han, C. W. Lee, J. Y. Lee, *Dyes Pigm.* **2018**, *151*, 75.
- [48] H. L. Lee, K. H. Lee, J. Y. Lee, *Adv. Opt. Mater.* **2020**, *8*, 2001025.
- [49] W. Huang, M. Einzinger, T. Zhu, H. S. Chae, S. Jeon, S.-G. Ihn, M. Sim, S. Kim, M. Su, G. Teverovskiy, T. Wu, T. Van Voorhis, T. M. Swager, M. A. Baldo, S. L. Buchwald, *Chem. Mater.* **2018**, *30*, 1462.
- [50] Q. Wang, Y.-X. Zhang, Y. Yuan, Y. Hu, Q.-S. Tian, Z.-Q. Jiang, L.-S. Liao, *ACS Appl. Mater. Interfaces* **2019**, *11*, 2197.
- [51] X.-D. Zhu, Q.-S. Tian, Q. Zheng, X.-C. Tao, Y. Yuan, Y.-J. Yu, Y. Li, Z.-Q. Jiang, L.-S. Liao, *Org. Electron.* **2019**, *68*, 113.
- [52] K. H. Lee, S. O. Jeon, Y. S. Chung, M. Numata, H. Lee, E. K. Lee, E. S. Kwon, M. Sim, H. Choi, J. Y. Lee, *J. Mater. Chem. C* **2020**, *8*, 1736.
- [53] Y. Li, J.-J. Liang, H.-C. Li, L.-S. Cui, M.-K. Fung, S. Barlow, S. R. Marder, C. Adachi, Z.-Q. Jiang, L.-S. Liao, *J. Mater. Chem. C* **2018**, *6*, 5536.
- [54] H. Li, J. Li, D. Liu, T. Huang, D. Li, *Chem. Eur. J.* **2020**, *26*, 6899.
- [55] R. K. Konidena, K. H. Lee, J. Y. Lee, W. P. Hong, *J. Mater. Chem. C* **2019**, *7*, 8037.
- [56] H. L. Lee, K. H. Lee, J. Y. Lee, W. P. Hong, *J. Mater. Chem. C* **2019**, *7*, 6465.
- [57] J. H. Yun, K. H. Lee, J. Y. Lee, *Chem. Eng. J.* **2020**, *400*, 125940.
- [58] Y. H. Park, H. J. Jang, J. Y. Lee, *Org. Electron.* **2020**, *82*, 105716.
- [59] S. K. Jeon, H.-J. Park, J. Y. Lee, *J. Mater. Chem. C* **2018**, *6*, 6778.
- [60] J. H. Yun, K. H. Lee, J. Y. Lee, *Dyes Pigm.* **2020**, *181*, 108549.
- [61] C. Li, C. Duan, C. Han, H. Xu, *Adv. Mater.* **2018**, *30*, 1804228.
- [62] D.-L. Sun, S. V. Rosokha, S. V. Lindeman, J. K. Kochi, *J. Am. Chem. Soc.* **2003**, *125*, 15950.
- [63] H. Tsujimoto, D.-G. Ha, G. Markopoulos, H. S. Chae, M. A. Baldo, T. M. Swager, *J. Am. Chem. Soc.* **2017**, *139*, 4894.
- [64] D. R. Lee, J. M. Choi, C. W. Lee, J. Y. Lee, *ACS Appl. Mater. Interfaces* **2016**, *8*, 23190.
- [65] J.-R. Cha, M.-S. Gong, T. J. Lee, T. H. Ha, C. W. Lee, *J. Korean Phys. Soc.* **2018**, *72*, 873.
- [66] X.-K. Chen, B. W. Bakr, M. Auffray, Y. Tsuchiya, C. D. Sherrill, C. Adachi, J.-L. Bredas, *J. Phys. Chem. Lett.* **2019**, *10*, 3260.
- [67] J. G. Yu, S. H. Han, H. L. Lee, W. P. Hong, J. Y. Lee, *J. Mater. Chem. C* **2019**, *7*, 2919.
- [68] X. Lv, Y. Wang, N. Li, X. Cao, G. Xie, H. Huang, C. Zhong, L. Wang, C. Yang, *Chem. Eng. J.* **2020**, *402*, 126173.
- [69] Y. Wada, H. Nakagawa, S. Matsumoto, Y. Wakisaka, H. Kaji, *Nat. Photon.* **2020**, *14*, 643.
- [70] X. Tang, L.-S. Cui, H.-C. Li, A. J. Gillett, F. Auras, Y.-K. Qu, C. Zhong, S. T. E. Jones, Z.-Q. Jiang, R. H. Friend, L.-S. Liao, *Nat. Mater.* **2020**, *19*, 1332.
- [71] H.-C. Li, X. Tang, S.-Y. Yang, Y.-K. Qu, Z.-Q. Jiang, L.-S. Liao, *Chin. Chem. Lett.* **2021**, *32*, 1245.
- [72] H. Miranda-Salinas, Y.-T. Hung, Y.-S. Chen, D. Luo, H.-C. Kao, C.-H. Chang, K.-T. Wong, A. Monkman, *J. Mater. Chem. C* **2021**, *9*, 8819.
- [73] X. Q. Wang, S. Y. Yang, Q. S. Tian, C. Zhong, Y. K. Qu, Y. J. Yu, Z. Q. Jiang, L. S. Liao, *Angew. Chem. Int. Ed.* **2021**, *60*, 5213.
- [74] T. Huang, Q. Wang, G. Meng, L. Duan, D. Zhang, *Angew. Chem. Int. Ed.* **2022**, *61*, 202200059.
- [75] S. Kumar, L. G. Franca, K. Stavrou, E. Crovini, D. B. Cordes, A. M. Z. Slawin, A. P. Monkman, E. Zysman-Colman, *J. Phys. Chem. Lett.* **2021**, *12*, 2820.
- [76] X. Wang, S. Wang, J. Lv, S. Shao, L. Wang, X. Jing, F. Wang, *Chem. Sci.* **2019**, *10*, 2915.
- [77] S. Shao, J. Hu, X. Wang, L. Wang, X. Jing, F. Wang, *J. Am. Chem. Soc.* **2017**, *139*, 17739.
- [78] C. Wang, H. Fei, Y. Qiu, Y. Yang, Z. Wei, Y. Tian, Y. Chen, Y. Zhao, *Appl. Phys. Lett.* **1999**, *74*, 19.
- [79] Y. Imai, Y. Nakano, T. Kawai, J. Yuasa, *Angew. Chem. Int. Ed.* **2018**, *57*, 8973.
- [80] J. L. Greenfield, J. Wade, J. R. Brandt, X. Shi, T. J. Penfold, M. J. Fuchter, *Chem. Sci.* **2021**, *12*, 8589.
- [81] C. Hao, L. Xu, H. Kuang, C. Xu, *Adv. Mater.* **2020**, *32*, 1802075.
- [82] E. Peeters, M. P. Christiaans, R. A. Janssen, H. F. Schoo, H. P. Dekkers, E. Meijer, *J. Am. Chem. Soc.* **1997**, *119*, 9909.
- [83] a) Y. Okamoto, *Prog. Polym. Sci.* **2000**, *25*, 159; b) Y. F. Wang, M. Li, J. M. Teng, H. Y. Zhou, W. L. Zhao, C. F. Chen, *Angew. Chem. Int. Ed.* **2021**, *60*, 23619.
- [84] a) T. R. Schulte, J. J. Holstein, L. Krause, R. Michel, D. Stalke, E. Sakuda, K. Umakoshi, G. Longhi, S. Abbate, G. H. Clever, *J. Am. Chem. Soc.* **2017**, *139*, 6863; b) J. Han, S. Guo, J. Wang, L. Wei, Y. Zhuang, S. Liu, Q. Zhao, X. Zhang, W. Huang, *Adv. Opt. Mater.* **2017**, *5*, 1700359.
- [85] a) M. Li, Y. F. Wang, D. Zhang, L. Duan, C. F. Chen, *Angew. Chem. Int. Ed.* **2020**, *59*, 3500; b) X. Li, Y. Xie, Z. Li, *Adv. Photon. Res.* **2021**, *2*, 2000136.
- [86] C. Liao, Y. Zhang, S.-H. Ye, W.-H. Zheng, *ACS Appl. Mater. Interfaces* **2021**, *13*, 25186.

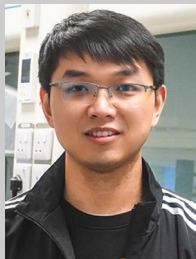
- [87] Y. F. Wang, M. Li, J. M. Teng, H. Y. Zhou, C. F. Chen, *Adv. Funct. Mater.* **2021**, *31*, 2106418.
- [88] W.-L. Zhao, Y.-F. Wang, S.-P. Wan, H.-Y. Lu, M. Li, C.-F. Chen, *CCS Chem.* **2022**, *1*.
- [89] S.-Y. Yang, Y.-K. Wang, C.-C. Peng, Z.-G. Wu, S. Yuan, Y.-J. Yu, H. Li, T.-T. Wang, H.-C. Li, Y.-X. Zheng, Z.-Q. Jiang, L.-S. Liao, *J. Am. Chem. Soc.* **2020**, *142*, 17756.
- [90] S.-Y. Yang, Z.-Q. Feng, Z. Fu, K. Zhang, S. Chen, Y.-J. Yu, B. Zou, K. Wang, L.-S. Liao, Z.-Q. Jiang, *Angew. Chem. Int. Ed.* **2022**, *61*, e202206861.
- [91] W.-L. Tsai, M.-H. Huang, W.-K. Lee, Y.-J. Hsu, K.-C. Pan, Y.-H. Huang, H.-C. Ting, M. Sarma, Y.-Y. Ho, H.-C. Hu, C.-C. Chen, M.-T. Lee, K.-T. Wong, C.-C. Wu, *Chem. Comm.* **2015**, *51*, 13662.
- [92] M. Wang, T. Chatterjee, C. J. Foster, T. Wu, C.-L. Yi, H. Yu, K.-T. Wong, B. Hu, *J. Mater. Chem. C* **2020**, *8*, 3395.
- [93] H. Tanaka, K. Shizu, H. Miyazaki, C. Adachi, *Chem. Comm.* **2012**, *48*, 11392.
- [94] T. Komino, H. Tanaka, C. Adachi, *Chem. Mater.* **2014**, *26*, 3665.
- [95] H. Tanaka, K. Shizu, H. Nakanotani, C. Adachi, *J. Phys. Chem. C* **2014**, *118*, 15985.
- [96] Y. Wada, K. Shizu, S. Kubo, K. Suzuki, H. Tanaka, C. Adachi, H. Kaji, *Appl. Phys. Lett.* **2015**, *107*, 183303.
- [97] H. Tanaka, K. Shizu, H. Nakanotani, C. Adachi, *Chem. Mater.* **2013**, *25*, 3766.
- [98] a) I. Marghad, D. H. Kim, X. Tian, F. Mathevet, C. Gosmini, J.-C. Ribierre, C. Adachi, *ACS Omega* **2018**, *3*, 2254; b) X.-F. Tan, P.-P. Wang, L. Lu, O. Bezikonnyi, D. Volyniuk, J. V. Grazulevicius, Q.-H. Zhao, *Dyes Pigment.* **2020**, *173*, 107793.
- [99] D. Chen, P. Rajamalli, F. Tenopala-Carmona, C. L. Carpenter-Warren, D. B. Cordes, C.-M. Keum, A. M. Z. Slawin, M. C. Gather, E. Zysman-Colman, *Adv. Opt. Mater.* **2020**, *8*, 1901283.
- [100] X. Cai, B. Gao, X. L. Li, Y. Cao, S. J. Su, *Adv. Funct. Mater.* **2016**, *26*, 8042.
- [101] S.-J. Woo, Y. Kim, M.-J. Kim, J. Y. Baek, S.-K. Kwon, Y.-H. Kim, J.-J. Kim, *Chem. Mater.* **2018**, *30*, 587.
- [102] T. A. Lin, T. Chatterjee, W. L. Tsai, W. K. Lee, M. J. Wu, M. Jiao, K. C. Pan, C. L. Yi, C. L. Chung, K. T. Wong, *Adv. Mater.* **2016**, *28*, 6976.
- [103] Z. Jiang, Z. Liu, C. Yang, C. Zhong, J. Qin, G. Yu, Y. Liu, *Adv. Funct. Mater.* **2009**, *19*, 3987.
- [104] W. Li, X. Cai, B. Li, L. Gan, Y. He, K. Liu, D. Chen, Y.-C. Wu, S.-J. Su, *Angew. Chem. Int. Ed.* **2019**, *58*, 582.
- [105] Y. Wada, S. Kubo, H. Kaji, *Adv. Mater.* **2018**, *30*, 1705641.
- [106] J. W. Sun, J. Y. Baek, K.-H. Kim, C.-K. Moon, J.-H. Lee, S.-K. Kwon, Y.-H. Kim, J.-J. Kim, *Chem. Mater.* **2015**, *27*, 6675.
- [107] J. W. Sun, J. Y. Baek, K.-H. Kim, J.-S. Huh, S.-K. Kwon, Y.-H. Kim, J.-J. Kim, *J. Mater. Chem. C* **2017**, *5*, 1027.
- [108] Y. Qi, Z. Weng, Y. Kou, L. Song, J. Li, J. Wang, S. Zhang, C. Liu, X. Jian, *Chem. Eng. J.* **2021**, *406*, 126881.
- [109] D. R. Anderson, J. M. Holovka, *J. Polym. Sci., Part A-1: Polym. Chem.* **1966**, *4*, 1689.
- [110] C. Krishnaraj, H. S. Jena, K. Leus, P. Van Der Voort, *Green Chem.* **2020**, *22*, 1038.
- [111] M. Y. Wong, E. Zysman-Colman, *Adv. Mater.* **2017**, *29*, 1605444.
- [112] Y. Hu, W. Cai, L. Ying, D. Chen, X. Yang, X.-F. Jiang, S. Su, F. Huang, Y. Cao, *J. Mater. Chem. C* **2018**, *6*, 2690.



Dianming Sun is currently a Royal Academy of Engineering Enterprise Fellow at the University of St Andrews. He received his PhD from the Beijing University of Chemical Technology in 2016 under the supervision of Prof. Zhongjie Ren and Prof. Shouke Yan. After that, he moved to the University of St Andrews with the support from the National Postdoctoral Program for Innovative Talents and focused on developing thermally activated delayed fluorescence (TADF) dendrimers. In 2019, he was then awarded a prestigious Marie Skłodowska-Curie Fellowship by the European Commission under the Horizon 2020 framework. His research interests cover molecular design, synthesis, photophysics, and organic light-emitting diodes (OLEDs) fabrication.



Changfeng Si graduated from Taiyuan University of Technology with a BS degree in Optical Information Science and Technology. He then received his MSc in Microelectronics and Solid-State Electronics from Shanghai University. Now, he is in the final year of his Ph.D. under the supervision of Prof. Eli Zysman-Colman at the University of St Andrews. His current research focuses on red TADF emitters for bioimaging and organic light-emitting diodes.



Tao Wang is currently a Marie Skłodowska-Curie research fellow at the University of St Andrews. Dr. Wang graduated from Anhui University in polymer materials and engineering with a Bachelor's degree in 2014. He then obtained his PhD in 2019 from the University of Science and Technology of China (USTC) under the supervision of Professors Guoqing Zhang and Xingyuan Zhang, where he mainly focused on the design of room-temperature phosphorescent polymers. After that, he joined the Hefei National Laboratory of Physical Science at the Microscale at the USTC as a postdoctoral fellow working with Professor Guoqing Zhang (2019–2020). He then moved to the University of St Andrew to work with Professor Eli Zysman-Colman. His research focuses on organic phosphorescence and thermally activated delayed fluorescence.



Eli Zysman-Colman obtained his Ph.D. from McGill University in 2003 under the supervision of Prof. David N. Harpp as an FCAR scholar, conducting research in physical organic sulfur chemistry. He then completed two postdoctoral fellowships, one in supramolecular chemistry with Prof. Jay Siegel at the Organic Chemistry Institute, University of Zurich as an FQRNT fellow and the other in inorganic materials chemistry with Prof. Stefan Bernhard at Princeton University as a PCCM fellow. He joined the department of chemistry at the Université de Sherbrooke in Quebec, Canada, as an assistant professor in 2007. In 2013, he moved to the University of St Andrews in St Andrews, UK, where he is presently Professor of Optoelectronic Materials, Fellow of the Royal Society of Chemistry, and past holder of a Royal Society Leverhulme Trust Senior Research Fellowship. His research program focuses on the rational design of (I) luminophores for energy-efficient visual displays and flat panel lighting based on organic light-emitting diode (OLED) and light-emitting electrochemical cell (LEEC) device architectures; (II) sensing materials employed in electrochemiluminescence; and (III) photocatalyst developing for use in organic reactions.